


<b>Title</b>	All optical systems for terabit network era
<b>Author(s)</b>	Fabbri, Simon
<b>Publication date</b>	2016
<b>Original citation</b>	Fabbri, S. 2016. All optical systems for terabit network era. PhD Thesis, University College Cork.
<b>Type of publication</b>	Doctoral thesis
<b>Rights</b>	<p>© 2016, Simon Fabbri.</p> <p><a href="http://creativecommons.org/licenses/by-nc-nd/3.0/">http://creativecommons.org/licenses/by-nc-nd/3.0/</a></p> 
<b>Embargo information</b>	No embargo required
<b>Item downloaded from</b>	<a href="http://hdl.handle.net/10468/3859">http://hdl.handle.net/10468/3859</a>

Downloaded on 2017-09-05T00:27:21Z



**UCC**

University College Cork, Ireland  
Coláiste na hOllscoile Corcaigh

# All optical systems for terabit network era

Simon Fabbri  
109222003



NATIONAL UNIVERSITY OF IRELAND, CORK

SCHOOL OF SCIENCE

DEPARTMENT OF PHYSICS

**Thesis submitted for the degree of  
Doctor of Philosophy**

2016

Head of Department: Prof. John McNerney

Supervisors: Prof. Frank Peters  
Prof. Andrew D. Ellis



# Contents

List of Figures . . . . .	iii
List of Publications . . . . .	vii
Acronyms . . . . .	xi
Acknowledgements . . . . .	xiv
Abstract . . . . .	xv
<b>1 Introduction</b>	<b>1</b>
1.1 Background . . . . .	1
1.2 Motivation . . . . .	2
1.3 Organization of the manuscript . . . . .	3
<b>2 Optical Comb Generators based on an external modulator</b>	<b>5</b>
2.1 Single frequency driven external modulator . . . . .	6
2.2 Multi-harmonic comb source . . . . .	11
2.2.1 Concept . . . . .	11
2.2.2 Step Recovery Diode based multi-harmonic comb source . . . . .	13
2.2.3 Up-conversion technique for multi-harmonic comb generation . . . . .	16
2.3 Hybrid comb generation . . . . .	19
2.4 Chapter summary . . . . .	23
<b>3 Experimental Implementation of a AO-OFDM Super-channel</b>	<b>24</b>
3.1 All-Optical Orthogonal Frequency Division Multiplexing . . . . .	24
3.2 Odd/Even comb source for experimental super-channel transmitter . . . . .	27
3.2.1 Odd/Even comb source concept . . . . .	28
3.2.2 Frequency shifting . . . . .	30
3.2.3 Odd/Even comb source implementation . . . . .	36
3.3 All-Optical OFDM transmitter . . . . .	37
3.3.1 Super-channel generation . . . . .	38
3.3.2 Transmitter stabilisation . . . . .	44
3.4 Chapter summary . . . . .	47
<b>4 Terabit Interferometric Drop, Add, and Extract multiplexer</b>	<b>48</b>
4.1 Concept . . . . .	49

4.2	Preliminary investigations for the experimental implementation of the TIDE node . . . . .	52
4.2.1	Experimental implementation of fiber based Mach-Zehnder interferometer . . . . .	52
4.2.2	Simulation . . . . .	54
4.3	Experimental implementation with single quadrature signal super-channel . . . . .	59
4.3.1	Optical Demultiplexing . . . . .	62
4.3.2	Optical Gating . . . . .	63
4.3.3	Optical Reshaping . . . . .	65
4.3.4	All-Optical TIDE node experimental results . . . . .	68
4.4	Experimental implementation with dual quadrature signal super-channel . . . . .	73
4.4.1	Experimental setup modifications . . . . .	73
4.4.2	QPSK channel reshaping . . . . .	74
4.4.3	All-Optical TIDE node experimental results . . . . .	77
4.5	Chapter summary . . . . .	79
<b>5</b>	<b>Conclusion</b>	<b>80</b>

## List of Figures

1.1	Concept of ROADM for ultra dense WDM links . . . . .	3
2.1	Simulated three line comb generation using a single MZM . . . . .	8
2.2	Five line comb generation using a single MZM . . . . .	9
2.3	Multi-harmonic comb generation concept . . . . .	11
2.4	Comb flatness versus driving harmonics power and bias voltage . . . . .	12
2.5	Schematic of SRD based comb generator . . . . .	14
2.6	RF spectrum from the electrical signal at different point in the electrical comb source circuitry . . . . .	15
2.7	Optical spectrum of multi-harmonic comb generated using an SRD as electrical source . . . . .	16
2.8	Schematic of the comb generator based the up-conversion electrical harmonic source . . . . .	17
2.9	RF spectrum from the electrical comb using the up-conversion technique . . . . .	17
2.10	Optical spectrum of the optical comb generated using the up-converter multi-harmonic scheme . . . . .	19
2.11	Schematic description of the hybrid comb . . . . .	20
2.12	Schematic of hybrid comb generator . . . . .	21
2.13	Optical spectrum of the 36 line comb generated using the hybrid comb source . . . . .	21
2.14	Electrical spectra of the 36 line comb output . . . . .	22
2.15	Optical spectrum of the 45 line comb generated using the hybrid comb source . . . . .	23
3.1	Impact on required OSNR of relative phase between adjacent sub-carriers and transmitter bandwidth on All-Optical OFDM . . . . .	26
3.2	Schemes for transmitter emulation . . . . .	28
3.3	Schematic of experimental OFDM transmitter . . . . .	29
3.4	SSB-SC concept using DP-MZM . . . . .	30
3.5	Experimental optical frequency shifting . . . . .	31
3.6	SSB-SC for different RF frequencies . . . . .	32
3.7	Frequency shifting at different wavelengths . . . . .	33
3.8	Experimental setup of the DP-MZM scheme with the stabilization . . . . .	34
3.9	SSB-SC performance over time with stabilisation circuitry . . . . .	35

3.10	Frequency shifting and comb generation of the generation of odd/even super-channel . . . . .	36
3.11	Optical comb obtained at the output of the odd/even structure . . . . .	37
3.12	BER versus frequency shifting extinction ratio . . . . .	38
3.13	Odd and Even channels optical spectrum . . . . .	39
3.14	BPSK AO-OFDM optical spectrum . . . . .	40
3.15	QPSK AO-OFDM optical spectrum . . . . .	41
3.16	$Q^2$ -factor versus OSNR . . . . .	42
3.17	Time alignment impact for BPSK AO-OFDM . . . . .	42
3.18	Impact of relative optical phase with adjacent channel . . . . .	45
3.19	Optical spectrum after FWM process . . . . .	46
3.20	Optical spectrum the monitor signal . . . . .	46
4.1	All-Optical Terabit Interferometric Drop, add, and Extract node . . . . .	50
4.2	Illustration of the reshaping functions . . . . .	51
4.3	Schematic of a fiber interferometer . . . . .	52
4.4	Interferometric channel suppression using fiber based MZI . . . . .	53
4.5	BER penalty for the added channel after the suppression of a single channel . . . . .	54
4.6	Sensitivity penalty versus sampling window . . . . .	55
4.7	Sensitivity penalty versus the gate ER . . . . .	56
4.8	OSNR penalty versus sampling window and gate input power. Polynomial fits are displayed for guidance. ch4 is the channel in the middle for the AO-OFDM super-channel, ch3 and ch5 are the adjacent channels. ch4' represents the channel that have been added in place of the extracted ch4. . . . .	57
4.9	Experimental setup of the BPSK AO-OFDM transmitter and of the proposed all optical ROADM . . . . .	60
4.10	Node sub-function: AO-OFDM demultiplexing . . . . .	63
4.11	Time window of the optical gating . . . . .	64
4.12	Optical spectrum of the optical gating . . . . .	65
4.13	Impact of the gating phase . . . . .	66
4.14	Different reshaping filter . . . . .	67
4.15	Different reshaping filter . . . . .	68
4.16	Spectrum at the TIDE node input, output, and channel extraction . . . . .	69
4.17	$Q^2$ -factor measurement for the five central channels BPSK modulated . . . . .	70
4.18	BER measurement in function of OSNR at receiver . . . . .	72

4.19 Experimental setup of the QPSK AO-OFDM transmitter and of the proposed all optical ROADM . . . . .	73
4.20 Spectrum of the channel before and after demultiplexing . . . .	74
4.21 Spectra of the different reshaping function . . . . .	75
4.22 Eyediagram and time trace of the reshaped QPSK channel . . .	76
4.23 Optical spectrum of the QPSK AO-OFDM . . . . .	77
4.24 $Q^2$ -factor measurement for the five central channels QPSK modulated . . . . .	78



I, Simon Fabbri, certify that this thesis is my own work and I have not obtained a degree in this university or elsewhere on the basis of the work submitted in this thesis.

*Simon Fabbri*

A handwritten signature in black ink, appearing to be 'S. Fabbri', with a large loop at the end.

## List of Publications

- C. O’Riordan, **S. J. Fabbri**, and A. D. Ellis. "Dual dual parallel Mach-Zehnder modulator as a variable multicarrier source." In Photonics Ireland, (2011).
- C. O’Riordan, **S. J. Fabbri**, and A. D. Ellis. "Variable optical frequency comb source using a dual parallel Mach-Zehnder modulator." In International Conference on Transparent Optical Networks (ICTON), (2011).
- P. Frascella, A. Cleitus, **S. J. Fabbri**, F. C. Garcia Gunning, P. Gunning, W. McAuliffe, D. Cassidy, and A. D. Ellis. "Impact of Raman amplification on a 2-Tb/s coherent WDM system." *Photonics Technology Letters*, vol. 23, no. 14, (2011).
- F. C. Garcia Gunning, P. Frascella, A. Cleitus, **S. J. Fabbri**, D. Rafique, S. Sygletos, P. Gunning et al. "All-optical OFDM and distributed Raman amplification: Challenges to enable high capacities and extend reach." In International Conference on Transparent Optical Networks (ICTON), (2012).
- **S. J. Fabbri**, S. Sygletos, and A. D. Ellis. "Multi-harmonic optical comb generation." In European Conference on Optical Communication (ECOC), (2012).
- **S. J. Fabbri**, C. O’Riordan, S. Sygletos, and A. D. Ellis. "Active stabilisation of single drive dual-parallel Mach-Zehnder modulator for single sideband signal generation." *Electronics letters*, vol. 49, no. 2, (2013).
- I. Phillips, M. Tan, M. F. Stephens, M. McCarthy, E. Giacomidis, S. Sygletos, P. Rosa, **S. J. Fabbri** et al. "Exceeding the nonlinear-Shannon limit using Raman laser based amplification and optical phase conjugation." In Optical Fiber Communication Conference (OFC), (2014).
- S. Sygletos, **S. J. Fabbri**, E. Giacomidis, M. Sorokina, D. Marom, M. F. C. Stephens, D. Klondis, I. Tomkos, and A. D. Ellis. "A novel architecture for all-optical add-drop multiplexing of OFDM signals". In European Conference on Optical Communication (ECOC), (2014).

- Klonidis, D., S. Sygletos, D. M. Marom, **S. J. Fabbri**, A. Ellis, E. Pincemin, C. Betoule et al. "Enabling transparent technologies for the development of highly granular flexible optical cross-connects." In International Conference on Transparent Optical Networks (ICTON), (2014).
- S. Sugavanam, **S. J. Fabbri**, S. T. Le, S. I. Kablukov, I. Lobach, S. Khorev, and D. V. Churkin. "Real-time heterodyned measurements of spatio-frequency dynamics in fibre lasers." In Nonlinear Photonics, NTu4A-4, (2014).
- **S. J. Fabbri**, S. Sygletos, E. Pincemin, K. Sugden, and A. D. Ellis. "First experimental demonstration of terabit interferometric drop, add and extract multiplexer." In European Conference on Optical Communication (ECOC), (2014).
- Sygletos, S., M. E. McCarthy, **S. J. Fabbri**, M. Sorokina, M. F. C. Stephens, I. D. Phillips, E. Giacomidis et al. "Multichannel regeneration of dual quadrature signals." In 2014 The European Conference on Optical Communication (ECOC), (2014).
- M. McCarthy, **S. J. Fabbri**, and A. Ellis. "Signal Processing Using Opto-Electronic Devices." In All-Optical Signal Processing, Springer International Publishing, (2015).
- S., Sygletos, **S. J. Fabbri**, M. Sorokina, and A. D. Ellis. "All-optical add-drop multiplexing of OFDM signals." Signal Processing in Photonic Communications, (2015).
- S. Sygletos, **S. J. Fabbri**, E. Giacomidis, M. Sorokina, D. M. Marom, M. F. C. Stephens, D. Klondis, I. Tomkos, and A. D. Ellis. "Numerical investigation of all-optical add-drop multiplexing for spectrally overlapping OFDM signals." Optics Express vol. 23, no. 5, (2015).
- **S. J. Fabbri**, S. Sygletos, A. Perentos, E. Pincemin, K. Sugden, and A. D. Ellis. "Experimental implementation of an all-optical interferometric drop, add, and extract multiplexer for superchannels." Journal of Lightwave Technology, vol. 33, no. 7 (2015).

- S. Sugavanam, **S. J. Fabbri**, S. T. Le, I. Lobach, S. I. Kablukov, S. Khorev, and D. V. Churkin. "Real-time heterodyne-based measurements of fiber laser spectral dynamics." In CLEO: Science and Innovations, JTh2A-50, (2015).
- S. Stylianios, **S. J. Fabbri**, F. Ferreira, M. Sorokina, A. Perentos, and A. D. Ellis. "All-optical add-drop multiplexer for OFDM signals." In International Conference on Transparent Optical Networks (ICTON), (2015).
- **S. J. Fabbri**, S. Sygletos, A. Perentos, E. Pincemin, K. Sugden, and A. D. Ellis. "Experimental demonstration of an all-optical interferometric drop, add, and extract multiplexer for OFDM super-channel." In Summer Topicals Meeting Series (SUM), IEEE, (2015).
- A. D. Ellis, I. D. Phillips, M. Tan, M. F. C. Stephens, M. E. McCarthy, M. A. Z. Al Kahteeb, M. A. Iqbal, **S. J. Fabbri** et al. "Enhanced superchannel transmission using phase conjugation." In European Conference on Optical Communication (ECOC), (2015).
- S. Sugavanam, **S. J. Fabbri**, S. T. Le, I. Lobach, S. Kablukov, S. Khorev, and D. Churkin. "Real-time high-resolution heterodyne-based measurements of spectral dynamics in fibre lasers." Scientific reports, vol. 6, (2016).
- A. D. Ellis, M. Tan, M. A. Iqbal, M. A. Z. Al-Khateeb, V. Gordienko, G. Saavedra Mondaca, **S. J. Fabbri** et al. "4 Tb/s Transmission Reach Enhancement Using 10x 400 Gb/s Super-Channels and Polarization Insensitive Dual Band Optical Phase Conjugation." Journal of Lightwave Technology, vol. 34, no. 8, (2016).



## Acronyms

<b>ADC</b>	Analog to Digital Converter
<b>ASE</b>	Amplified Spontaneous Emission
<b>ASK</b>	Amplitude Shift Keying
<b>AO-OFDM</b>	All-Optical Orthogonal Frequency Division Multiplexing
<b>BER</b>	Bit Error Rate
<b>BPSK</b>	Binary Phase Shift Keying
<b>CW</b>	Continuous Wave
<b>DAC</b>	Digital to Analog Converter
<b>DLI</b>	Delay Line Interferometer
<b>DP-MZM</b>	Dual-Parallel Mach-Zehnder Modulator
<b>DSP</b>	Digital Signal Processing
<b>EDFA</b>	Erbium Doped Fiber Amplifier
<b>ER</b>	Extinction Ratio
<b>EVM</b>	Error Vector Magnitude
<b>FEC</b>	Forward Error Correction
<b>FFT</b>	Fast Fourier Transform
<b>FSR</b>	Free Spectral Range
<b>FWHM</b>	Full Width at Half Maximum
<b>FWM</b>	Four Wave Mixing
<b>HNLF</b>	Highly Non-Linear Fiber
<b>IQ Modulator</b>	Dual-Parallel Mach-Zehnder Modulator
<b>LO</b>	Local Oscillator
<b>MZI</b>	Mach-Zehnder Interferometer
<b>MZM</b>	Mach-Zehnder Modulator
<b>NRZ</b>	Non Return to Zero

**OFC** Optical Frequency Comb  
**OFDM** Orthogonal Frequency Division Multiplexing  
**OSA** Optical Spectrum Analyzer  
**OSNR** Optical Signal to Noise Ratio  
**PZT** Piezoelectric Module  
**QAM** Quadratic Amplitude Modulation  
**QPSK** Quadrature Phase Shift Keying  
**RF** Radio Frequency  
**RZ** Return to Zero  
**ROADM** Reconfigurable Optical Add Drop Multiplexer  
**SMSR** Side-Mode Suppression Ratio  
**SOA** Semiconductor Optical Amplifier  
**SRD** Step Recovery Diode  
**TIDE** Terabit Interferometric add, Drop, and Extract  
**WDM** Wavelength Division Multiplexing  
**WSS** Wavelength Selective Switch

Je dédicace ce manuscrit à ma compagne Kerstin, à ma famille et mes amis.



## **Acknowledgements**

First, I would like to thank my supervisor Professor Andrew Ellis for giving me the opportunity to work under his supervision in two world class research institutes. I highly appreciated his advice and shared experiences both inside the lab and outside.

I would also like to thank Professor Frank Peters for acting as my academic supervisor.

I would like to thank Dr Stylianos Sygletos for his discussion, advices, and strong support during our collaboration,

My special thanks goes to all my colleagues from the Tyndall National Institute and from the Aston Institute of Photonic Technologies for the nice research environment I experienced. I would like to thank particularly Dr Colm O’Riordan, Dr John O’Dowd, Dr Fatima Gunning, Dr Thavamaran Kanesan, Dr Mary McCarthy, Dr Ian Phillips, and Dr Paul Harper for their support and their contribution to the lab.

## Abstract

The continuous growth of the network capacity demand drives the development of the optical fiber networks. Since optical super-channels carrying multi-Terabit/s transmissions are the next evolution of the optical links, future transmitters and receivers systems will be required to handle vast volume of information while maintaining reasonable power consumption and cost. In addition, when point to point links are approaching the fundamental limit of standard fiber, the efficient use of the entire transmission window for optical networks will only be achieved through flexible super-channels compatible with flexible optical nodes.

This thesis describes the research work carried out to investigate the future optical systems that will support the Terabit era networks. All-optical systems are presented, allowing for high spectral efficiency in future networks, from the comb sources to the optical nodes. The following manuscript firstly reports on the development of optical combs based on external modulators to provide transmitters with a large number of optical carriers. Then, the implementation of an experimental all-optical super-channel through the use of optical signals and wavelength manipulations is described. Finally, a novel all-optical node called Terabit Interferometric add, Drop, and Extract (TIDE) is presented. With a management of the super-channel components in the optical domain, the optical node offers transparency and flexibility while maintaining the high spectral efficiency of the super-channel carrying links.

An optical frequency comb source was developed, generating a high quality 9 line comb with a spectral flatness  $< 0.3$  dB and side-mode suppression ratio  $> 20$  dB. A single Mach-Zehnder modulator was driven with a low power multi-harmonic electrical signal. Furthermore, a large 36 line comb was obtained by the addition of a two cascaded modulators comb source driven with a 90 GHz signal. The implementation of an all-optical Orthogonal Frequency Division Multiplexing (OFDM) super-channel, using a high quality single sideband modulation scheme based on a dual-parallel Mach-Zehnder modulator, allowed for the development and test of the all-optical TIDE node. The interferometer based structure was capable of managing (add, drop, and extract) channel from a super-channel strictly in the optical domain. In this manuscript, we prove that it is possible to extract channels even with overlapping spectrum super-channel aggregation for both single and dual quadrature modulation formats.



# Chapter 1

## Introduction

### 1.1 Background

Less than one century ago, humanity entered into an era, now dubbed the Information Age, where seemingly infinite quantities of knowledge, data, and discussion can be exchanged in an instant without limitation of geographic location. Once supported by copper wires and wireless communications, the gargantuan flow of information is nowadays mainly transferred through optical fibers [1,2]. The continuous growth of network capacity has been made possible with the implementation of Wavelength Division Multiplexing (WDM) systems [3] and the development of reconfigurable optical filters offering the option to select, direct and remove particular wavelengths without affecting the rest of the signal transported on the link [4,5]. By bringing optical channels closer and closer, single optical fibers have been demonstrated to be able to carry tens of terabits of data per second in point to point links [6] and terabit/s systems are commonly deployed by operators. In addition, the development of high-speed electronics opened the way for higher modulation formats such as QPSK and m-QAM [7]. As the number of channels rapidly increased, multi-wavelength light source systems, called Optical Frequency Comb (OFC) sources [8–10], have been developed to reduce the inventory and power consumption required for large numbers of lasers, along with the number of wavelength locking and stabilisation circuitry. Then, the use of multi-wavelength sources paved the way for super-channels carrying ultra dense WDM as the comb sources fixed the frequency difference between adjacent channels. The rise of different types of super-channel types, from Nyquist WDM to Orthogonal Frequency Division Multiplex-

ing (OFDM), requires Reconfigurable Optical Add Drop Multiplexer (ROADM) technologies compatible with the difficult spectral manipulation of overlapping channel spectra in the case of OFDM or highly rectangular spectra in the case of Nyquist WDM. Furthermore, as the Erbium Doped Fiber Amplifiers [11] have shown for optical links, flexible all optical nodes [12] are needed to release the optical link's potential with the benefit of reducing the latency [13], the power consumption [14], and the cost [15] by maintaining the difficult to upgrade high-speed electronics at the edge of the network.

This thesis reports the investigations towards future flexible all optical networks with the development of optical comb sources, all optical super-channel systems, and finally all optical nodes compatible with the most challenging channel aggregation type.

## 1.2 Motivation

The work reported in this thesis was motivated by the need to develop optical systems capable of providing the future network capacity growth. The work was focused on three points:

- Develop novel comb sources that offer large numbers of carriers for super-channel generation using standard external modulator devices.
- Implement an experimental optical super-channel transmitter as a test bed for future transmission, modulation format exploration and networking experiments
- Implement an all-optical node for future optical super-channel routing in high capacity networks

Fig.1.1 illustrates an optical node or ROADM with a set of channels passing through, of which one is extracted i.e. removed from the link to be received or transferred and a new one is added at the freed spectral position. Because of the high channel density, the optical channel selection is incomplete and so crosstalk from adjacent channels degrades the channel dropped and the channel added. This figure hence illustrates the problem this work is considering with on one hand a demand for a higher number of channels and rising spectral efficiency, and on the other hand the capability to manage each individual channel transiting on the network to reach an optimum use.

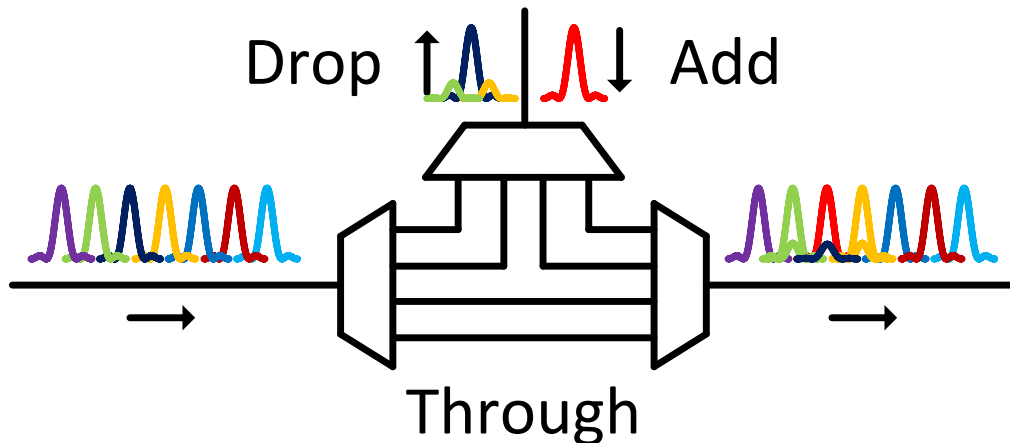


Figure 1.1: Concept of ROADM for ultra dense WDM links

### 1.3 Organization of the manuscript

The thesis is organized in three parts:

- The first part is centered on optical frequency comb generation using electro-optic modulators, in different configurations from single Mach-Zehnder modulators (MZM) driven by a single frequency microwave signal to cascaded modulators driven by multi-harmonic signals. This section presents the first demonstration of a high quality 9 line comb source based on a single MZM, and the extension to a flat 36 line comb using a hybrid source [10].
- The second part is centered on the implementation of an experimental All-Optical Orthogonal Frequency Division Multiplexing (AO-OFDM) carrying single and dual quadrature modulation format. The transmitter is based on an odd/even structure supported by a dual-parallel Mach-Zehnder modulator based frequency shifter. A full characterization of the signal translation using the modulator was performed and reported [16]. In addition, a super-channel transmitter stabilisation circuit is described.
- The last part introduces the Terabit Interferometric Drop, Add, and Extract (TIDE) multiplexer. A novel architecture for optical reconfigurable add, drop multiplexer is described [17]. Preliminary simulations are shown before the first experimental implementation of an All-Optical node [18,19]. Each function of the optical ROADM is described and experimentally im-

plemented. Finally, the node is used to replace one channel from an AO-OFDM super-channel [20]. In this chapter, the first real-time implementation of an optical node capable of managing super-channels formed of spectrally over-lapping channels is presented [21, 22].

It is to be noted that many devices used in this work, as well as the optical medium linear and non-linear effects, are thoroughly described and explained in the literature, such as Agrawal *Nonlinear Fiber Optics* [23] and *Fiber Optic Communication System* [24], Hui and O'Sullivan *Fiber Optic Measurement Techniques* [25], Gnauck *Optical phase-shift-keyed transmission* [26], or Essiambre *Capacity limits of optical fiber networks* [7]. Description will only be extended when relevant to the understanding of the experiments reported.

## Chapter 2

# Optical Comb Generators based on an external modulator

We have seen in the previous chapter the trends toward the generation of super-channel carriers using optical comb sources in order to reduce the quantity of laser sources and stabilization systems associated with the transponder in addition to maintaining an exact frequency spacing between sub-channels.

Of particular importance is the potential role of an optical comb in the development of transmitter units for advanced multi-carrier signal formats, i.e. Orthogonal Frequency Division Multiplexed signals (OFDM), considered for next generation optical networks. In this context, it is important to take into account the potential integration of the comb generator component in order to obtain cost effective and compact transmitters [27,28].

In this chapter, we investigate comb sources based on external modulators as a system delivering a high quality optical comb. In the first part of this chapter, optical sideband generation is described for a standard balanced MZM. The second part of this chapter is focused on the development of a multi-harmonic comb generator as a source of an excellent quality comb. The third section presents the extension of those results towards the generation of large numbers of subcarriers as required for a high capacity super-channel.



## 2.1 Single frequency driven external modulator

Future transmitters are expected to be used with multi-wavelength sources with requirements such as equally distributed power between carriers, stable phase relation between adjacent carriers and controlled frequency spacing. The external Mach-Zehnder modulators have very attractive features such as a bias control coupled with a periodic transfer function allowing the control of the optical comb generated spectral shape. They also offer flexibility in the control of the line frequency spacing, the independence in the choice of the central wavelength, as well as the potential for integration [29]. The spectral flatness defines the homogenous power distribution between each subcarrier: an important indicator as it dictates the need for a power flattening filter in the transmitter. Similarly, the Side Mode Suppression Ratio (SMSR) must be taken into account for the design of the system to avoid the need to insert an optical bandpass filter after the comb source to reduce the crosstalk with adjacent super-channels in the case of dense flexible networking. The design of an optical transmitter is a place of numerous trade-off in terms of capacity, power consumption, price, or footprint to cite a few. Optical comb sources are trading the flexibility of a bank of laser for a smaller footprint, a smaller inventory, and a stable frequency spacing between comb lines per example. Small flatness and high value of SMSR can reduce the requirement on pre-transmission filter that would equalize the different channels to maintain similar performance over long distance and reject the unwanted sideband so adjacent super-channels in the optical link are unaffected. While flatness requirement is depending on the transmission, SMSR greater than 20 dB can be considered a goal for a dense link with a ratio of the optical power between the unwanted channel and the data carrying channels lower than 1%. Furthermore, greater SMSR can optimize the gain capacity of the link optical amplifiers by limiting the residual components and hence the overall link OSNR budget. Similarly, the system design determines the amount of insertion loss or OSNR degradation tolerated, and consequently the type of comb source and the presence of EDFAs.

A Mach-Zehnder modulator driven by a sine wave signal creates symmetrical sidebands on both sides of the optical carrier entering the device as demonstrated below [30]. Let  $v(t)$  be a sinusoidal voltage applied to the modulator and defined by  $\epsilon$  as the bias voltage normalized to the voltage required to shift the optical phase by  $\pi$  [31],  $\alpha$  as the similarly normalized amplitude, and  $\omega$  the

signal frequency:

$$v(t) = V_\pi(1 + \epsilon) + \alpha V_\pi \cos(\omega t) \quad (2.1)$$

then the field at the output of the intensity modulator is described as:

$$E(t) = \cos\left(\left(\frac{\pi}{2}\right)\left((1 + \epsilon) + \alpha \cos(\omega t)\right)\right) \cos(2\pi\nu_0 t) \quad (2.2)$$

where  $\nu_0$  is the optical carrier frequency.

In order to underline the sideband generation, equation 2.2 can be approximated as a finite series of Bessel functions (or an infinite series for an exact approximation [32, 33]) and for the first three pairs of sidebands presented as :

$$\begin{aligned} E(t) = & \frac{1}{2} J_0\left(\alpha \frac{\pi}{2}\right) \cos\left(\frac{\pi}{2}(1 + \epsilon)\right) \cos(2\pi\nu_0 t) \\ & - J_1\left(\alpha \frac{\pi}{2}\right) \sin\left(\frac{\pi}{2}(1 + \epsilon)\right) \cos(2\pi\nu_0 t \pm \omega t) \\ & - J_2\left(\alpha \frac{\pi}{2}\right) \cos\left(\frac{\pi}{2}(1 + \epsilon)\right) \cos(2\pi\nu_0 t \pm 2\omega t) \\ & + J_3\left(\alpha \frac{\pi}{2}\right) \sin\left(\frac{\pi}{2}(1 + \epsilon)\right) \cos(2\pi\nu_0 t \pm 3\omega t) + \dots \end{aligned} \quad (2.3)$$

The new sidebands can be clearly observed from the components of equation 2.3 with a rigorous frequency spacing equal to integers of the driving signal frequency and where the amplitude of the sideband is determined by the driving voltage through the Bessel function and the bias voltage through the first trigonometric function of each term. With appropriate biasing, sidebands are generated symmetrically on both sides of the modulated carrier, given by the  $\pm$  symbols in equation 2.3.

While phase modulators are also capable of generating optical combs [34, 35], the lack of bias control make it impossible to obtain more than three comb lines with a flatness lower than 6 dB. For example using a phase modulator, the only degree of freedom available to control the comb shape is the normalized amplitude  $\alpha$  so a single equation can be resolved such as :

$$J_0\left(\alpha \frac{\pi}{2}\right) \cos(2\pi\nu_0 t) = J_1\left(\alpha \frac{\pi}{2}\right) \cos(2\pi\nu_0 t \pm \omega t) \quad (2.4)$$

When using MZMs, the additional control given by the bias voltage controlling the optical path difference in the interferometric structure allows, from equation 2.3, for a rectangular spectrum consisting up to five lines. Consequently, by controlling the drive signal power and the bias voltage, it is possible to tailor

the optical comb produced. In the MZM case, the amplitude  $\alpha$  is used to power align the central component and the second order components, then the second degree of freedom provided by the voltage bias  $\epsilon$  is used to control a second group of lines, here the first order components to equalized the comb lines. Since there is no solution for  $J_0(x) = J_1(x) = J_2(x) = J_3(x)$ , flat optical comb larger than 5 lines requires supplementary degrees of freedom in the form of additional devices for example.

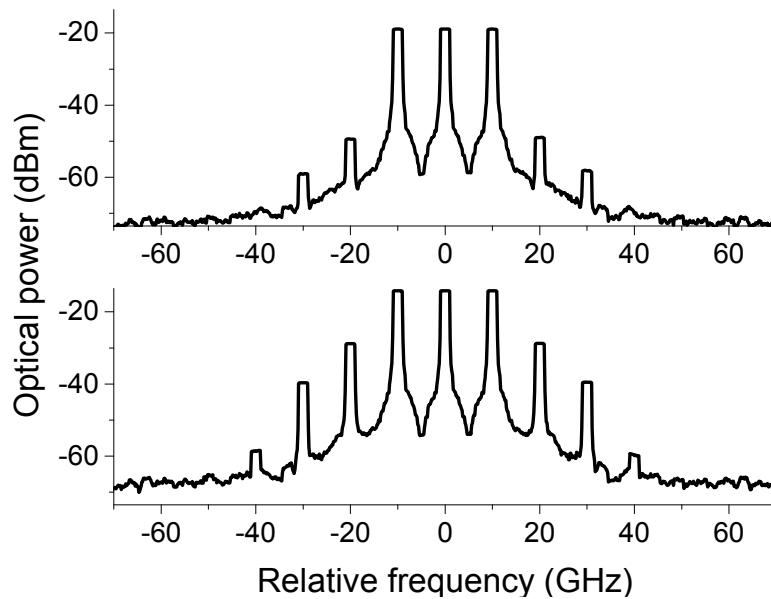


Figure 2.1: Three line comb generation simulation for a single MZM driven with 10 GHz signal for different driving amplitude. Top:  $V_{RF} = 0.3V_{\pi}$  and bottom  $V_{RF} = 0.7V_{\pi}$ . Simulated resolution: 2 GHz, rectangular

Figure 2.1 is the result of simulations using VPI Transmission Maker where a continuous signal was modulated by a 10 GHz signal through the transfer function of a standard MZM. The optical spectrum analyzer is emulated with a 2 GHz rectangular resolution. The modulator was set to have 6 dB insertion loss and an extinction ratio of 35 dB with the applied voltage normalized to the  $V_{\pi}$  for both the RF signal and the DC signal. The top spectrum of figure 2.1 is the output of the MZM when driven with  $V_{RF} = 0.3V_{\pi}$  and the bottom spectrum was observed for  $V_{RF} = 0.7V_{\pi}$ . It is interesting to observe the evolution of the spectrum when a higher driving signal is applied to the modulator as stronger sidebands are generated, broadening the comb spectrum. The lower power comb matches the high quality criteria defined previously as the flatness and SMSR gives a rectangular shape. However, in order to achieve equal power with a lower amplitude signal, the modulator needs to be biased closer to the null point of the device

transfer function to strongly attenuate the central carrier in order to match the first order sidebands power.

As the driving signal is further increased in amplitude, a five line comb is generated as the broadest flat comb obtainable using a single MZM. The generation of the 5 line comb can be understood from equation 2.3, where the bias voltage  $\epsilon$  is clearly affecting every second sideband alternatively and the RF signal is controlling the strength of the sidebands. The single driving signal-bias combination is consequently obtained when the optical power of the carrier and the pair of second sidebands are equal and the bias is then tuned to align the pair of first sidebands to observe a perfectly flat spectrum. Figure 2.2 illustrates the result of this configuration with the simulation result at the top and the experimental result at the bottom. The experiment was performed using a Fujitsu LiNbO<sub>3</sub> based modulator. The experimental comb obtained was characterized by a spectral flatness of 0.53 dB and a side-mode suppression ratio (SMSR) close to 15 dB similar to the simulation that demonstrated 0.1 dB flatness and 14.9 dB SMSR.

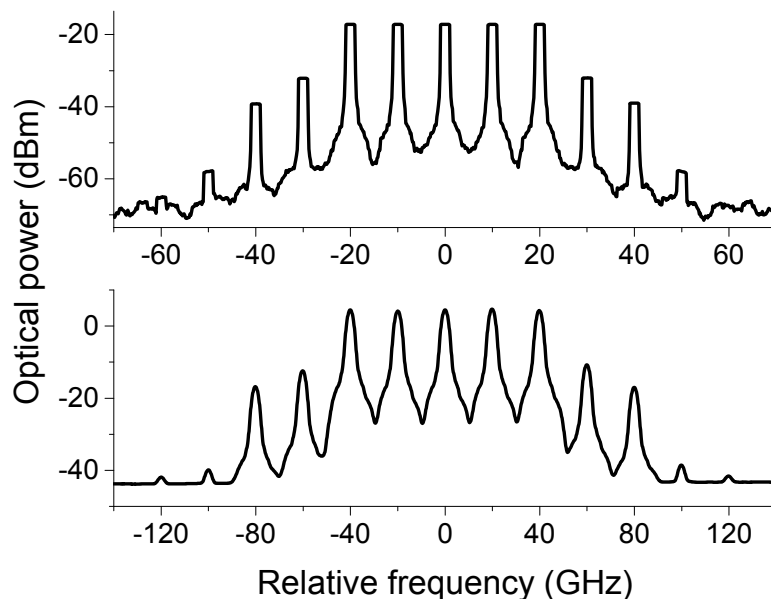


Figure 2.2: Five line comb generation simulation (top) and experimental (bottom) for a single MZM driven with 10 GHz and 20 GHz signal respectively

While we have shown that single MZMs are good devices to generate a high quality wide comb, it is common practice to extend the spectral width of the comb generator by adding modulators in parallel [36–38] and/or in series [8, 39]. The use of additional devices is a source of limitations towards their implementation in telecom systems such as additional insertion losses, system com-

plexity, and larger footprint. It however allows the drive power to be spread over multiple devices to increase the total power tolerance [40] and offer additional degrees of freedom to tailor the resulting comb.

In this section, we investigated the simplest comb source consisting of a single amplitude modulator capable of generating a multi-wavelength signal with constant phase relation and frequency locked subcarriers, equal power for each of the channels and good differentiation between the comb and the unwanted sidebands surrounding the comb.

## 2.2 Multi-harmonic comb source

### 2.2.1 Concept

While standard techniques using external optical modulators drive the devices with high RF power to generate optical comb lines, the work reported in this section was focused on decreasing the complexity and power consumption of such systems. When looking at the sideband generation from a MZM, the power required to generate additional spectral components increases rapidly and often requires extra devices due to the input power tolerance and the damage threshold of the modulators.

As wider combs are needed, the required electrical power per sideband generated increases. Another way to generate multiple carrier combs is to drive the optical modulator with a series of signals with different frequencies [10,41–45]. Similar to previously described comb sources, a laser is used as a light source, which is then injected into a MZM before being detected using an OSA for the optical part, and an RF signal, originated from a local oscillator, is used to drive the modulator. The main difference is that the RF signal is manipulated through frequency multiplication, power splitting, and amplification to obtain a set of RF harmonics.

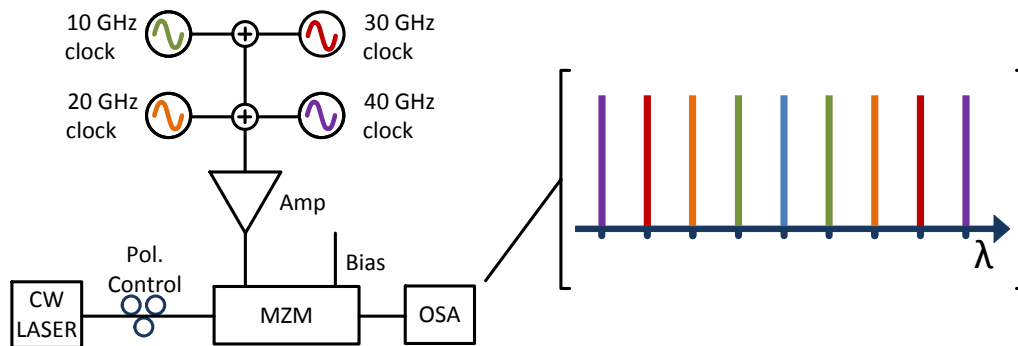


Figure 2.3: Multi-harmonic comb generation concept. On the left side: schematic of a Mach-Zehnder modulator driven by an RF signal obtained by the sum of four independent clock sources. On the right: Corresponding optical spectrum at the output of the comb source centered on the laser wavelength, sideband colors matching the driving signal RF component colors. For example, the sidebands colored in orange are due to the 20 GHz signal injected to the optical modulator

Figure 2.3 presents the ideas of the multi-harmonic comb generation where in-

stead of applying a strong RF signal to the modulator, an electrical comb drives the modulator at a fraction of the standard comb source power. Similar to the three line comb shown previously in figure 2.1 in which a high quality comb was obtained, each pair of sidebands is directly generated by the related RF harmonic. The DC bias voltage predominantly controls the level of the central carrier. In this scheme, the studies were aiming towards a power efficient rectangular shaped optical comb so that the amplitude of the driving signal was constrained to a power level for which each electrical harmonic would generate a 3 line comb if used independently. The low power mode used to generate the multi-harmonic comb allows for high flexibility in the number of subcarriers since the addition of RF harmonic would create only the corresponding sideband, per example if additional carriers are required by the network manager. It is to be noted that the use of high power driving signals to generate additional comb lines where the drive signal comprises such a flat electrical comb resulted in an unequal power distribution over the comb because of the highly complex relationship between the sidebands generated by each RF harmonic.

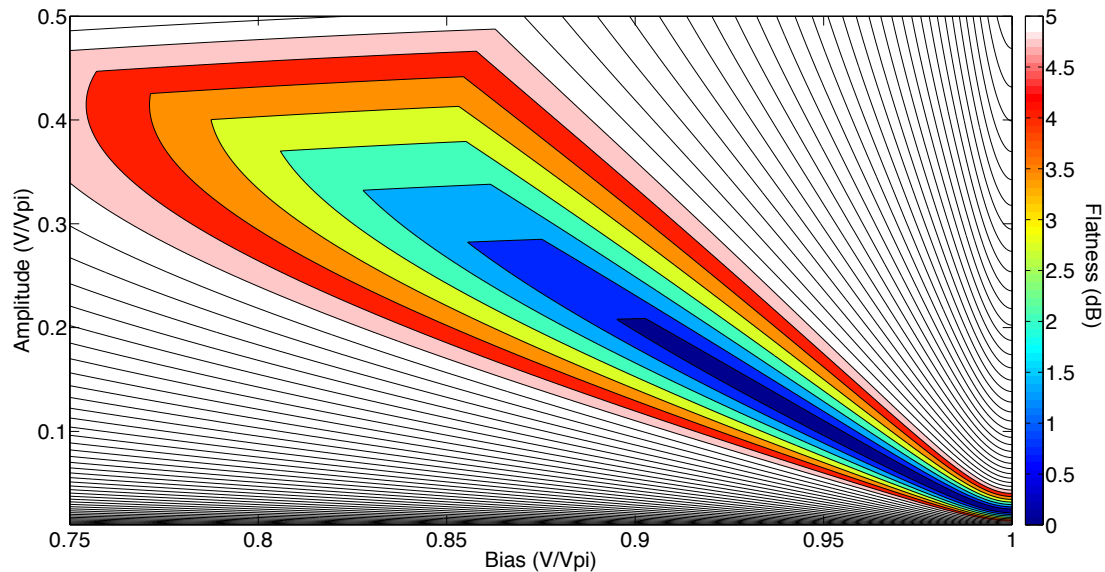


Figure 2.4: Flatness in dB of simulated 9 line comb driven by 4 harmonics of equal power for different combination of bias voltage and driving voltage

Similar to the 3 line comb generator, the trade-off between comb quality and output optical power is present in the multi-harmonic comb scheme. Figure 2.4 is the result of the Matlab simulation where the flatness of a 9 line comb generated through a modulator driven by 4 RF harmonic, of equal power, was determined as a function of the modulator bias voltage and the driver amplitude. The lower right corner corresponds to the modulator being biased at null and

little RF power is needed to match the sideband power to the carrier level. As the driving power increases, more light is allowed through the device and so the bias is moving away from the minimum transmission point. Because of the increase of electrical power, combs generated by each harmonic are broadened and this causes interference between different tributaries to occur at each sideband with the consequence that the flatness degrades. Hence a trade off occurs, depending on the system design, between the comb flatness that is optimum for low RF amplitude and the lower insertion loss that is depending on the bias voltage. In an ideal system, the multi-harmonic comb generator offers many control points, as there are independent power and phase controls on each of the RF tributaries. The amplitude control becomes useful for medium power driving the modulator where the impact from the interference is of few dB whereas the phase control is mandatory for high driving voltage since the interference at each sideband is strong between the tributaries.

In this section, the concept of the multi-harmonic comb generation is presented where an electrical comb is driving a optical frequency converter to generate high quality optical combs for optical communications. A first implementation is presented in the following subsections and we will discuss the different types of electrical comb sources studied.

### 2.2.2 Step Recovery Diode based multi-harmonic comb source

In the concept presented previously, the RF components used to drive the optical modulator are presented as independent sources and fully controlled. In order to reduce the inherent complexity of numerous electrical oscillators, here the electrical comb source was generated from a single microwave clock source using a step recovery diode (SRD) before driving an optical modulator. A step recovery diode is a semiconductor junction diode that has a special doping profile such that it shows significant conduction when reversed biased. Like a normal pn-diode, the SRD conducts when forward biased but continues for a short time as stored charge is removed in the reverse cut-off region [46]. The fast transition in the current characterizes the SRD and is the source of a narrow pulse train in the time domain and a richer spectrum in the frequency domain. It is commonly used as an electronic multiplier, comb generator and pulse sharpener. In this experiment, a non-standard frequency SRD [47] driven by a well power controlled



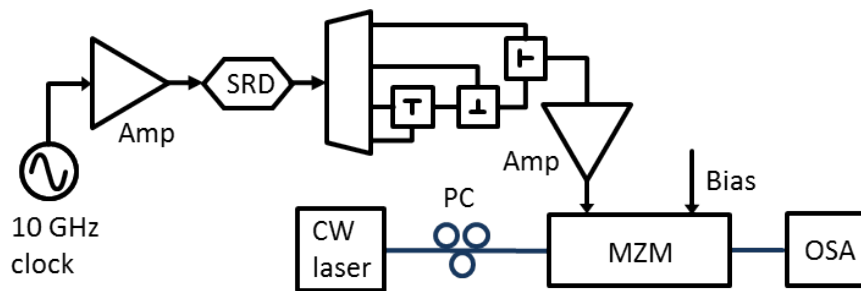


Figure 2.5: Schematic of the comb generator based on a SRD electrical harmonic source. Triangle: electrical amplifier, trapezoid: frequency interleaver, square: RF power divider

10 GHz signal from a clock source generated harmonics equally spaced by 10 GHz. Because of the bandwidth limitation of the RF spectrum analyzer, cables, modulator, and amplifier, the first three harmonics obtained were studied and manipulated. The electrical system displayed in figure 2.5 was set such that the original clock signal was amplified up to 27 dBm, the maximum power tolerated by the SRD. The output signal was made up of a set of 10, 20, 30, and 40 GHz components, with a strong power roll-off as the frequency increases.

The electrical comb was then carried through an appropriate high bandwidth cable to the input of an electrical dis-interleaver, which has the function to separate each RF component. By appropriate attenuation and recombination of the different signals using power combiners, the output of the network of RF cables gave a set of equal power RF harmonics. Few dB power adjustment was added during the amplification with the three stage device before applying the electrical comb to the optical modulator.

The electrical power of the RF components has been measured using a 30 Hz to 50 GHz Agilent RF spectrum analyzer, set with a span of a 1 MHz. The different levels are displayed in figure 2.6. The output of SRD when driven with a 27 dBm 10 GHz signal produced the harmonics with decreasing power with frequency. Since the difference of power between components is close to 6 dB, the cascaded structure of power combiners delivered relatively equal power for each component before the driving amplifier. The three stage nature of the amplifier used (a broadband 50 GHz Centellax device) allowed for some frequency response control so the electrical comb at the output of the amplifier is within 2 dB of the target pre-emphasis required to match with the frequency response of the optical modulator, as well as the attenuation consequent of the cable bandwidth. The resulting optical spectrum is presented in figure 2.7 which

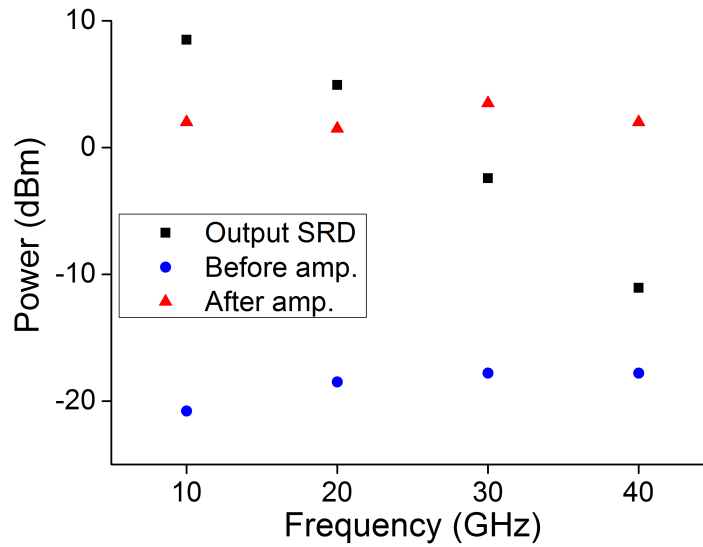


Figure 2.6: RF spectrum from the electrical signal at different point in the electrical comb source circuitry. Before amplifier: input of amplifier with pre-emphasis to compensate for SRD roll-off. After amplifier: output including amplifier bias adjustment. Values for optimized optical comb and stepped back through system

is the spectrum of the experimental implementation of the concept where 4 RF components are applied to a MZM device to generate a high quality optical comb.

The low power from the electrical signal, approximately a third of the modulator  $V_{\pi,RF}$ , generated a high quality optical comb by generating strong first sidebands and weak secondary sidebands for each frequency. Near perfect flatness was consequently observed at 0.3 dB along with an SMSR of 20.4 dB. Higher levels of control could easily be added to the electrical comb source by modifying the RF combination from passive to active system in which each component is allocated an individual electrical amplifier. In this section, the first iteration of the multi-harmonic comb generator is implemented, based on an electrical comb source SRD. However, the use of the SRD required a high power driving signal with a very accurate power control as the diode is highly sensitive and has no tolerance to excessive power. The required performance could only be obtained by driving the SRD within 0.5 dB of the damage threshold.

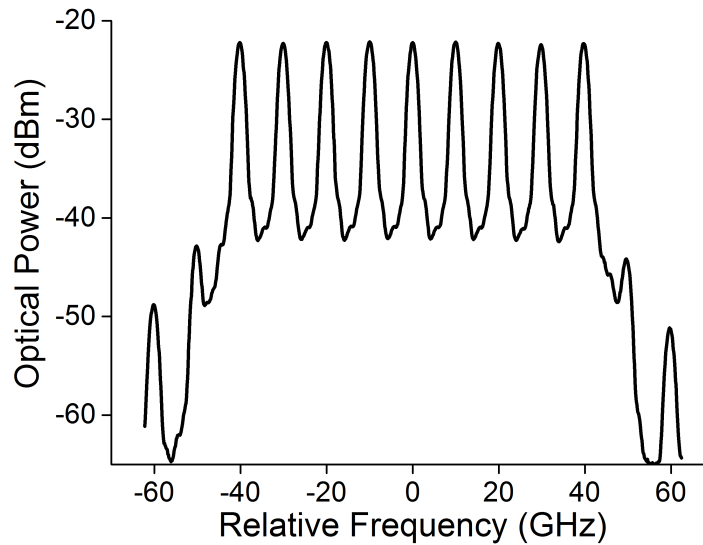


Figure 2.7: Optical spectrum of multi-harmonic comb generated using an SRD as electrical source

### 2.2.3 Up-conversion technique for multi-harmonic comb generation

In this experiment, we implement a different RF system in order to reduce the total supplied power. While the use of an SRD and dis-interleaver electrical comb source is suitable for a large number of lines (2.5GHz spaced comb line over 40GHz per example), the up-conversion technique described here requires less total supplied power. The 10 GHz 4 line electrical comb source was generated from single clock source followed by a frequency multiplier conjointly with a broadband mixer. The 10 GHz RF signal issued from the oscillator was branched into two paths. One part of the signal was frequency multiplied by a factor of three in order to obtain a 30 GHz signal that would then be mixed with the second part of the 10 GHz signal. At the output of the mixer 20 GHz and 40 GHz signals are generated. Passive attenuators and biased mixer were included in order to allow some of the original 10 GHz and 30 GHz to be transferred and to consequently obtain a set of 4 equally spaced frequencies of equal powers.

The schematic in figure 2.8 shows two important components as a frequency multiplier and a broadband mixer. The broadband mixer is performing a non-linear process equivalent to a multiplication of the signals at its two input ports. As result, the output is a signal of frequency equal to the composite of the sum of the two input signal frequencies as well as the their difference. Formally, if  $f_1$

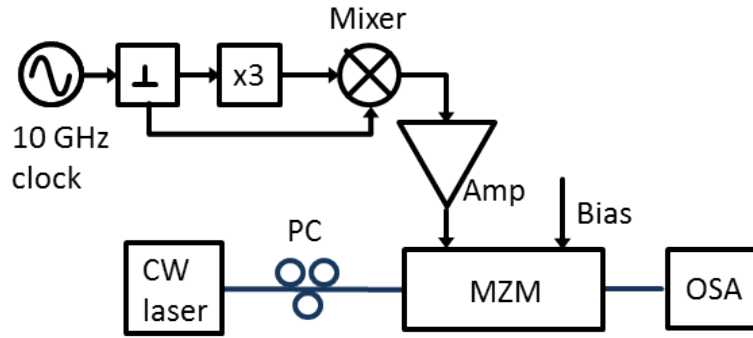


Figure 2.8: Schematic of the comb generator based the up-conversion electrical harmonic source. Inverted T: RF power divider, x3: frequency multiplier

represents the frequencies contained in the signal in port 1 and  $f_2$  representing similarly the frequencies at port 2 then the signal observed at the output is:

$$\cos(f_1 t) * \cos(f_2 t) = \frac{1}{2} * (\cos((f_2 + f_1)t) + \cos((f_2 - f_1)t)) \quad (2.5)$$

As the mixer down or up converts the electrical signals from one carrier frequency to another, the RF comb generation scheme described here is referred as an up-conversion technique to differentiate it from the SRD solution described in section 2.2.2.

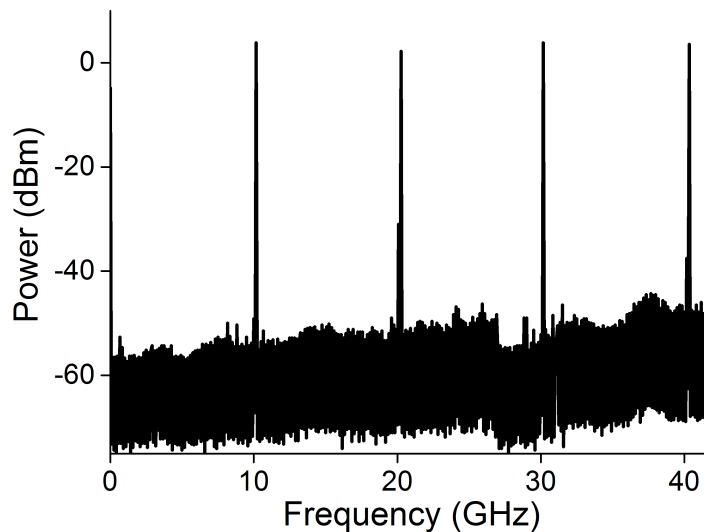


Figure 2.9: RF spectrum from the electrical comb using the up-conversion technique

The electrical power of the signal RF component applied to the modulator was

measured as 3.7, 2.3, 3.8, and 3.2 dBm for the 10, 20, 30, and 40 GHz harmonics respectively. The overall signal applied to the modulator is hence lower than 10 mW whereas standard comb generators either drive the modulator with the highest power tolerated ( $\sim 1$ W) and/or spread the driving power through additional optical devices [39]. Furthermore, the electrical generation of the harmonics is in this case requiring a small amount of power with only two active devices: the frequency multiplier and the three stage electrical amplifier. When compared with standard comb sources, the electrical amplifier trades off a low gain and low output power for a broad bandwidth.

If the power consumption is considered for the electrical part of the optical comb generator, the original clock source was providing a 10 dBm 10 GHz signal, of which a portion was frequency tripled using an active discrete frequency multiplier drawing 0.6 W from the power supply. The three stage electrical amplifier driving the optical modulator required less than 3.4 W from the power supply as a result of the low power needed at the input of the MZM.

The electrical comb was applied to the MZM device and the resulting optical comb is presented in figure 2.10. The generated optical comb showed a spectral flatness of 0.3dB and a SMSR better than 16dB. While the flatness was the same than the previous SRD implementation, the SMSR was a few dB lower due to a higher amplitude drive signal. Lower unwanted sidebands can be obtained by reducing the electrical power at the output of the drive amplifier, as the second order sidebands degrading the SMSR would be of lower intensity.

The up-converter scheme was implemented in order to demonstrate it as a potential source of electrical comb compatible with the multi-harmonic comb generator scheme, it has the advantage of higher power efficiency compared to the SRD technique. In either case, a high quality 9 line comb was generated with excellent flatness and high side mode suppression ratio.

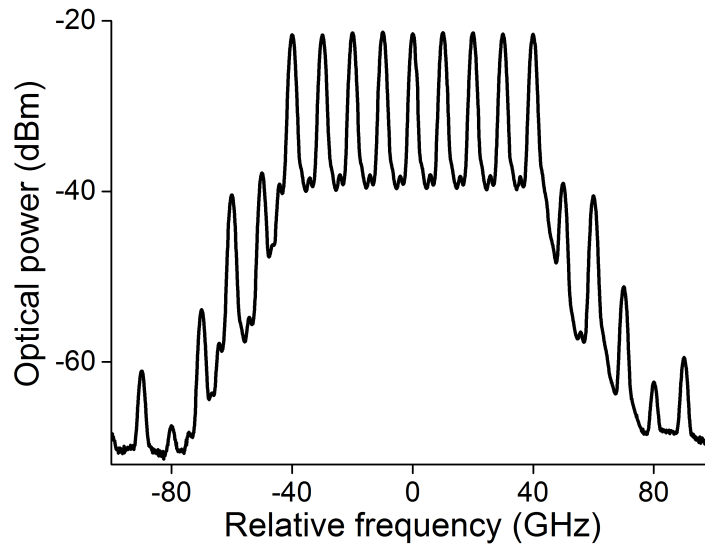


Figure 2.10: Optical spectrum of the optical comb generated using the up-converter multi-harmonic scheme

## 2.3 Hybrid comb generation

While the comb generator described in the previous section would be a capable source for a 400Gb/s transceiver assuming PM-QPSK modulation format ( $9 \times 2 \times 22.3$  Gbit/s), optical network providers are investigating multi terabit/s super-channels. The multi-harmonic technique presented in the previous parts is limited by the electrical bandwidth of the optical modulator, in this section the output of the up-converter comb source is used as a laser source to a second comb generator composed of two polarization modulators in cascade. In this experiment, an optical comb with a narrow frequency spacing was used as an optical input for a large frequency spacing comb source. The first one being the 9 line multi-harmonic comb and the second being a 90 GHz spacing comb obtained from two cascaded MZMs.

A comb source composed of two cascaded modulators each of them driven by 45 GHz signals is capable of generating seven flat comb lines. The two cascaded amplitude modulators had been extensively investigated by Healy et al. [8] when the system had been implemented. A downside of using such widely spaced comb lines is that in order to use a high spectral efficiency format, like OFDM for example, the data channels need to be modulated at a high baud rate for which transmitters are not widely available, in addition to altering the granularity of the network. Using higher numbers of lower speed sub-channels im-

prove the flexibility as well as maintaining total throughput through sub-channel aggregation [48]. The combination of the nine line comb source with the wide comb source offers a high number of sub-channel carriers of high quality. In order to use the 9 line comb as the seed light source for the cascaded modulators, it is easy to see the need for a comb spacing for the second comb generator equal or larger than the bandwidth of the original comb. Consequently, the second comb generator would require a spacing greater than the 90 GHz bandwidth of the multi-harmonic generator. However, such a high microwave frequency is difficult to obtain, amplify, and transmit. The approach presented here entails frequency doubling using an optical modulator by suppressing every second comb line by biasing either at the null or at the peak, so that a 45 GHz driven comb generator provides a 90 GHz spaced optical comb, as depicted in figure 2.11. While the cascaded modulators can provide seven lines separated

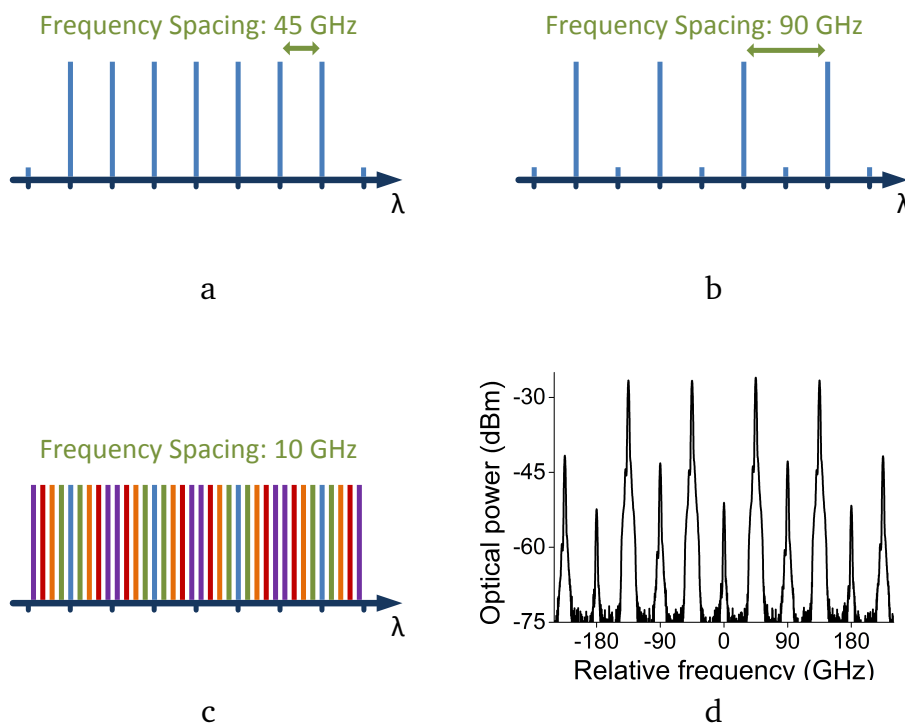


Figure 2.11: Schematic description of the hybrid comb. a) 7 line comb source generated from cascaded optical modulators. b) Suppression of every second line by appropriate biasing of the modulators (at null). c) 36 line comb from the hybrid comb source (Colors represent component associated with RF frequencies from the multi-harmonic comb generator, as presented by Fig.2.3). d) Experimental optical spectrum of the 4 line comb obtained from the cascaded comb source with twice the frequency spacing with the multi-harmonic comb source switched off.

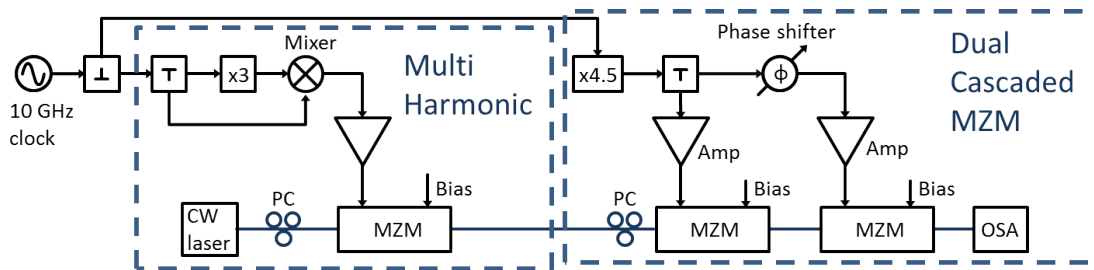


Figure 2.12: Schematic of the hybrid comb generator, with the multi-harmonic comb source as first comb source and two cascaded MZM as comb extension

by 45 GHz, the modulators were biased at null so the even components of the comb were suppressed, as the optical spectrum analyzer shows in figure 2.11d for a CW signal at the input.

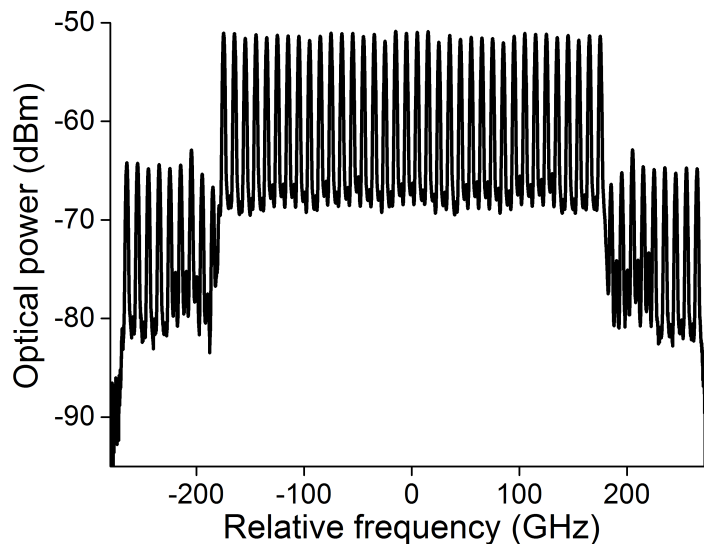


Figure 2.13: Optical spectrum of the 36 line comb generated using the hybrid comb source

The experimental scheme is shown in figure 2.12. The two comb architectures were synchronized by using an active frequency multiplier so that a single 10 GHz clock source was feeding the comb generators and consequently the frequency spacing between comb lines was kept constant. The output of the hybrid comb generator is shown in figure 2.13 with neat rectangular shape. The flatness was measured to be 1.2 dB and the SMSR greater than 10 dB for a 36 line 10 GHz spacing.

Fig.2.14 shows the measurement made using a broadband photodiode connected to a RF spectrum analyzer of the 36 line comb. The four initial harmonics



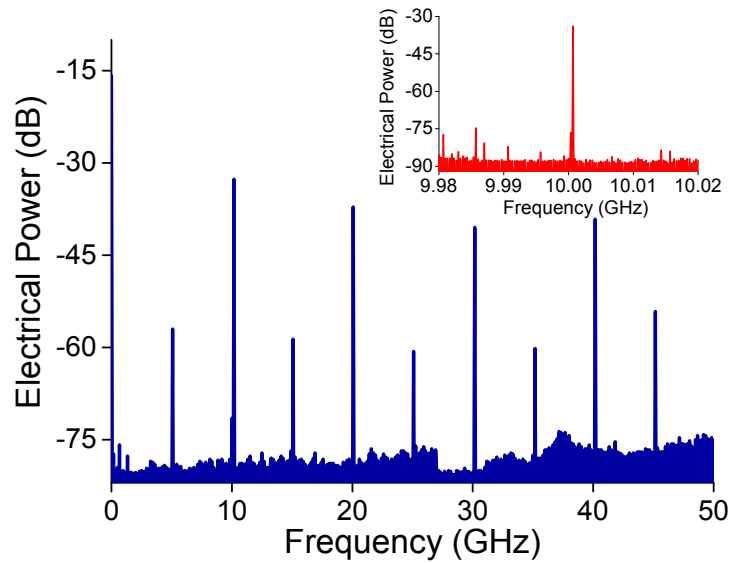


Figure 2.14: Electrical spectra of the 36 line comb output. Resolution bandwidth: 10 kHz (Insert: 1 kHz)

were clearly observable at the frequencies 10, 20, 30, and 40 GHz, confirming the maintained frequency spacing. Additional 5 GHz components were present due to the limited extinction ratio of the unwanted component of the 45 GHz comb. Indeed, from Fig.2.11d, it can be seen that the unwanted side-modes were suppressed by 15 dB. The unwanted 5 GHz components could be removed further by inserting a delay line interferometer of free spectral range (FSR) of 10 GHz or by employing higher extinction ratio MZMs.

By re-biasing at peak the 45 GHz comb modulators, the number of comb lines was extended to 45 through a 5 line frequency doubled comb as presented in figure 2.15. While the 9 additional comb lines had been obtained, poor flatness performance was demonstrated at 6.4 dB whereas the SMSR maintained a good 14.7 dB. The strong roll-off was due to the maximum input power tolerated by the second stage optical modulators ( $<28$  dBm) and the spectrum was acquired for driving voltage at the damage limit given by the manufacturer. An appropriate electrical amplifier and low  $V_{\pi}$  modulator would make possible a larger flat comb as described in [8]. In the case represented by figure 2.15, the cascaded MZM comb source was set to generate a 9 line comb, and with the appropriate biasing at a peak transmission of the modulators, a 5 line comb of 90 GHz frequency spacing was achieved.

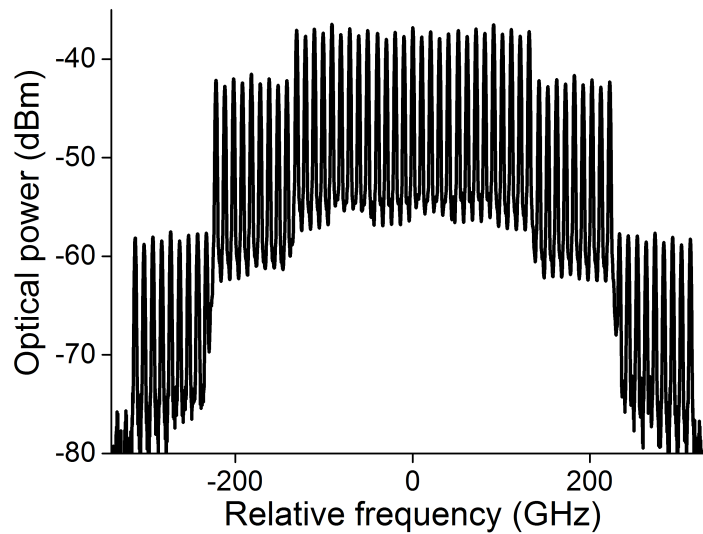


Figure 2.15: Optical spectrum of the 45 line comb generated using the hybrid comb source. First stage composed of the 9 line comb generated by the multi-harmonic comb generator, second stage composed of two cascaded modulators

## 2.4 Chapter summary

In this chapter, the comb generation mechanism for external modulator based sources has been presented, to underline the limit of a single frequency driving signal. A new concept, the multi-harmonic comb generation, was described as well as implemented in different ways in order to obtain a power efficient high quality comb source for future integrated transceivers. Even through the 9 line comb generated using the multi-harmonic source was based on a single drive MZM, SMSR and flatness were found to be higher than experiments reported based on more advanced devices [37, 41, 45, 49–51]. Further investigations were carried out to obtain high quality broad comb sources for multi-Terabit per second transmission and a 36 line comb source was demonstrated [10].

## Chapter 3

# Experimental Implementation of a AO-OFDM Super-channel

In this chapter, we consider the implementation of an experimental All-Optical OFDM transmitter. Firstly, we consider the optical OFDM transmission format and through Matlab simulation identify the limiting parameters. Following the preliminary simulation, the experimental implementation of an odd/even super-channel emulator is reported. The experimental super-channel generated is then studied and a stabilization circuit is added to the transmitter.

### 3.1 All-Optical Orthogonal Frequency Division Multiplexing

Orthogonal Frequency Division Multiplexing (OFDM) is an extension of Wavelength Division Multiplexing (WDM) where with certain conditions a channel is theoretically not affected by the adjacent channels. While in WDM the channels are simply separated by large guard band, in OFDM the spectrum of a channel overlaps with the spectrum of adjacent channels. In the condition that the channel spacing is strictly equal to the symbol-rate, the crosstalk due to adjacent channels is reduced and thus channels can be transmitted in a very spectrally efficient way [52–58]. All-Optical OFDM (AO-OFDM) is the aggregation of single carrier channels with a separation equal to the symbol-rate and a sinc-function matched filter. The attainment of these two conditions is the condition required for orthogonality between adjacent channels and thus crosstalk free transmis-

sion. For non-ideal match filters, the optical carriers generated by optical comb sources are used in order to obtain constant relative phase between adjacent channels.

The Matlab environment was developed in order to gain understanding of the limitations and requirement of AO-OFDM. The program was simulating eight channels single polarization AO-OFDM modulated with BPSK at a rate of 10 Gb/s. Eight independent  $2^{14}$  bit long patterns generated by a random function were up-sampled by a factor 32. A coherent receiver was emulated, limited by a Gaussian filter with a bandwidth equal to twice the baud rate representing the electrical bandwidth of the photodiodes and electronics. The received signal was retimed and phase compensated using standard algorithms [59]. Noise loading with additive white gaussian noise was obtained by modifying the noise spectral density  $N_0$  in order to investigate the impact of optical signal to noise ratio (OSNR) per subcarrier [60].

$$N_0 = \frac{P_{average}}{(OSNR * B_{ref} * N_{subcarrier})} \quad (3.1)$$

where the OSNR is the ratio required,  $P_{average}$  is the total average power of all sub-carriers,  $N_{subcarrier}$  the number of subcarriers, and  $B_{ref}$  is the commonly taken equivalent to the 0.1 nm resolution bandwidth at a wavelength of 1550 nm. The subcarrier to be received was selected using the transfer function of three cascaded delay line interferometers (DLI) as an approximation to the Fast Fourier Transform (FFT) derived in [61].

$$H_p = \prod_{p=0}^{N_{order}-1} \frac{(1 + \exp(-i(\omega - \omega_0)T_p + \varphi_p))}{2} \quad (3.2)$$

with  $H_p$  as filter transfer function,  $N_{order}$  as the FFT order,  $\omega$  as optical frequency,  $\omega_0$  as filter center,  $T_p$  the time delay defined as:

$$T_p = \frac{T}{2^{N_{order}-p}} \quad (3.3)$$

and  $\varphi_p$  the phase shift defined as:

$$\varphi_p = \frac{2m\pi}{2^{N_{order}-p}} \quad (3.4)$$

For a high order FFT filter, the transfer function is converging toward the sinc function which is the ideal match filter for AO-OFDM.

The Bit Error Rate was determined using the Monte Carlo method where multiple sets of data were simulated until the standard deviation relative to the BER value was lower than 0.1 [62]. Diverse variables were used to test the performance such as the relative phase difference between subcarrier, OSNR, transmitter rise time, demultiplex filter and the receiver bandwidth. Fig.3.1 illustrates the transmitter bandwidth limitations as a function of the phase relation between adjacent subcarriers and the subsequent impact via the minimum required OSNR to achieve a BER of  $5 * 10^{-4}$ .

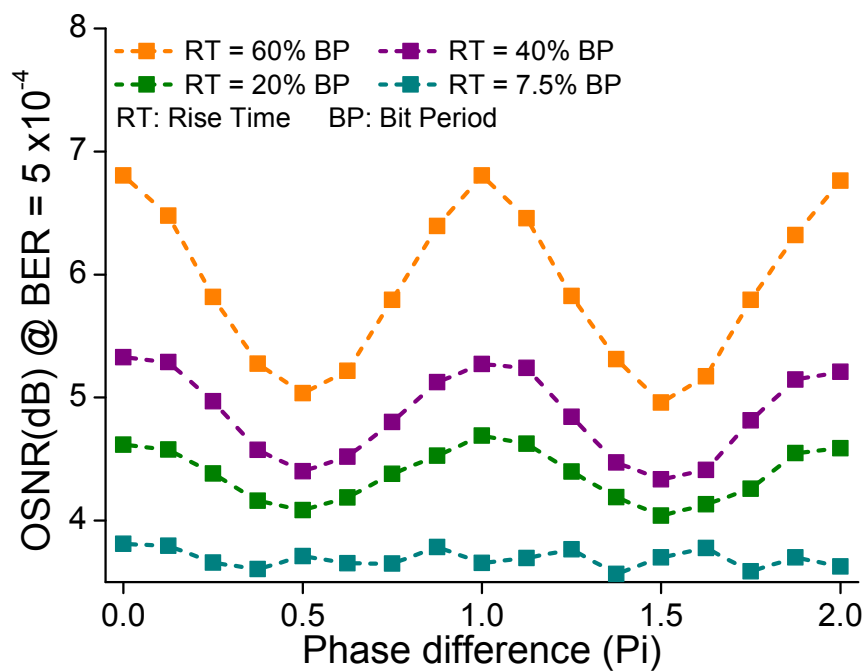


Figure 3.1: Impact on required OSNR of relative phase between adjacent subcarriers and transmitter bandwidth on All-Optical OFDM. Points are connected to highlight the phase difference impact

The super-channel transmission performances are dependent on the orthogonality conditions that allows channel to be spectrally overlapping without crosstalk. While the frequency spacing equal to the baud rate condition is obtained by using an optical comb, and hence not considered during this simulations, the transmitter matched filter implementation is limited. In the case of an OFDM super-channel, the ideal matched filter is a sinc function in the spectral domain, and similarly a rectangular pulse in the time domain. When the rise time of the pulse increases, the frequency response deviates from the match filter and the orthogonality is degraded. Consequently, the crosstalk due to the adjacent chan-

nels degrades the performance of the channel under consideration. In Fig.3.1, as the rise time increases, the penalty due to such loss of orthogonality is illustrated by a higher OSNR requirement. Typical systems deliver bandwidth large enough to have rise time in the range of 20 % of the bit period.

Furthermore, for poorly matched transmitter, for example in the case of a rise time greater than 40 % of the bit period, the phase relation between adjacent channels has a large impact on the required OSNR with optima when the phase difference is  $\pm\pi$ . Large bandwidth transmitters can be implemented without phase control and maintain constant performances. In addition, it is to be noted that the phase control crosstalk mitigation is optimum for single quadrature modulation format such as BPSK [63] and has a lower impact in dual quadrature format.

Similarly to the transmitter, the demultiplexing of an embedded channel is dependent on the quality of the matched filter. If a perfectly sinc shaped channel is demultiplexed from the super-channel by a coarse approximation of the matched filter, then the phase control is then a tool to optimize the performance.

Finally, the simulation results confirm the degradation of performance when a sharp transition cannot be achieved. Furthermore it also shows the potential improvement in OSNR requirement provided by the control of the optical phase between subcarriers.

## 3.2 Odd/Even comb source for experimental super-channel transmitter

Optical frequency comb sources are commonly used as the platform for optical OFDM generation due to their inherent match with the orthogonal frequency spacing along with a constant phase relation between subcarriers.

In this section, the transmitter set up used in this thesis will be described from the comb source used to emulate the super-channel carriers to the structure providing channel data different to the adjacent ones. Firstly, the concept of the odd/even comb source is described. This is followed by an extensive look at the critical Frequency Shifting function used, which was based on a Dual-Parallel Mach-Zehnder modulator. Then the comb source and the odd/even structure are combined to generate the set of carriers that support the experimental super-channel.

### 3.2.1 Odd/Even comb source concept

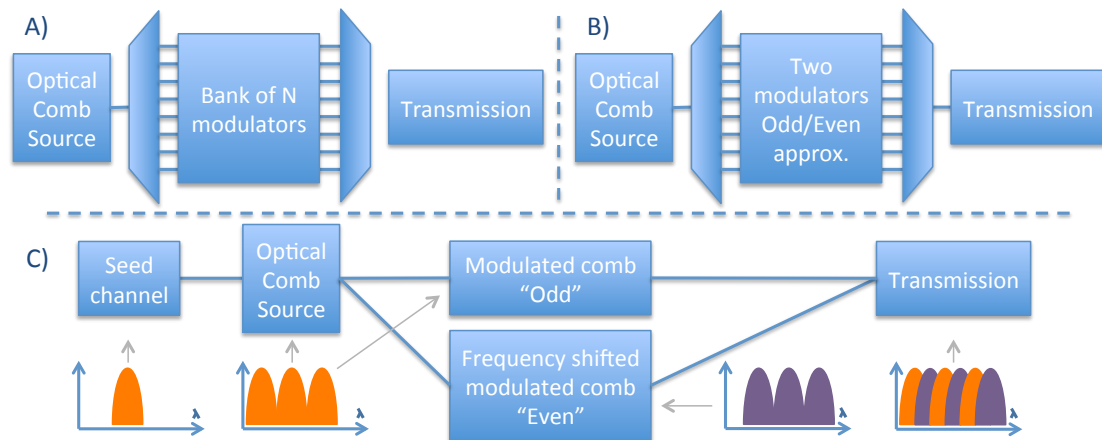


Figure 3.2: Schemes for transmitter emulation. A) Realistic transmitter: different data per channels, B) Experimental emulator: odd/even channels from two data modulators, and C) Experimental emulator for this super-channel: optical comb source and frequency shifting function based odd/even structure requiring a single data modulator. Inserts represent the steps to generate an experimental 6 channel super-channel as used in [64].

Due to the limited availability of equipment in a laboratory environment, it is common to emulate a super-channel transmission system by employing a single channel source before duplicating the signal by assigning it to multiple carriers [65–69]. While a high number of decorrelated data patterns would give a most realistic transmission performance [70, 71], only a few sets of data are generally used such as in the odd/even configuration where every second carrier is supporting the same data, as shown by Fig.3.2 B). While the experiments presented in these two papers [72] and [63] show that using only two channels gives a slightly optimistic performance, transmitter emulation using only two independent data paths still allows for useful preliminary proof of concept experiments, especially when the experimental implementation is in support of extensive numerical simulations using fully independent channels, as presented here. The transmitter developed in this chapter is similar to the system presented in [63] as the relative phase of adjacent subcarriers are controlled, as developed in section 3.3.2. In this experiment, the comb source was based on a combination of a first stage 5 line comb source using a single MZM and a second stage Frequency Shifting based odd/even structure as illustrated by Fig.3.2 C). This structure requires a single data modulator and hence is a simplification of the standard emulators that are based on two high quality data transmitters and periodic filters.

Fig.3.3 presents the experimental implementation. Firstly, the MZM was driven, with approximately  $2 V_{\pi}$ , by a 20 GHz sine wave and biased to generate a 20 GHz spaced five line comb, to obtain five channels. In order to maintain strict frequency spacing between channels, the same 10 GHz RF master clock source was used throughout the system. An additional five channels, frequency shifted by 10 GHz were generated using a parallel path structure. The first arm of this structure contained an optical frequency shifter, using a dual-parallel MZM driven by the electrical signal frequency provided by the system clock source [73]. The unshifted frequency and negatively shifted components after the frequency conversion were suppressed by more than 30 dB with respect to the positive frequency shifted channels [16]. The second arm contained an attenuator, a polarization controller, an optical delay line, and an optical phase shifter. The two arms were recombined, interleaving the two sets of five channels to form the ten line AO-OFDM transmitter. The two arms were mismatched by a strict integer number of bit periods by adding fiber in one arm to ensure time alignment but decorrelated data patterns (the fiber length equivalent of 5 bit periods). In addition, the two paths were polarization aligned and power equalized. An additional polarization beam splitter was positioned at the output of the AO-OFDM transmitter in order to guarantee polarization alignment of the odd and even sub-channels.

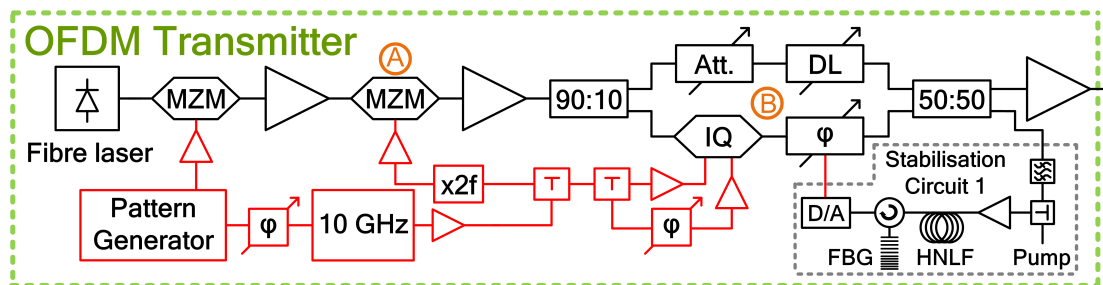


Figure 3.3: Schematic of the experimental OFDM transmitter based on single channel transmitter (MZM driven by the pattern generator), optical comb source ((A), MZM driven by a doubled frequency clock), and odd/even structure (B). Polarization controllers not pictured for clarity. Black and red lines signify optical and electrical paths respectively. MZM: Mach-Zehnder modulator, Att.: optical attenuator, DL: optical tunable delay line, IQ: Dual-parallel Mach-Zehnder modulator (Frequency shifter),  $\varphi$ : tunable electrical phase shifter, triangles represent optical or electrical amplifiers. Stabilization circuit described in 3.3.2



### 3.2.2 Frequency shifting

The 5 line comb source based on a MZM was described in the second chapter of this manuscript (point A in Fig.3.3). Here we describe the frequency shifting function represented by an IQ modulator at point B in Fig.3.3. The concept of external modulator based frequency shifting is presented and conceptually explained. Further the experimental implementation and testing is carried out using commercially available devices. Finally, the long term stabilization of the frequency conversion is observed and maintained with the implementation of a phase locked loop feedback circuitry.

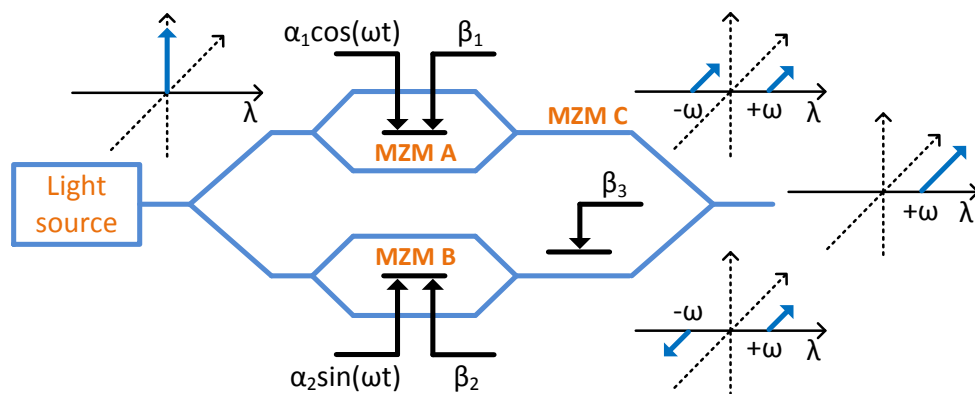


Figure 3.4: SSB-SC concept using DP-MZM

The frequency shifting of an optical signal can be obtained by interferometrically beating two identical three line combs with a specific phase difference such as only one carrier is maintained after carrier suppression, as shown by figure 3.4. The experimental implementation of the carrier suppressed frequency shifting was initially done using a commercially available JDSU DPMZ modulator. The device had sub-MZM extinction ratios above 25 dB, and  $V\pi$  of 5.2 V, 4.5 V, and 6 V for the RF electrodes, the bias electrodes, and the phase electrode respectively. The RF bandwidth of the modulator was 16 GHz. The electrical microwave signal originated from a Centellax clock synthesizer with a bandwidth of 13 GHz, before being filtered using a bandpass electrical filter with a transmission window from 8 to 11.5 GHz in order to reduce any additional unwanted frequency components. The RF signal was then amplified using an SHF broadband amplifier with a bandwidth of 70 kHz - 15 GHz and saturation power of 26 dBm. The microwave signal was then split in two parts to be applied to the two RF inputs

of the DPMZM, with phase control on one of the path. The RF signal applied to the sub-MZM was formed of 10 GHz, 20 GHz and 30 GHz frequencies with power measured as 16.8 dBm, -27.2 dBm, and -51.2 dBm respectively that indicate a clean driving signal and consequently a sideband generation limited to the fundamental 10 GHz contribution.

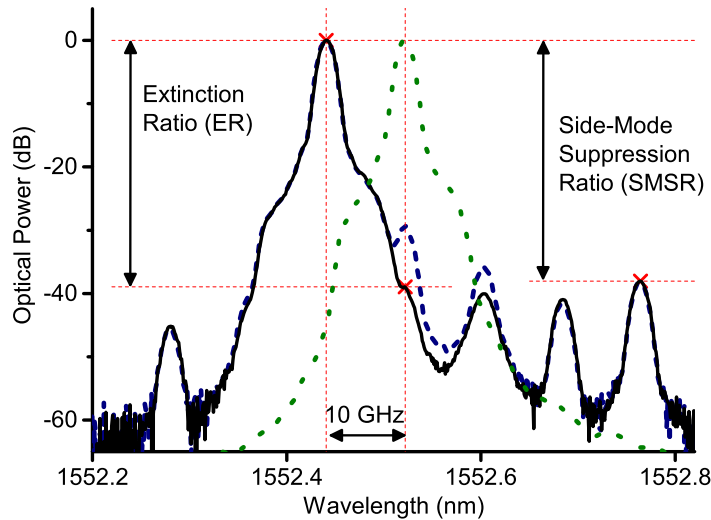


Figure 3.5: Optical spectrum of 10 GHz SSB-SC generated signal. Optimized (solid line), non-optimized (dashed line), input optical carrier (dotted line)

Fig.3.5 is the optical spectrum at the output of the DPMZM tuned as a frequency shifting device. The dotted line represents the optical signal at the input of the modulator. The dashed line and the continuous line are the translated optical signal.

The frequency shift was equal to the 10 GHz driving frequency and the remaining unwanted sidebands are equally spaced too. As the electrical and optical phase delays were both equal to  $\pi/2$ , the symmetry around the carrier is broken and one of the sidebands is suppressed, as shown with dashed lines in figure 3.5. In addition, when the two sub-MZM are accurately biased at the null (within the 10mV resolution of the power supplies used), the resulting spectrum is then carrier suppressed. The resulting spectrum is described as optimized in figure 3.5, when the polarization was aligned with the modulator axis, the carrier suppressed by biasing at null both of the sub-MZMs, the RF powers driving the sub-MZM were balanced (within 0.1dB), and the two phase variables were properly set. The performance of the frequency shift can be defined by two factors, illustrated in Fig.3.5:

- the Extinction Ratio (ER), describing the difference of power between the translated and the original signals
- the Side Mode Suppression Ratio (SMSR), describing the difference of power between the translated signal and any other unwanted components generated during the frequency shifting.

For a 16.8 dBm RF driving power applied to each of the two parallel MZMs, and with corresponding bias voltages of 3.3 V and 6.2 V respectively, the performance observed with this modulator were a high ER of 39 dB and a SMSR of 38.1 dB, delivering a clear frequency shift.

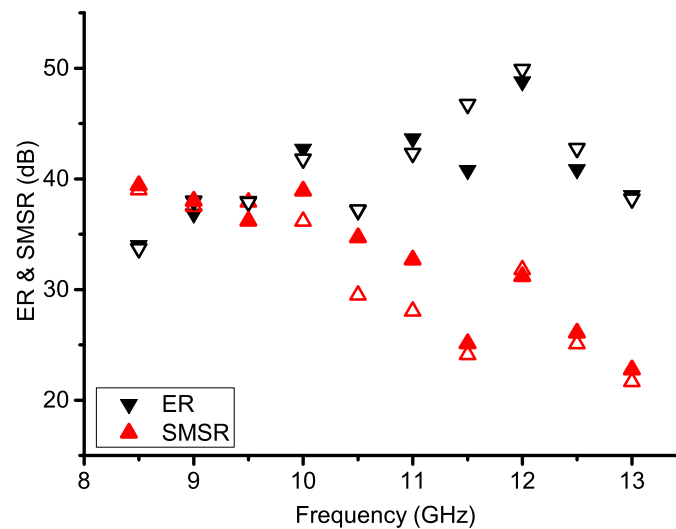


Figure 3.6: SSB generation at different shift frequencies: blue shift (filled symbol), red shift (open symbols). Driving voltage fine tuned to follow the modulator RF transfer function

To determine the applicability for further implementation in an optical transmitter or network sub-system, the flexibility of the frequency shifter system was investigated. Firstly, Fig.3.6 depicts the results of the corresponding ER and SMSR measurements against the RF driving frequency with either blue or red shifting of the generated SSB signal with respect to the input optical carrier. ER values above 35 dB were obtained for frequencies higher than 9 GHz, approaching even 50 dB at 12 GHz. The limited resolution bandwidth of our optical spectrum analyzer ( $\sim 0.02$  nm) did not allow accurate measurements below 8 GHz. The SMSR performance seems to be more dependent on the characteristics of the DP-MZM as it follows the frequency response of the modulator and decreases with frequencies above 10 GHz. All the measured SMSR values were

nonetheless above 20 dB. The difference between blue and red shift are believed to be due to phase misalignment and/or notches in the frequency response of the sub-MZMs.

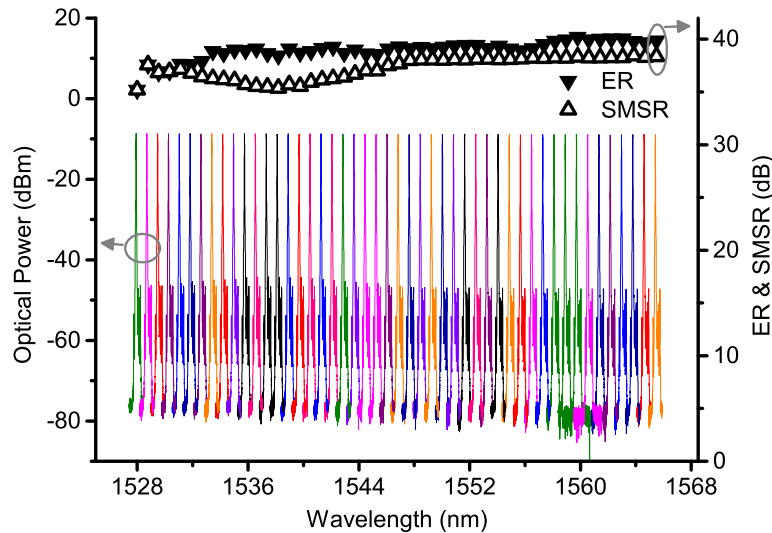


Figure 3.7: SSB-SC generation over C-band. Optical spectra and corresponding ER and SMSR values

Secondly, the optical frequency tunability has been tested through a scan of the communication transmission C-band spreading from 1530 nm to 1565 nm. Measurements have been taken every 100 GHz following the ITU-grid using a tunable laser source of linewidth lower than MHz. The frequency shifting was equal to 10 GHz and only tuning of the bias voltages ( $<100\text{mV}$ ) was performed to maintain optimum performance. As the modulator is designed for the whole transmission window, the ER and SMSR values were consistent for each data point across the C-band. Nevertheless, a drop in the SMSR is noticed in the lower part of the spectrum. Fig. 3.7 shows that the minimum values are still above 35 dB for the ER and SMSR. A very stable output optical power for the generated SSB tones was also observed.

While the RF frequency change performance measured is inherently related to the particular frequency response of the modulator used, it is to be noted that the experimental device is a commercially available component initially designed for data modulation. Multiple configurations can be investigated to design a specialized component that produces ER and SMSR greater than 50 dB over a wide range of electrical and optical frequencies [74]. Such high values are only required in particular cases, later in this chapter, Fig.3.12 shows that

an ER greater than 20 dB is sufficient for the super-channel implementation.

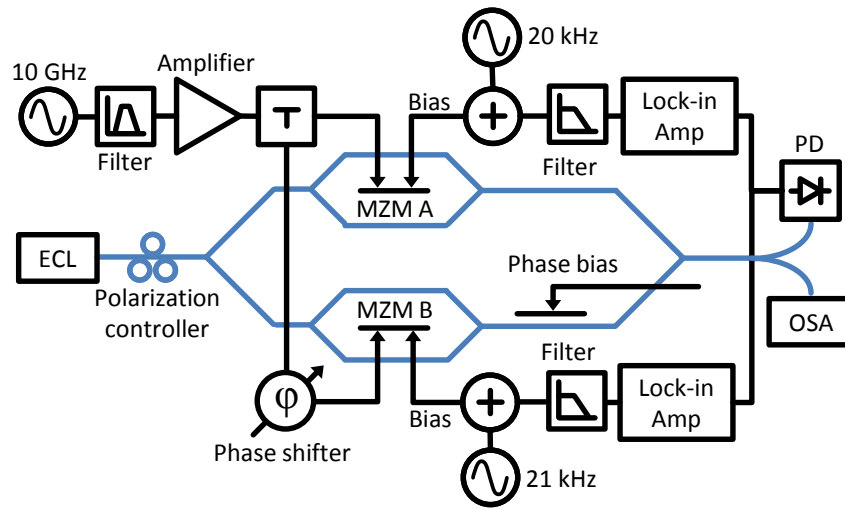


Figure 3.8: Experimental setup of the DP-MZM scheme with the stabilization for the generation of an SSB-SC optical signal

Finally, a stabilized SSB-SC generation scheme based on the use of a single drive DP-MZM and a feedback control loop was designed and tested. The scheme maintained high performance in terms of ER and SMSR over a whole day, which in addition to the different modulation frequencies and operating wavelengths that have been demonstrated, prove its high potential for practical application in future optical transmitter units.

The SMSR and extinction ratios were critically dependent on the device biasing which suffered from the well know thermally induced variation. Consequently, a stabilization circuit is required for long time usage of the frequency shifting sub-system. From experimental monitoring, it was observed that the sub-MZM dominated the variation over time. The microwave phase control and signals driving the modulator were sufficiently stable over time, the optical phase required a realignment daily whereas the bias voltages had to be realigned to compensate small variations every few hours. A high resolution Optical Spectrum Analyzer (OSA) [75] or a Fabry-Perot scanning filter can of course be used in conjunction with a control algorithm implemented in, for example, a LabView program to provide appropriate control signals based feedback. However in the laboratory such techniques require the monopolization of complex and valuable equipment. More generally the optical monitoring would be impractical if the optical signal is carrying data that would result in a broader spectrum of the range of the frequency shift. As described above, drifts from the optimum biasing point of the two sub-Mach-Zehnder modulators affects the performance of

the frequency shifter. Long term stability at the optimum operation condition has been achieved, with a feedback loop scheme shown in Fig.3.8 that applied separate control of each sub-MZM bias. This was enabled by two electrical dithering tones of 10 mV amplitude, at 20 and 21 kHz, added on the respective bias voltages. The dither was consequently transferred mainly on the residual portion of the original optical carrier because at null the center frequency is much more sensitive to bias than the frequency shifted components. The induced variations were extracted from the monitored optical signal with the help of high gain lock-in amplifiers, after being detected using a low speed photodiode. The fundamental tones were kept to the minimum to ensure an optimum extinction of the carrier. The two loops were closed with lowpass electrical filters of 40 Hz bandwidth, enabling efficient compensation of the slow drift effect.

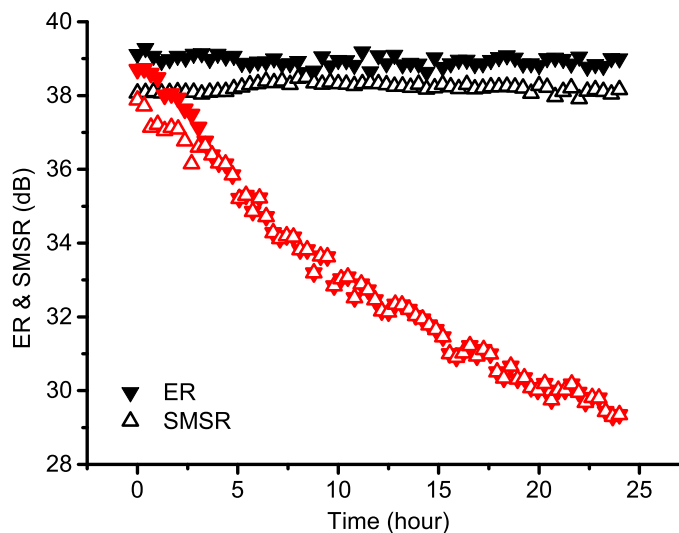


Figure 3.9: SSB modulation stability over time (24 h): stabilisation enabled (black) and disabled (red)

Fig.3.9 depicts the results of long-term measurements for the ER and SMSR of a 10 GHz SSB-SC generation process. After 24 hours of operation in a laboratory environment, the stabilization loop maintained, with small variations, a high ER level of  $\sim 35$  dB and a SMSR level of  $\sim 38$  dB. The ER and SMSR peak-to-peak variations calculated from the set of data are 0.77 and 0.45 dB respectively. Without feedback control the ER and SMSR figures degraded severely to 30 dB.

The performance of DP-MZM based frequency shifter has been investigated before its implementation as part of a odd/even comb source for experimental super-channel transmitter. Electrical frequency tunability and input wavelength

transparency has been demonstrated. In addition, long period stability has been obtained through the use of low frequency feedback system.

### 3.2.3 Odd/Even comb source implementation

As the use of a DP-MZM device has been validated for frequency shifting, the experimental setup was then implemented to generate two combs of 5 line frequency shifted by 10 GHz with respect to each other. The combination of the two combs corresponds then to the odd/even set of carriers that will support the super-channel generation.

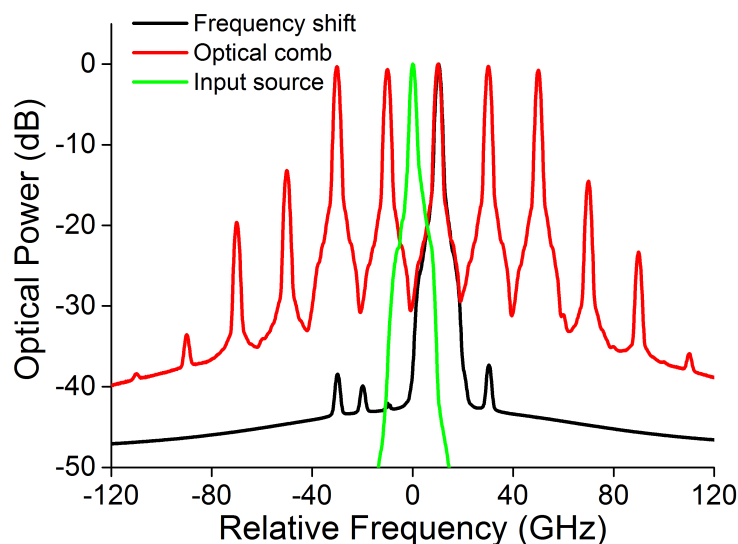


Figure 3.10: Frequency shifting and comb generation of the generation of odd/even super-channel

Initially the comb and odd/even structure was tested without the transmitter section, following Fig.3.3. The input light source was a fiber laser of very narrow linewidth and high spectral purity. A polarization controller was followed by a single drive MZM driven by a 27.5 dBm 20 GHz RF signal in order to generate a 5 line comb. A comb flatness of  $\sim 0.5$  dB and SMSR  $> 12$  dB were observed. The comb signal then entered a two arm structure through a 90:10 coupler, the strong signal going to a DP-MZM after a second polarization controller. The sub-MZM were driven by two independent narrow band amplifiers delivering 16.7 dBm and 16.9 dBm respectively as to maximize the SMSR, the second harmonics at 20 GHz were measured as  $< -27$  dBm. Finally, the insertion loss of the overall connectors, polarization controller and frequency shifting function

was estimated  $\sim 15$  dB. Fig.3.10 shows the high quality frequency shift and the combination of the two stages resulting into the frequency shifted 5 line comb.

While the DP-MZM device used to investigate the frequency shifting in the previous section of this chapter wasn't available, the modulator used in the setup described in the further sections and chapter had similar characteristics of frequency response and stability. Fig.3.10 shows lower performance in the frequency shifting ER but values remaining above the 30dB carrier and side-mode suppression. The unshifted comb signal was balanced in power, time and polarisation within the second arm of the odd/even structure as to obtain the odd/even comb required for the transmitter. Fig.3.11 shows the resulting comb, with flatness and SMSR similar to the 5 line comb.

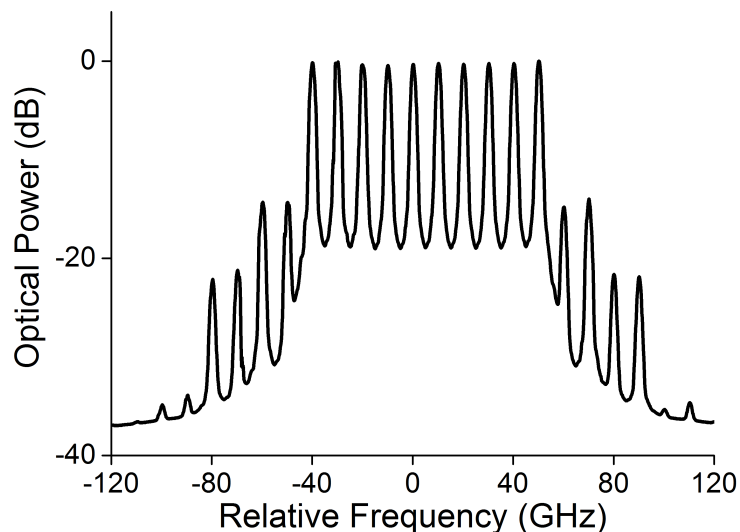


Figure 3.11: Optical comb obtained at the output of the odd/even structure

The input of the odd/even comb generator was then replaced with a data channel to obtain the super-channel. Channel generation and results are presented in the next section.

### 3.3 All-Optical OFDM transmitter

In this section, the odd/even structure coupled with the comb source will be used to copy the signal from a single channel to generate an experimental super-channel. The section is split in two parts, with initial focus on the modulated



signal and the overall super-channel performance in a back-to-back configuration, and then a description of the stabilization circuit implemented to control the phase relations between adjacent channels.

### 3.3.1 Super-channel generation

The data channel was obtained by phase modulating the optical signal from a fiber laser of kHz linewidth. Single quadrature format was implemented with BPSK by driving a Mach-Zehnder modulator with a binary signal of amplitude close to twice the  $V_{\pi}$  of the device [26, 76]. A pulse pattern generator (PPG) generated a 10 Gb/s  $2^{15}$ -1 bits long pattern, which was passed through a broadband electrical amplifier to a high bandwidth optical Mach-Zehnder modulator to impose BPSK modulation on the cw signal. Note that the same electrical clock source was used for both the transmitter and the comb source in order to maintain strict frequency spacing between channels equal to the symbol rate of the seed channel.

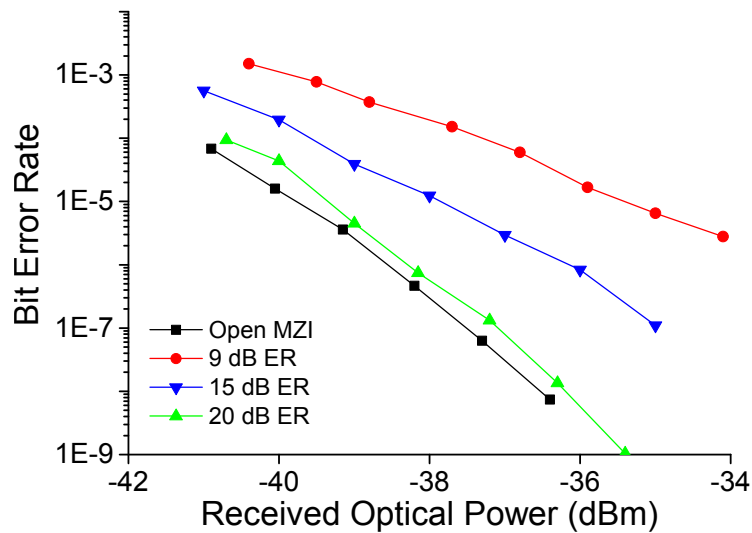


Figure 3.12: BER of DPSK channel versus frequency shifting extinction ratio. Curve for added channel with no other channel, and for a interferometrically suppressed channel with an extinction ratio of 9, 15, and 20 dB.

Initially, the transmitter was used in conjunction with a DPSK direct detection system. This consisted of an optical attenuator, pre-amplifier, delay line interferometer (DLI) with a free spectral range (FSR) of half the symbol rate, and a broad optical filter (1nm), followed by a second EDFA amplifier before a 32 GHz

bandwidth photodiode followed by a broad bandwidth data amplifier. In order to confirm the required extinction ratio of unwanted comb components, two different signals were sent to the receiver with a difference of power representing the ER. Two parallel arms were set of different length with an attenuator for one side, in order to determine the impact of a degraded suppression of the carrier in the frequency shifting function. This experiment was used to confirm the capability of this implementation of the odd/even generation for a super-channel transmitter. The Bit Error Rate was measured over 10 seconds through DPSK direct detection for different simulated frequency shifter ER. Fig.3.12 clearly shows that while high ER is required to maintain performance in the super-channel, a  $>20$  dB ER had little impact compared to the reference channel and thus the performance of the frequency shifting technique is acceptable [77, 78].

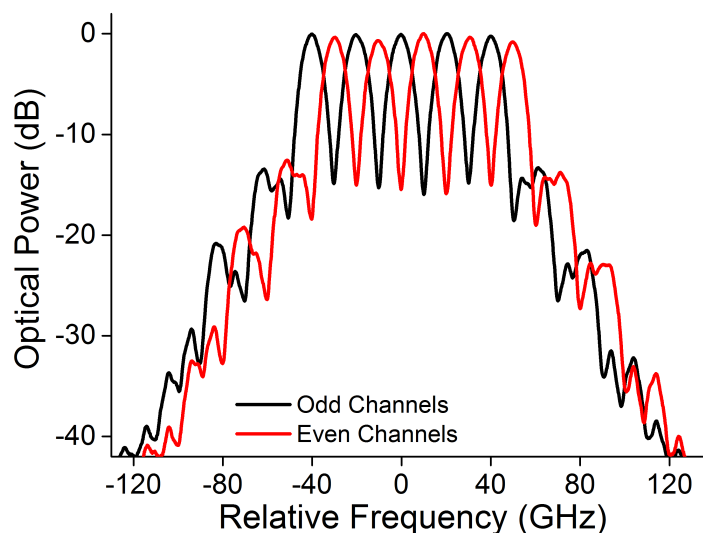


Figure 3.13: Odd and Even channels optical spectrum

As the frequency shifting function was demonstrated to conform to the multiplexing requirement, the super-channel transmitter was implemented using a single light source, a single clock source, a single channel transmitter, a comb source, and finally the odd/even function as illustrated in Fig.3.3. Fig.3.13 shows the optical spectrum at the two outputs of the odd/even structure, with one set of 5 BPSK channels frequency shifted by the symbol-rate frequency. The similarity of the two sets of channels confirms the low impact of the frequency shifting action and thus led to Fig.3.14 representing the final AO-OFDM super-channel at the output of the experimental transmitter. In addition to the power and time alignment, a polarization beam splitter was added at the output of the

odd/even structure in order to maintain each carrier in the same polarization and thus maximizing the channel overlap.

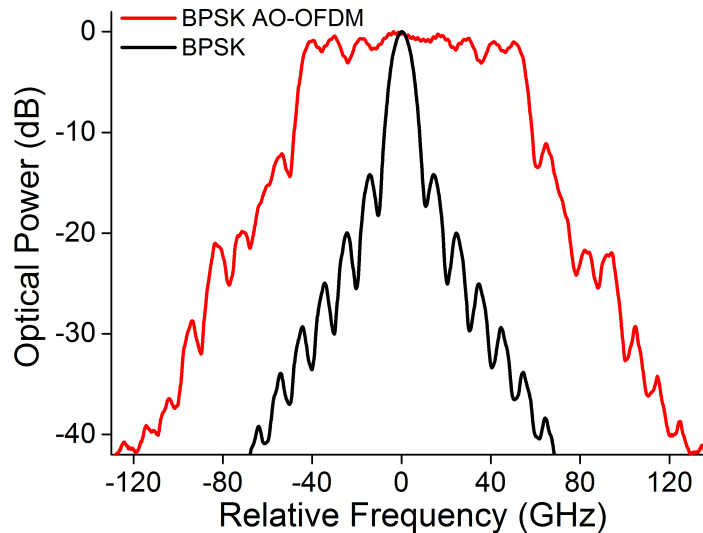


Figure 3.14: BPSK AO-OFDM optical spectrum and seed channel

A modification of the seed channel generator allowed an upgrade of the modulation format from single quadrature (BPSK) to dual quadrature (QPSK) in order to reach the higher spectral efficiency required for future optical links. The PPG and Mach-Zehnder modulator were replaced by a Arbitrary Waveform Generator and an IQ modulator. The symbol rate was maintained at 10 Gbaud and consequently the comb generator remained unaffected. Fig.3.15 shows the spectrum of the QPSK AO-OFDM super-channel.

Independently of the modulation format and the number of channels, a heterodyne coherent receiver of analog bandwidth of 36 GHz was used. The coherent receiver employed a second independent fiber laser forming a local oscillator (LO), tunable over 1nm, which was set to within 100 MHz of the channel to be measured. The frequency alignment of the channel to be received and LO laser was monitored by making the optical carriers beat at a broadband photodiode connected to a RF spectrum analyzer. The wavelength of the transmitter seeding fiber laser was defined as the central channel. Adjacent channels were measured by detuning the LO wavelength by  $\pm n\Delta f$  where  $\Delta f$  is the symbol-rate.

Because of the limited tuning range inherent to fiber lasers, only the central channels were measured, those however have the most interaction due to the presence of adjacent channels and thus are the more interesting. The AO-OFDM

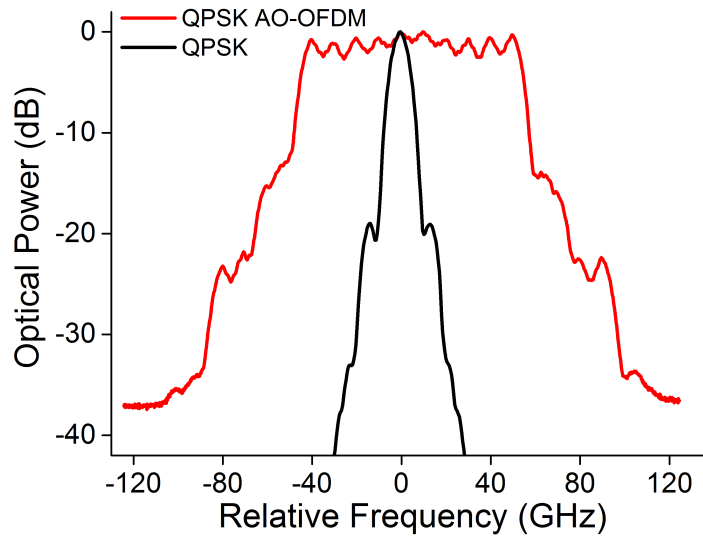


Figure 3.15: QPSK AO-OFDM optical spectrum and seed channel

signal was sampled at the receiver at approximately 8 samples per bit. Channel selection was performed using a digitally implemented sinc-function matched filter. Channel estimation was achieved off-line using typical digital signal processing (DSP) algorithms for clock recovery, polarization rotation, and frequency offset compensation [79, 80]. System performance was evaluated based on the  $Q^2$ -factor, in dB, calculated from the error vector magnitude following the expression  $Q^2 = 10 \log(\frac{1}{EVM^2})$  from [81].

A noise loading section was placed before the coherent receiver in order to detect excessive penalties due to the channel multiplexing into a super-channel. An optical attenuator was placed at the input of the receiver EDFA to limit the optical power and force the amplifier into a degraded OSNR regime. Because of the back-to-back implementation of the test, a second attenuator was placed before the receiver optical amplifier to achieve a highly degraded OSNR. A broadband optical filter was placed after the first EDFA in order to reduce the out of band ASE noise level and particularly the low wavelength ASE peak. Fig.3.16 confirms the transmitter and receiver implementation as high  $Q^2$ -factors were obtained for BPSK and QPSK in both single channel and super-channel configuration. While the curves are converging for low OSNR due to the performance estimation determined from the EVM values,  $Q^2$ -factor values above the 7 % hard decision FEC threshold (8.3 dB) [82] were used as reference for the experiment using the super-channel transmitter, as reported in the next chapter.

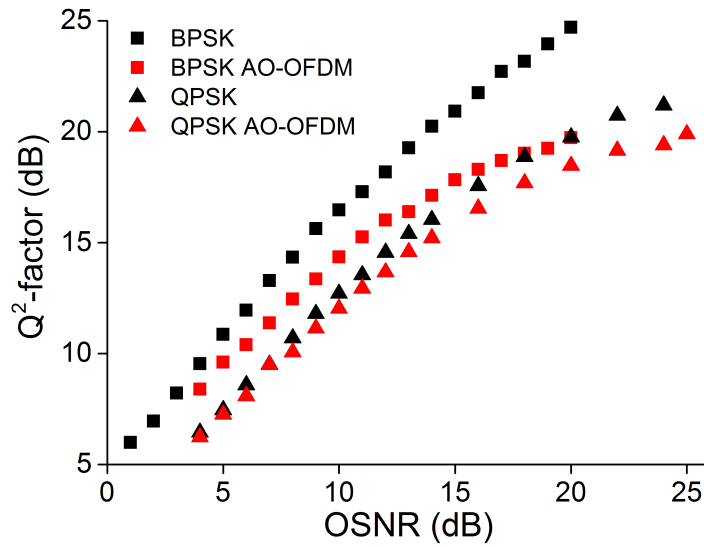


Figure 3.16:  $Q^2$ -factor versus OSNR for seed channel (black) and AO-OFDM super-channel (red) with BPSK (square symbol) and QPSK (triangle symbol) modulation format.

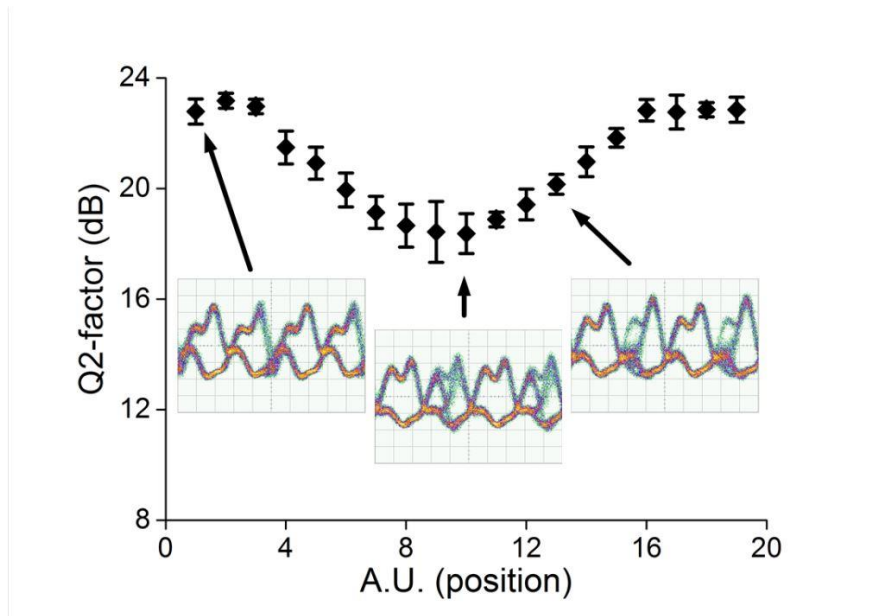


Figure 3.17: Adjacent channel time alignment impact for BPSK AO-OFDM

The impact of the time alignment of the channels, described as affecting the super-channel performance [63, 83, 84], has been measured to control the appropriateness of this experimental implementation with previously published work by tuning the electrical time delay between the seed channel and the comb source. The mechanical delay had a tuning range equal to the symbol-rate (100ps). Fig.3.17 shows up to 5 dB penalty in the  $Q^2$ -factor as the crosstalk

is not contained at the bit transition point, as the inserted eye-diagrams illustrates at different delay positions (two bit period). Additional time alignment was obtained by path matching the odd/even structure so as to differentiate the two paths by 5 bits, with a few percent uncertainty due to the oscilloscope time resolution.

An experimental AO-OFDM super-channel transmitter has been implemented. The odd/even structure coupled with an optical comb source provided ten channels carrying single and dual quadrature modulated signal required for further network experiments.

### 3.3.2 Transmitter stabilisation

Unless either guard bands or ideal filters and pulse shapes are used, AO-OFDM transmitters typically benefit from a phase stabilization circuit to contain the residual crosstalk. Optical matched filters can be difficult to achieve for All-Optical OFDM mainly because the bitrate is in the higher range of electronic systems, limiting the quality of time transitions, but requires narrow filtering by optical standards, making the required control of filter shape difficult to achieve. Whereas near-ideal rectangular waveforms can be obtained from DSP at low symbol-rates, practical optical devices don't allow advanced spectral profiles such as the sinc function required for OFDM. Hence, realistic system results show residual inter-channel crosstalk at the receiver. The relative phase between adjacent subcarriers can be used to control the position of the crosstalk in the bit period. This allows a reduction in the signal-crosstalk beating at the decision point and so maintain the performance even for lower bandwidth transmitters and receivers. The insertion of a piezo electric ceramic module (PZT) in the odd/even structure allowed the control of the relative phase between adjacent channels and consequently the time position control of the crosstalk within the bit period, similar to Fig.3.17. A computer controlled low voltage digital-to-analog converter was used to control the high voltage driver required to expand the PZT and stretch the optical fiber spooled around it providing the optical phase change [85]. Using a BPSK AO-OFDM super-channel the impact of the relative phase between adjacent channels has been measured for the central channel by varying the PZT control voltage. The estimated range of phase variation was greater than  $\pi$ .

While the data in Fig.3.18 clearly shows that no phase control is required for the coherent receiver setup to mitigate the crosstalk penalties, it has been shown that the optical demultiplexing, implemented in the next chapter, requires the use of crosstalk mitigation such as the relative phase control [86–88] to make the adjacent channels phase orthogonal to the central channel. Indeed, the bandwidth of the channel used as seed for the AO-OFDM super-channel was large enough that no phase control is required with the high bandwidth receiver, as seen with Fig.3.1. But in order to maintain performance using unmatched filter to demultiplex channels, the phase control stabilization was implemented. The principle used here is the conversion through the use of Four Wave Mixing (FWM) with an arbitrary laser pump of the relative phase of adjacent subcarriers into an amplitude variation that can be directly detected. FWM is a nonlinear

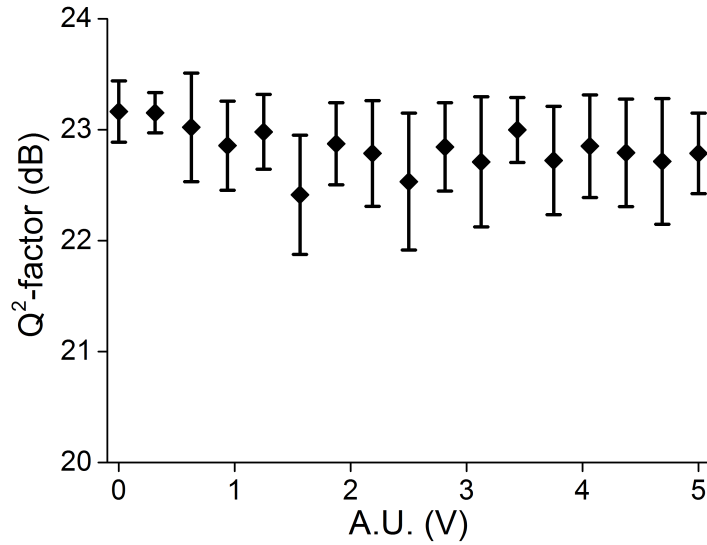


Figure 3.18: Impact of relative optical phase with adjacent channel. Phase variation greater than  $\pi$

process occurring due to the response of bound electrons in the fiber to the propagation optical signal. Commonly used for optical signal processing, it has been well described [23, 89]. In this case, two photons of different frequencies are annihilated and two photons of different frequencies are created, such as  $\omega_1 + \omega_2 = \omega_3 + \omega_4$ .

A couple of AO-OFDM channels were filtered, combined with a pump signal positioned at 320 GHz from the AO-OFDM laser source before being amplified up to 0.5 W. The signal and pump were inserted into a 400m HNLF spool, of nonlinear coefficient  $\gamma: \sim 7W^{-1}.km^{-1}$ . One of the FWM products generated by the interaction between two adjacent sub-channels and the pump is dependent on the relative phase variation between the sub-channels [88, 90]. Because of the symmetrical FWM process, a narrow Fiber Bragg Grating (FBG) filter was positioned at 320 GHz on the other side of the super-channel before a low speed photodiode [91].

Fig.3.19 shows the broad spectrum at the output of the HNLF due to the nonlinear wave mixing between the filtered AO-OFDM channel and the pump signal. The spectral components created on the right of the super-channel are shown in Fig.3.20 where the monitor signal is shown in two states of in-phase and out-phase after the FBG, representing the relative phase between adjacent channels that have been filtered.



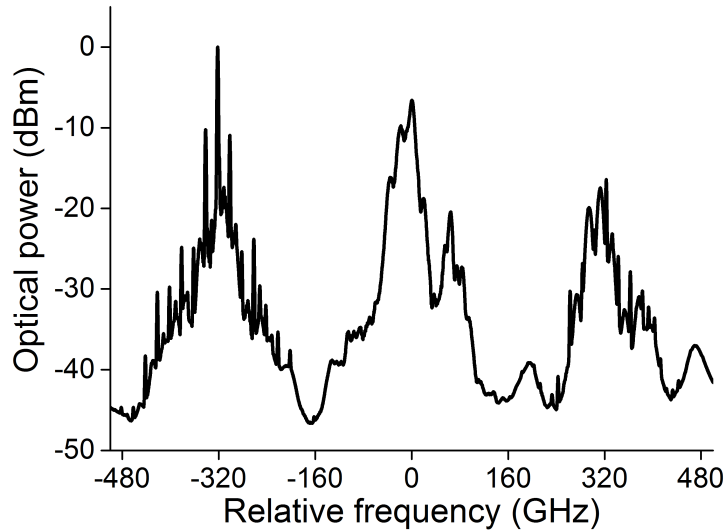


Figure 3.19: Optical spectrum after FWM process. Centered on the central channel from the AO-OFDM super-channel. Pump situated at -320 GHz

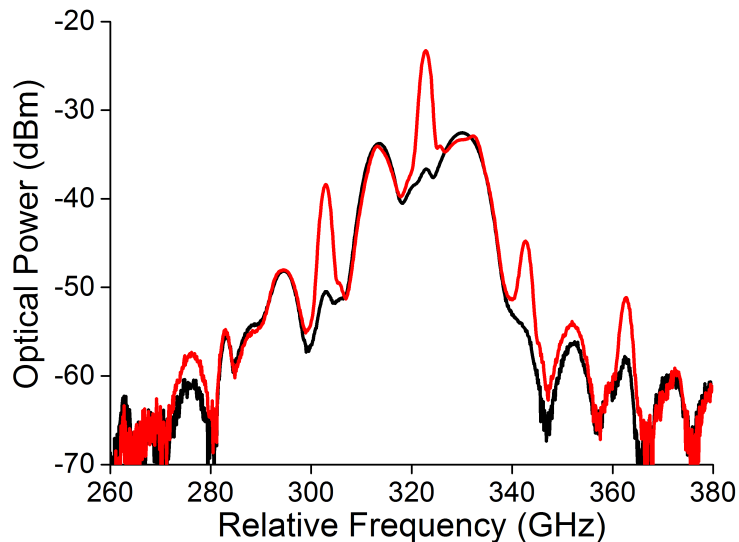


Figure 3.20: Optical spectrum of the filtered monitor signal after the FWM process. Adjacent channels in phase (red) and out of phase (black), the power difference detected by a photodiode was used to stabilize the relative phase between adjacent channels.

The total optical power variation at the photodiode was approximately 13 dB between an in-phase adjacent subcarriers and  $\pi/2$  phase difference. A computer controlled low speed ADC/DAC was used to implement the stabilization loop by controlling the high tension voltage applied to a PZT stretcher.

To account for dual quadrature modulation, the transmitter phase stabilization circuitry was modified by tuning the pump closer to the filtered channels in order to select the monitor wavelength using the same FBG as previously, as QPSK is modulation stripped on the fourth harmonic.

The AO-OFDM experimental transmitter has been completed by the addition of a stabilization circuit to compensate for finite bit transition due to imperfect transmitter components. It has been shown that the relative phase between the channels must be controlled to minimize crosstalk, as illustrated by Fig.3.1 and in the literature [63]. In addition, the stabilization setup will be of great importance for the next chapter as a channel from the AO-OFDM super-channel is optically demultiplexed.

### 3.4 Chapter summary

In this chapter, an experimental All-Optical OFDM super-channel has been implemented for single and dual quadrature modulation formats. A succinct description of AO-OFDM channel aggregation was first described and simulation results were presented to describe the impact of electrical bandwidth and optical phase control on super-channel transmitters. The implementation of the odd/even frequency shifting based structure followed, with an extensive description of the frequency translation using a DP-MZM device [16]. The third part described the final implementation of the super-channel transmitter by adding a data carrying channel as seed to the odd/even structure, completed by the implementation of the stabilization circuitry. In conclusion, the construction of the super-channel transmitter allowed the routing experiment developed in the next chapter.

## Chapter 4

# Terabit Interferometric Drop, Add, and Extract multiplexer

We have seen in previous chapters that the development of a frequency locked and phase locked multi wavelength optical source realized through an optical comb generation allowed for spectrally dense transmission, up to a point where channel spectra overlap. Such super-channel creation permits an optimum usage of the transmission window provided by existing amplification technology. However the use of extremely dense wavelength division multiplexing requires a new node structure to be implemented in future super-channel capable networks.

As the load on the optical networks steadily grows, an optimum utilization of the legacy optical fiber infrastructure is essential. Only flexible super-channel based optical networks can make use of the entire transmission window available [92]. While many research groups are approaching the fundamental limit of standard fiber point-to-point systems [93], optical networks require the use of Reconfigurable Optical Add/Drop Multiplexers (ROADM) [94]. The convergence of flexible super-channels capable of carrying Tb/s of data with optical flexible nodes is paramount to extend the benefit of optical link capacity to optical networks. Future optical networks will require the high granularity necessary to aggregate and extract data from an optical link with a range going from the single channel to multi-terabit wide super-channel. Different channel types have the potential to form super-channels for these future networks with small spectral guard band such as OFDM [95, 96] and Nyquist WDM [97, 98] or even with overlapping spectra such as All-Optical OFDM (AO-OFDM) [99–103]. High

performance optical filters such as those used in [95] allow for a diminution of the guard-band while maintaining a high quality signal. However, the guard-band remains finite. Recently, solutions compatible with overlapping spectra have been presented conceptually [104, 105] with a preliminary demonstration using FWM [106]. The extract function of the node, which consists in removing a particular channel from a super-channel to free the spectrum allocated, can be obtained using an interferometric solution. It offers the advantage of dropping the channel of interest from the super-channel without impacting the adjacent channels. When reaching the optical node, the super-channel is divided in two paths, the through arm and the channel extraction arm. While one path is unaltered, the channel to be dropped is demultiplexed from the super-channel and reshaped. The reshaped signal is then interferometrically combined with the original super-channel, and the relative phase is adjusted for destructive interference. This approach offers the possibility to implement ROADMs with guard-band free and overlapping spectrum. A recent proof of concept has been implemented emulating an interferometer composed of an electrical and optical path [106]. However, the scheme proposed is quite complex since it requires the use of a coherent receiver and a high-speed transmitter as part of the node. Moreover, the interferometric structure was associated with a complex Four Wave Mixing (FWM) process to insert new data in the super-channel.

In this chapter, the Terabit Interferometric Drop, Add, and Extract (TIDE) multiplexer will be introduced. This scheme is an all-optical node or reconfigurable optical add drop multiplexer (ROADM) that can be used with optical super-channels. The following section of this chapter will cover the conceptual presentation of the TIDE multiplexer. Preliminary simulation results are then presented and specific requirements are drawn for the experimental implementation. The different functions of the node are then further discussed through their implementations, in particular the optical demultiplexing, the optical gating and the optical reshaping. Experimental demonstrations are discussed for both single quadrature modulation format using Binary Phase Shift Keying and dual quadrature modulation format with Quadrature Phase Shift Keying.

## 4.1 Concept

A new architecture is proposed, called Terabit Interferometric Drop, add and Extract (TIDE) multiplexer, to facilitate all-optical switching of sub-channels

within the OFDM signal band, see Fig.4.1. Switching is performed in two layers, with the upper layer selecting the super-channel using typical Wavelength Selective Switch (WSS) units. The super-channel to manipulate is removed from the optical link and transferred to the lower layer where sub-channel switching is performed, with an interferometric setup that allows coherent subtraction of the dropped signals and the addition of the new. Contrary to the previous approaches, this scheme makes use of purely all-optical methods, such as FFT/i-FFT filtering and time domain sampling, to replicate the waveform of any sub-channel for the extract operation. Clock recovery, carrier extraction and phase locking units will be also needed for data and frequency synchronization within the node to make possible an in-line operation in a transmission link.

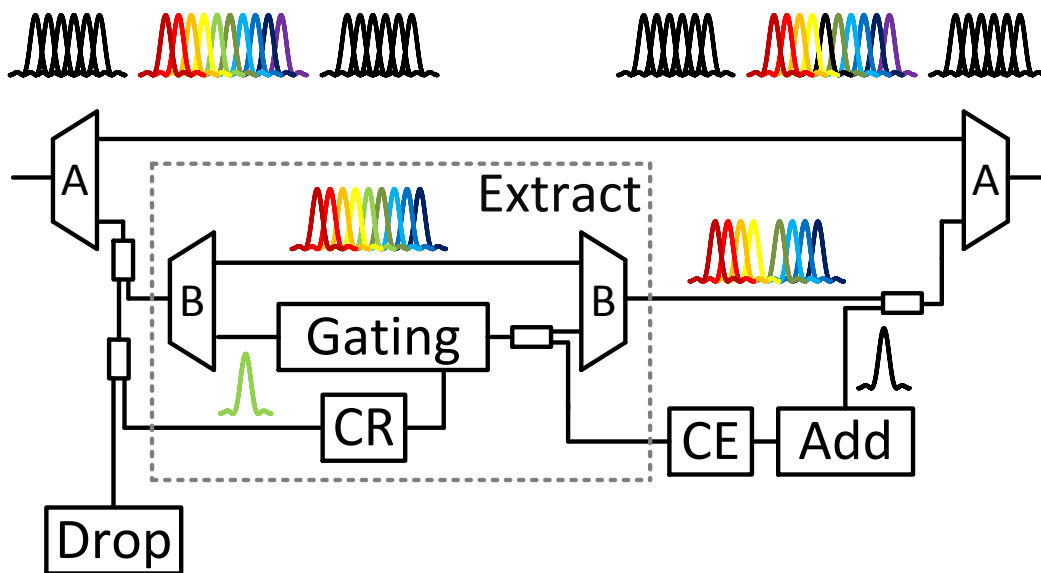


Figure 4.1: All-Optical Terabit Interferometric Drop, add, and Extract node. Optical filter A: coarse WSS for super-channel selection, optical filter B: fine WSS for channel selection. CR: clock recovery. CE: carrier extraction.

Fig.4.2 illustrates the replication of the sub-channel to be extracted from the super-channel in three eye-diagrams. On the top, the signal (in black) after the demultiplexing of a sub-channel from the super-channel is shown when FFT filters are used. The eye-diagrams are narrow and the adjacent channel crosstalk (in orange) is dominating the bit period, and thus removing the crosstalk is required to obtain the clear copy of the sub-channel for the interferometric suppression. The channel demultiplexing is hence completed by a sampling function and a reshaping, illustrated in Fig.4.2 by (B) and (C) respectively, obtained by an optical gate and an optical FFT filter. In the central part of the figure,

the signal is shown as a Return-to-Zero (RZ) signal cleared from crosstalk using a temporal rectangular function. The data carried by the sub-channel is at this point fully demultiplexed. However, the FFT filtering function is required to match the copied sub-channel to the one contained in the super-channel, as shown in the bottom part of the figure. Residual crosstalk can remain in the reshaped sub-channel copy in the function of the gating window and FFT filtering implementation, as simulation results presented further in this chapter illustrate.

Fig.4.2 represents a ideal FFT filter with a characteristic trapezoid eye diagram, from the convolution of two rectangular transfer functions, the data pulse train and the filter in the time domain. The approximation of the matched filter during the experimental implementation results in a closing of the eye due to an excess of crosstalk from the adjacent channels. Hence the control of the relative phase can improve the performance, as seen with Fig.3.1, by maintain the crosstalk out of the decision point.

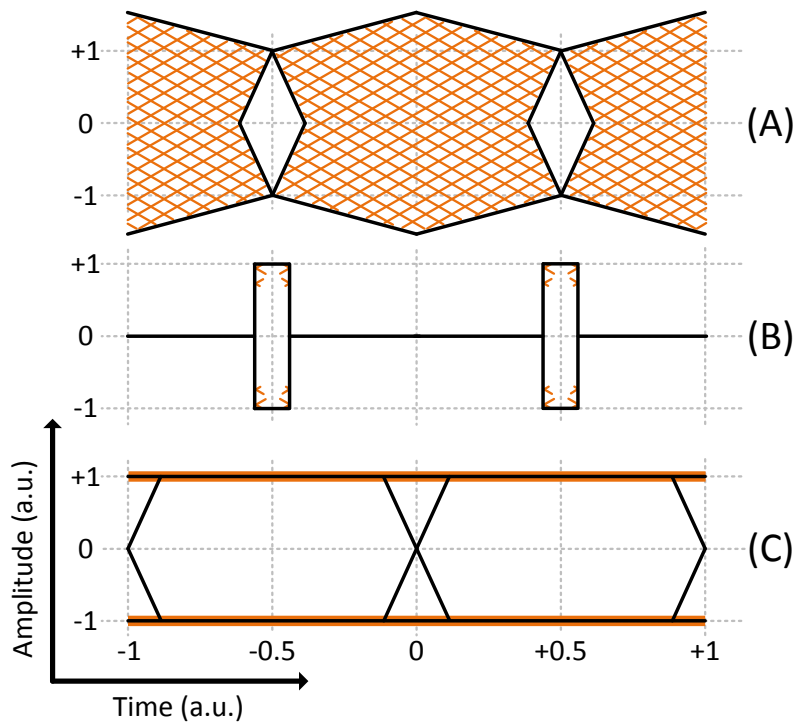


Figure 4.2: Illustration of the reshaping functions for BPSK signal. (A): After channel demultiplexing, narrow eye with large crosstalk (in orange) from adjacent channels, (B): After gating, crosstalk rejected, and (C): After reshaping, copy of the channel to be extracted without the super-channel crosstalk. Eye-diagrams of two bit periods

## 4.2 Preliminary investigations for the experimental implementation of the TIDE node

In this section, the implementation of the all-optical node is studied by testing a simplified experimental setup and simulations are carried out to determine the requirement of the sub-systems such as the optical gating extinction ratio and sampling window duration.

### 4.2.1 Experimental implementation of fiber based Mach-Zehnder interferometer

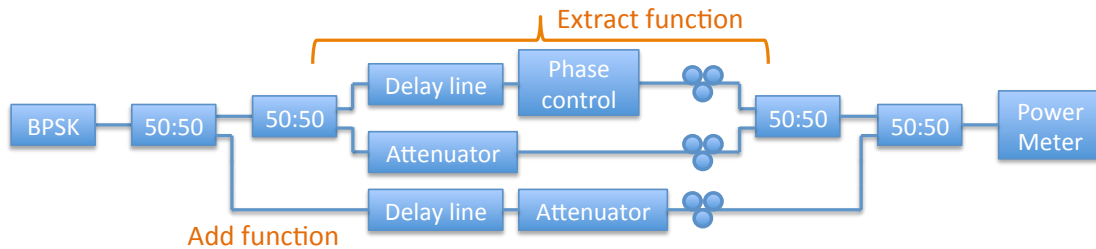


Figure 4.3: Schematic of a fiber interferometer. Extract function: fiber interferometer implemented to investigate the suppression of an optical channel, Add function: emulation of the insertion of a new channel at the same spectral position than the extracted channel. BPSK: Transmitter, Attenuator: Variable optical attenuator, Phase control: Optical phase control using PZT based fiber stretcher.

In order to investigate the potential of the channel suppression, a simple fiber interferometer (illustrated in Fig.4.3) was set up to measure realistic extinction ratio (ER) and penalty due to the remainder of the suppressed channel on an added one. For this experimental investigation, a simple BPSK transmitter was set up, consisting of a 10 Gbit/s  $2^{31} - 1$  PRBS signal produced by a Pulse Pattern Generator driving an optical MZM modulator biased at the null. The phase modulated optical signal entered a fiber interferometer through a 50:50 coupler, one arm of which contained a polarization controller, an optical variable attenuator, and a PZT fiber stretcher based optical phase shifter whereas the second arm contained a polarization controller followed by an variable optical delay line. The two paths were length aligned within the resolution of the oscilloscope used i.e. few picoseconds. The two arms were then recombined using a second 50:50 coupler, and the optical power and polarization were tuned to obtain the highest extinction ratio.

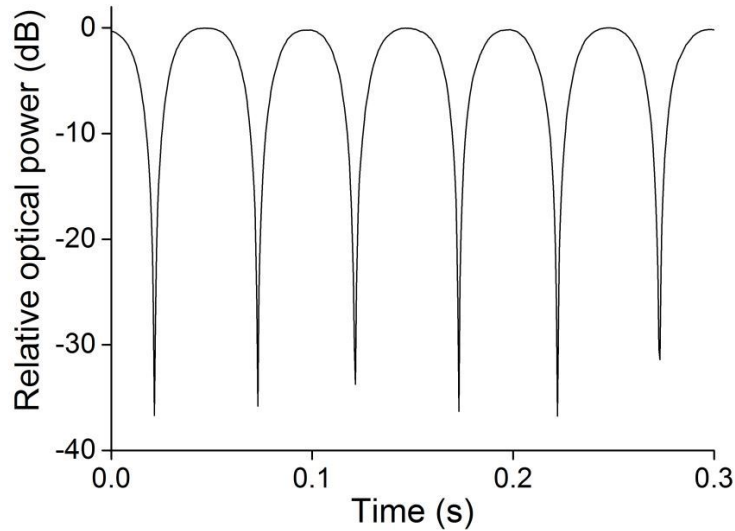


Figure 4.4: Interferometric suppression using fiber based MZI.

Fig.4.4 presents the normalized power variation at the output of the MZI when a periodic voltage ramp was applied to the PZT ceramic controlling the optical phase difference between the two interferometer arms. It can be seen that the ER of the fiber based MZI reaches more than 30 dB. To determine the penalty due to incomplete channel suppression, a third arm was added to the interferometer with sufficient length to decorrelate the data, as well as an additional optical attenuator to emulate the addition of a new channel at the spectral position of the extracted channel. The extract MZI was maintained in the interferometric suppression point by detecting the power at its output with a low speed photodiode of which an ADC measured a voltage. A Labview program was written to maintain and close the feedback loop by controlling the voltage applied to the PZT phase shifter. The stabilized MZI extinction ratio was maintained higher than 20 dB.

Fig.4.5 presents the BER versus the received optical power of the original BPSK channel and the added channel after the extraction. The DPSK receiver was composed of an optical attenuator, a pre-amplifier, a DLI of half the baud rate, followed by a second EDFA amplifier. The optical signal was down converted to the electrical domain using a HP 32 GHz bandwidth photodiode followed by a broad bandwidth data amplifier being before input to an error detector. The BER measured was determined by a data acquisition period of 10 seconds. As seen in the previous chapter with Fig.3.12, once the channel is suppressed by more than 20dB relative to the new channel added at the same spectral position,



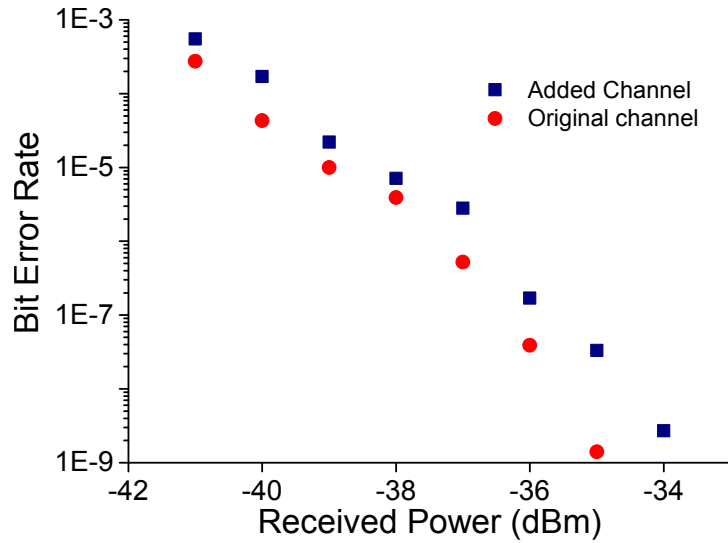


Figure 4.5: BER penalty for the added channel after the suppression of a single channel.

little impact on performance can be observed.

In summary, a preliminary implementation of a optical fiber based MZI was used to confirm the potential of channel extraction using the interferometric suppression that is the core to the TIDE node. High extinction ratio was observed when amplitude, polarization, and time position were aligned. In addition, the fiber interferometer stabilization feedback loop allowed to measure the penalties due to the insertion of a new channel in place of the extracted channel, with little penalty for ER of 20 dB.

### 4.2.2 Simulation

In this part, preliminary numerical simulations of the optical TIDE multiplexer have been carried out in order to plan the experimental implementation and determine the requirements and limitations [17]. In these simulations, the extraction and addition of a channel from a BPSK OFDM super-channel was investigated. The super-channel was composed of seven independent data carrying 10 Gb/s BPSK channels equally spaced by 10 GHz. The transmitter function was bandwidth limited by a second order Gaussian electrical filter resulting in a non-perfect (non-rectangular) pulse shape with a 10ps rise time. As described previously, the penalty associated with a lack of orthogonality due to such slow

transitions can be moderated through adjacent channel relative phase control, thus a  $\pi/2$  phase difference was coded between carriers. Characterization of the super-channel performance before and after the node was evaluated using the direct error counting iterative Monte-Carlo method [62], providing the BER estimation with less than 10% relative error. The performance degradations are plotted relative to the node input figures. While the interferometric suppression function was tested experimentally, numerical simulation offered the tools to determine the optimum transfer function for the complex optical gating function at the core of the TIDE node. Combined with the optical reshaping, the sampling function is critical for the extraction of a sub-channel from the link as to clear the crosstalk, as pictorially shown in the previous section.

The matched filter *sinc* shaped optical function for the demultiplexing and reshaping representing the optical FFT and iFFT were used, and a rectangular gating window width was modified to establish its effect at the output of the node on the channel added in place of the extracted channel as well as the adjacent channels for which minimum impact is required. Fig.4.6 shows the impact of

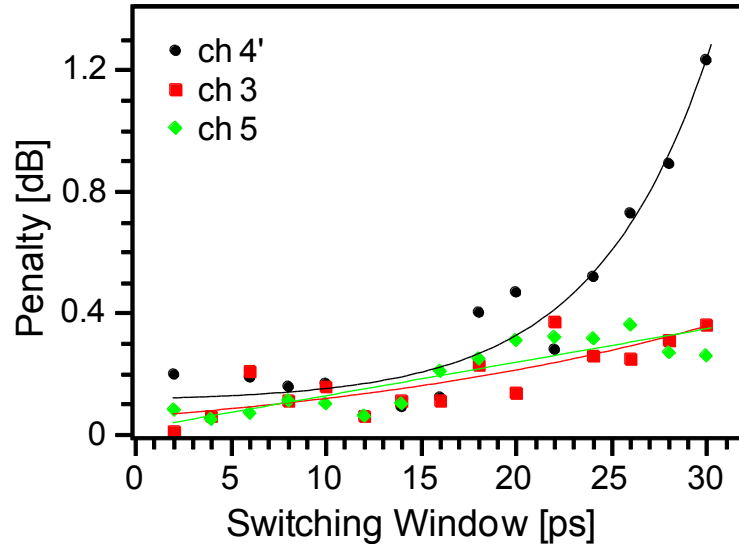


Figure 4.6: Sensitivity penalty versus sampling window. Polynomial fits are displayed for guidance. ch4 is the channel in the middle for the AO-OFDM super-channel, ch3 and ch5 are the adjacent channels. ch4' represents the channel that has been added in place of the extracted ch4.

the optical gate width on the three central channels of the OFDM super-channel, of which the channel 4' is the channel added after the extraction of channel 4.

The manipulated channel is showing most of the penalty when the gating window is broadening as more in-band crosstalk is sampled. It is observed that there is an optimum sampling window width between 10% to 17% of the bit period. For this set of simulations, the ER of the gating was set at unrealistically high values, with a rectangular window of either 0 or 1. However, in optical gating experimental implementations [107–110], more limited extinction ratios are observed. A study of the impact of residual unwanted crosstalk is presented

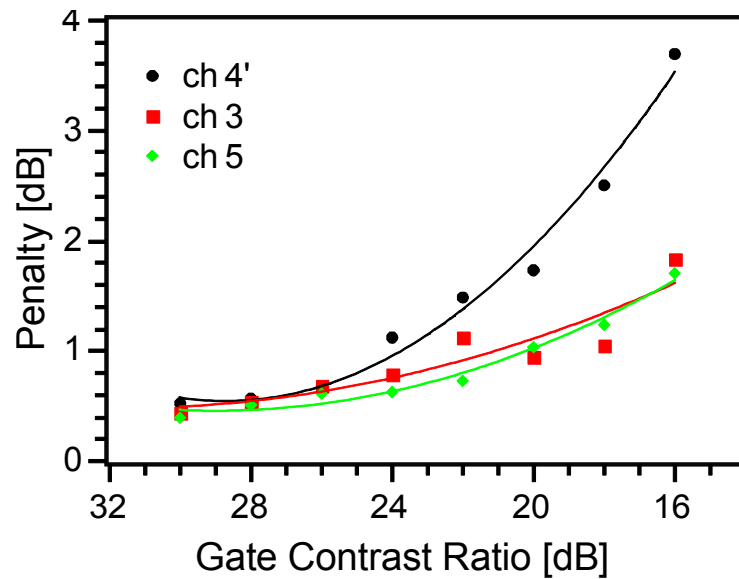


Figure 4.7: Sensitivity penalty versus the gate ER. Polynomial fits are displayed for guidance. ch4 is the channel in the middle for the AO-OFDM super-channel, ch3 and ch5 are the adjacent channels. ch4' represents the channel that has been added in place of the extracted ch4.

in Fig.4.7 where the penalty associated is determined for different extinction ratio values. A greater impact can be observed at ER lower than 26 dB as the penalty is rapidly increasing for the added channel. From these two results an optimum gating function is deduced, with a gating window narrower than 15 ps or 15% of the duty cycle along with a suppression ratio greater than 26 dB.

The final step of theoretical sampling analysis was to include the effects of ASE noise emitted by the optical amplifiers that are part of the TIDE node. It is to be noted that the signal at the input of the node had a large OSNR during this simulations in order to focus on the degradation intrinsic to the scheme. The noise addition to the pulse can be problematic as the sampling window narrows and thus reduces the total signal power. Indeed, as the noise is a random vari-

able, even as the variance of the signal is maintained, noise sampling leads to an increase of the noise variance [111]. Fig.4.8 depicts the sensitivity penalty for the added channel as a function of the switching window and for different gate input power levels. The demultiplexing filter and reshaping filter were set as matched. The extinction ratio was set greater than 30 dB so the direct impact of the sampling window and the OSNR degradation can be highlighted. Three main regions can be identified, corresponding to three sampling window ranges. The central one shows the lowest degradation of the central sensitivity, from 10 ps to 20 ps, for a wide range of input power. Larger signal sampling results in higher degradation as seen previously due to crosstalk not being excluded. The main impact of the presence of a ASE noise source in the node is located in the sub 10 ps wide window range, where the channel power at the input of the gate range from -2 dBm to +10 dBm. Low power at the output of the optical gating is the result of a narrow selection of the total signal power and thus the system functioning in a lower OSNR regime at the output of the reshaping filter.

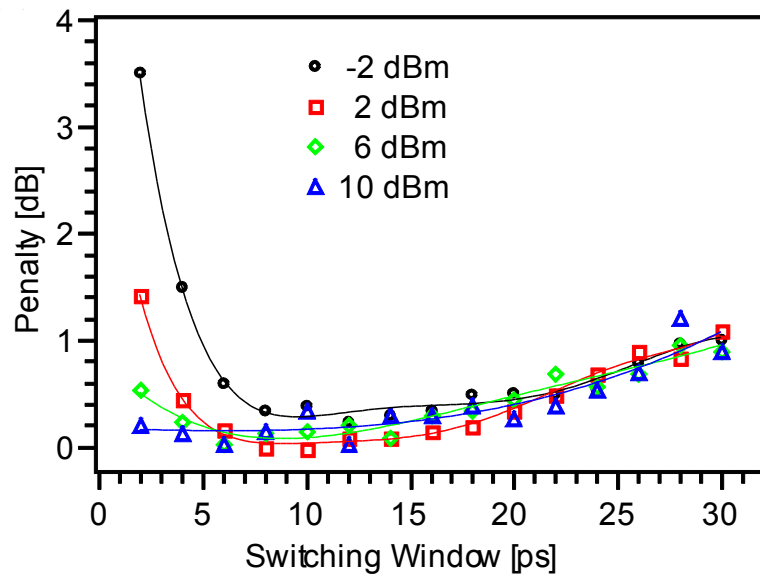


Figure 4.8: OSNR penalty versus sampling window and gate input power. Polynomial fits are displayed for guidance. ch4 is the channel in the middle for the AO-OFDM super-channel, ch3 and ch5 are the adjacent channels. ch4' represents the channel that have been added in place of the extracted ch4.

From analytical simulations, optimum performance regions had been determined and provided direction to design and implement the experimental system. For the optical gating, a contrast ratio greater than 30 dB and an optical

switching window in the range from 10 ps to 20 ps is required. In addition, to reduce the sensitivity degradation at the output of the TIDE node, the optical gating implementation is required to be able to tolerate more than 0 dB optical power as input.

In conclusion, the gating window width was optimized using numerical simulations where a tradeoff between short widths and long pulse widths exists. A narrow pulse train approaches the ideal Dirac comb which would sample only the bit pattern required at the ideal sampling instant and avoid residual crosstalk, whereas a larger pulse reduces the impact of sampling induced noise enhancement. More intuitively, in order to maximize signal energy, the gate selects as much of the middle part of the eye diagram as possible whilst still suppressing the adjacent parts influenced by the residual crosstalk.

### 4.3 Experimental implementation with single quadrature signal super-channel

With the valuable indicators obtained in the previous section using a simplified experiment and analytical simulation, the experimental implementation of the Terabit Interferometric add, Drop, and Extract node was undertaken. The experimental demonstrator system was composed of two main parts, starting with the BPSK AO-OFDM transmitter and then followed by the interferometric extraction. The extraction function is divided into sub-functions in this section, such as the optical demultiplexing of the channel to be extracted, the optical gating or optical sampling function used to re-time and remove crosstalk, and finally the reshaping function used to match the channel in the two arms of the interferometer to efficiently suppress the drop data from the super-channel. In addition to the transmitter and the interferometric extraction, the add function, the fiber interferometer stabilization circuitry, and the coherent receiver completed the set-up. The AO-OFDM transmitter was the one previously described, seeded by a fiber laser with a kHz class linewidth positioned at a wavelength of approximately 1552.7 nm, then modulated using a pulse pattern generator (PPG) generating a 10 Gb/s  $2^{15} - 1$  bits long pattern resulting in a 10 Gb/s BPSK channel. The ten channel 100 Gb/s AO-OFDM super-channel was polarization aligned by minimizing the optical power of one of the two outputs of a polarization beam splitter at the output of the transmitter. On the receiver side, a second independent fiber laser acted as LO for the coherent receiver, with the light source tuned within 100 MHz of the center of the channel of interest. In the case of AO-OFDM, the signal was sampled at approximately 8 electrical samples per bit before applying a sinc-function matched filter. Standard DSP algorithms were employed as described in the previous chapter [80].

Fig.4.9 is a schematic description of the experimental implementation of the TIDE node, used to demonstrate the all-optical ROADM function for AO-OFDM. The AO-OFDM transmitter is extensively described in the previous chapter with a laser source being externally modulated by a MZM, followed by an optical comb generator and then an odd/even super-channel emulator. The most complex function for a node capable of routing sub-channels in a very dense WDM or overlapping spectrum, described as Extract function, is contained in the blue frame, formed of path A and path B. The path A represents the through path, receiving 10% of the optical power of the AO-OFDM super-channel. It contains

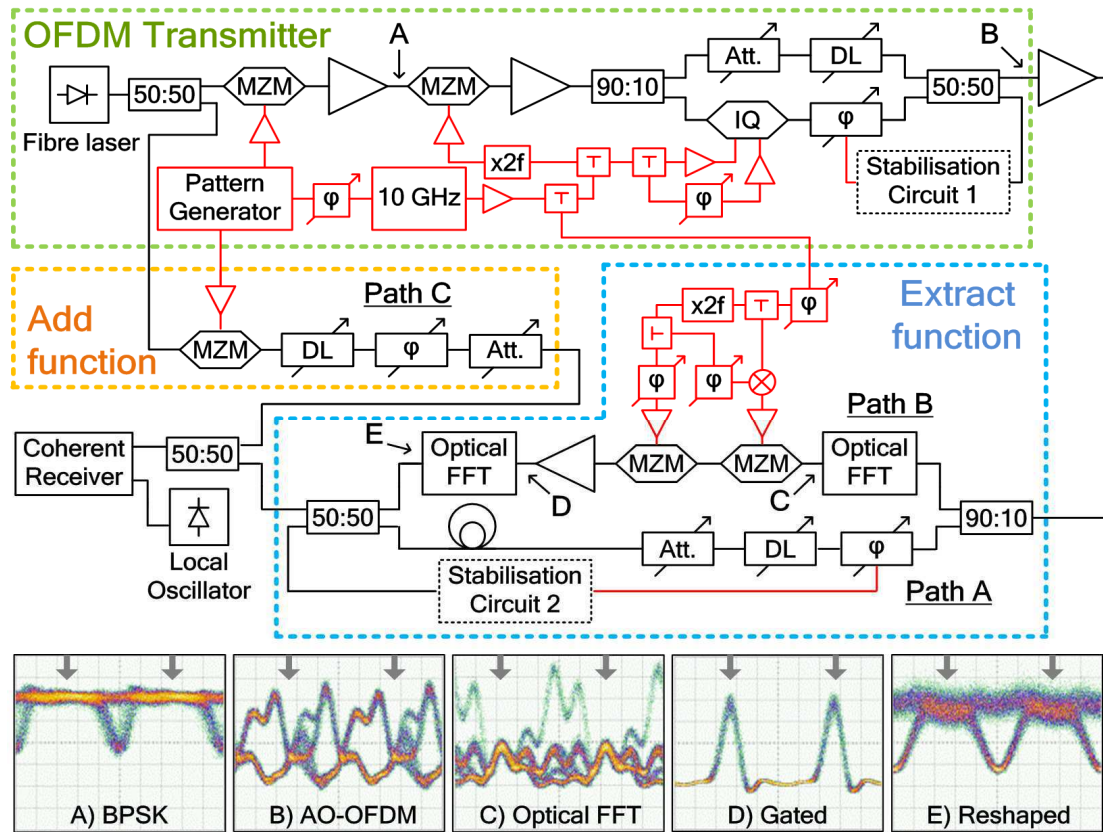


Figure 4.9: Top: Experimental setup of the BPSK AO-OFDM transmitter (top, green frame) and of the proposed all optical ROADMs with drop and extract function (bottom, blue frame, path A and B) and emulation of the add function (middle, orange frame, path C). Polarization controllers and monitoring couplers not pictured for clarity. Black and red lines signify optical and electrical paths respectively. MZM: Mach-Zehnder modulator, DL: tunable delay line,  $\varphi$ : tunable phase shifter, Att.: tunable attenuator, IQ: dual parallel MZM,  $\otimes$ : mixer, triangles represent optical or electrical amplifiers. Bottom: Intensity eye diagrams at various points: A) individual channel before super-channel multiplexing, B) BPSK AO-OFDM super-channel, C) demultiplexed channel after optical channel selection through optical FFT filter, D) sampled channel after optical gating, and E) reshaped channel prior to interferometric extract operation. Arrows represent the center of the eye. Time window equals to two bits period.

a fiber wrapped piezo-electric ceramic cylinder used as an optical phase control, followed by an optical delay line used to exactly match the paths A and B. Power and polarization control was contained in path A, concluded by a 50:50 optical coupler. Path B represents the channel extraction and reshaping function used to interferometrically suppress it from the super-channel when path A and B are combined. It consists of three sub-functions, channel demultiplexing, optical gating, and channel reshaping, described in sub-section 4.3.1, 4.3.2, and 4.3.3

respectively. The path B consists of an optical FFT to demultiplex a channel, followed by two MZMs performing the optical gating. Due to the total optical power decrease after the signal sampling, an optical amplifier was required to maintain the OSNR performance of the node, as described by the analytical simulation. The return-to-zero coded channel was then reshaped into a non return-to-zero waveform with a second optical FFT before being recombined with the super-channel signal. When the two paths were summed with the out of phase signals for the channel to be extracted, the allocated spectrum was freed to be filled with a new channel. Since a channel was extracted from the super-channel, a new channel could be introduced at the same frequency. For the experimental demonstration, the add function was implemented by adding a third arm to the optical interferometer, named path C in Fig.4.9. The add path had to be carefully aligned to the two other arms both in power, polarization, and time. The time delay was set to be an exact integer number of bits and the polarization alignment was controlled using a polarization beam splitter at the output of the node. The new channel to be combined into the AO-OFDM super-channel was generated using the second port of the pattern generator through a different data modulator to the AO-OFDM transmitter. However, the optical carrier originated from the same laser so the added channel was well aligned to the freed spectrum after the drop function. Optical carrier extraction has been previously demonstrated and could be readily implemented in order to obtain a system with solely an external optical reference [112]. While the AO-OFDM super-channel transmitter was completed with a stabilisation circuit, the added channel wasn't phase controlled relative to the adjacent channels as the detection was realized without optical demultiplexing. Indeed at the difference of the approximation of the matched filter obtained during the implementation of the optical FFT, both the transmitter and the digital filter at the receiver were of sufficient quality as to have a small phase dependent impact on the overall performances. As it has been seen in Fig.3.18, the digital filter used to demultiplex the channel at the receiver mitigates the need for the optical phase control of the adjacent channels.



### 4.3.1 Optical Demultiplexing

The first sub-function of the extract part of the node is the demultiplexing of the channel to be dropped and extracted from the super-channel. The use of cascaded DLI based optical FFT had been successfully proved to be an appropriate AO-OFDM demultiplexer [61]. Optimum FFT filters require  $n$ -stages following the rule described as:  $2^n \geq N$  to demultiplex a channel of a AO-OFDM super-channel,  $N$  channels wide. While the AO-OFDM signal generated at the transmitter was composed of ten channels, only a two stage optical FFT was implemented due to inventory limitation. An optical filter of 0.4 nm was set to suppress the unfiltered channels due to the lack of the third and fourth order DLI required for an optimum FFT operation.

The signal from a 20dBm optical amplifier was placed at the input of the TIDE node to maintain a low noise figure for the OADM. The 90% output of the first coupler of the node implementation was selected as the input for the optical demultiplexer, with an initial polarization control before the polarization dependent Kyliia DLI used for the channel selection. A first DLI of FSR twice the symbol-rate suppressed every second channel whereas a second DLI of FSR four times the symbol-rate suppressed every fourth channel. Since much of the measurement occurred for the central channel and since the AO-OFDM super-channel was ten channels wide, the channels positioned at four times the symbol-rate from the channel of interest were not filtered. In order to complete the channel selection, a Gaussian shaped 50 GHz optical filter was added after the DLIs.

Fig 4.10 shows the selection of a channel from the AO-OFDM super-channel, with the clear suppression of the first three pairs of adjacent channels as expected from a second order optical FFT filter. However a poor suppression of the  $\pm 40$ GHz channels is clearly visible as the slow roll-off of the optical 0.4 nm filter attenuated the unwanted channel only by approximately 8 dB. Since the channels are phase modulated for the demonstration and the odd/even nature of the experimental AO-OFDM super-channel, the amplitude modulation due to the poor side-bands suppression has no impact on the transmission and the extraction function was achieved. The eye-diagram C) of Fig4.9 clearly shows a crosstalk free time during each bit period. The next sub-function, optical sampling, was hence required to fully demultiplex the channel to be extracted from the super-channel.

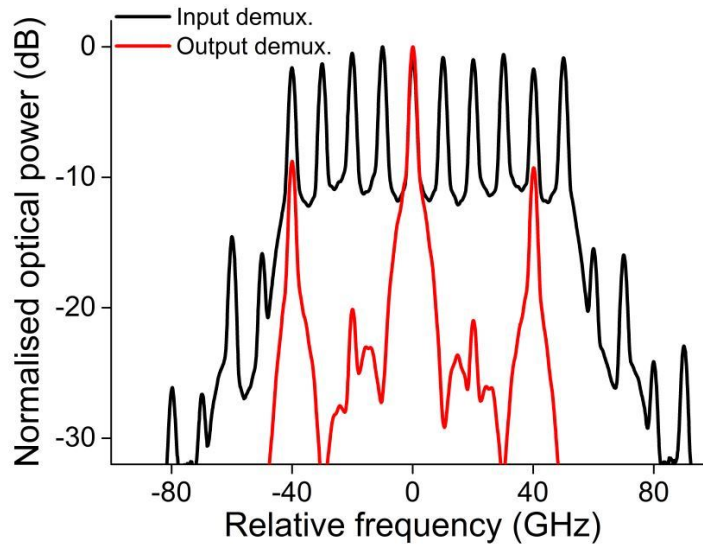


Figure 4.10: Spectrum of the ASK AO-OFDM super-channel at the input of the node (black) and spectrum of the channel demultiplexed for the reshaping (red).

### 4.3.2 Optical Gating

In order to extract this channel from the AO-OFDM super-channel, the dropped channel needs to be reshaped, so that it may be interferometrically subtracted from the AO-OFDM signal. Since low crosstalk is only obtained at the optimum sampling instant (indicated by arrows in Fig4.9 A), B), C), D), and E), an optical gate was used after the FFT based filter to remove the crosstalk at other possible sampling times. The level of this crosstalk is of course influenced by imperfect filtering in the TIDE node and finite transmitter bandwidth, both of which impact the adjacent channels orthogonality required in OFDM. The optical gate selects the time period corresponding to the dropped channel bit during each OFDM symbol. From the numerical simulation, we know that high power is required at the input of the gate in order to maintain low sampling noise. In addition, long time stability is highly important for the optical node to work. In the light of those requirements, the Mach-Zehnder modulator based solution [109] was selected for the experimental implementation of the optical gating. Others gating techniques based on Electro-Absorption Modulator (EAM) [107] or Semiconductor Optical Amplifier (SOA) [108] can not provide the high ER while maintaining losses low, the full band wavelength flexibility, nor the tolerance for high power input.

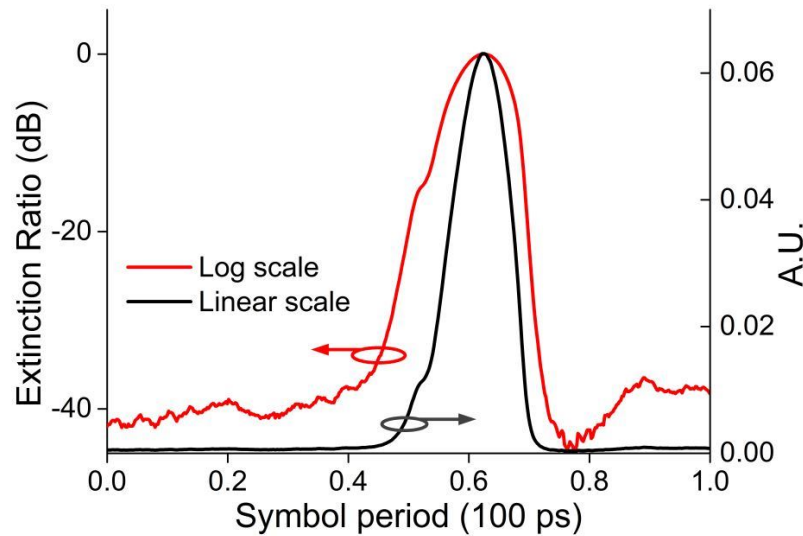


Figure 4.11: Optical pulse obtained from the optical gating cascaded MZMs structure when time scanned using few picoseconds wide pulse.

The optical sampling in the node was obtained by driving two optical MZMs so they produce a short pulse train. The first MZM was driven by a strong 20 GHz RF signal and biased at quadrature to produce a narrow pulse train. The second MZM suppressed every second pulse. To maximize this suppression, the drive signal for this MZM was obtained by modulating the 20 GHz signal by a 10 GHz RF signal using a broadband mixer and time aligning the resultant electrical pulse. The sampling window obtained has a FWHM of 11.6 ps and an extinction ratio greater than 35 dB, as shown by Fig 4.11.

Fig 4.12 shows the spectral broadening of the demultiplexed channel due to the optical time gating, with the first stage providing higher repetition rate narrow pulses while the second stage gives a RZ-BPSK signal at the original symbol-rate. The sampled output is shown in Fig 4.9 D) where a phase modulated RZ signal is observed, free of any noticeable crosstalk. With the combined demultiplexing and gating functions, the channel to be extracted from the super-channel was successfully differentiated from the AO-OFDM signal going through the optical node. The resulting return-to-zero data pattern obtained is clear from crosstalk from the adjacent channels by the FFT-like filtering and the optical sampling.

In order to determine the requirement in term of phase alignment accuracy, the reshaped channel (the optical reshaping sub-function will be described in next section) was received using a coherent receiver and optical wide-band oscillo-

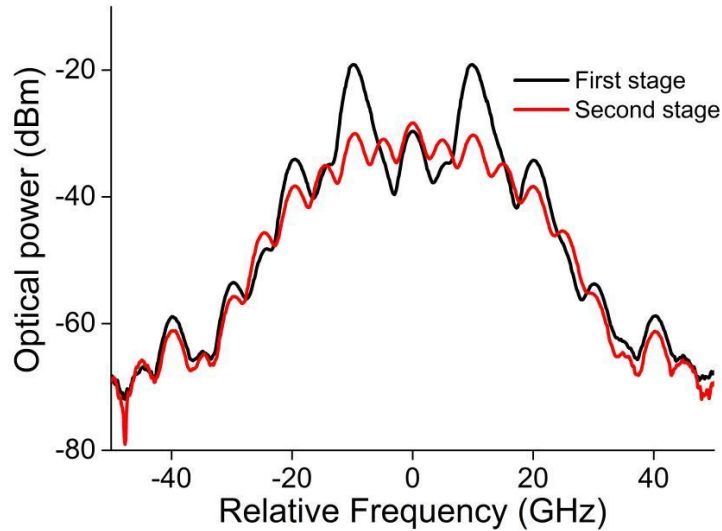


Figure 4.12: Optical spectrum obtained from the optical gating cascaded MZMs structure at the output of the first and second MZM.

scope.

$Q^2$ -factor penalties induced by misaligned sampling timing with a selection of corresponding eye-diagrams of the resulting reshaping are shown in Fig 4.13. In addition to showing the impact of the time alignment of the optical gating on the reshaping of the extracted channel (measured at point E) in Fig 4.9), the narrow operating range shown in the figure confirms the requirement for a narrow optical gating window to reduce the residual crosstalk and so obtain a clear RZ-BPSK signal.

### 4.3.3 Optical Reshaping

The optical reshaping of the channel to be extracted is the last sub-function in the parallel path before the recombination and interferometric suppression from the AO-OFDM super-channel. Conceptually, it consists of a FFT function that transforms the pulsed bit pattern into a rectangular bit of time length equal to the inverse of the symbol-rate, as for a standard NRZ single channel. As has been explained previously, only an approximation of the FFT function could be implemented so a preliminary study had been carried out to determine the filter giving the reshape closest to a single channel. For this experiment and due to the DLI available at the time, the super-channel used was composed of ten

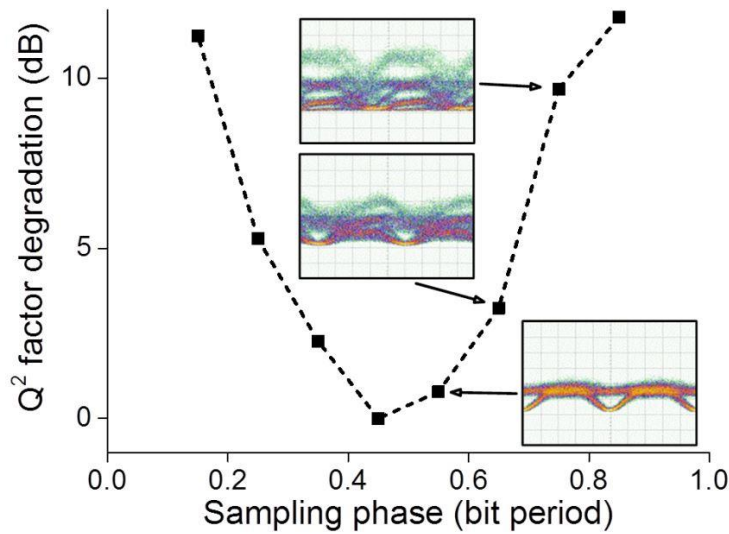


Figure 4.13: Q<sup>2</sup>-factor degradation for the reshaped AO-OFDM channel as function of the time position of the optical sampling within the period, eye-diagrams showing the reshaped BPSK channel for different sampling position.

10.7GHz ASK coded channels. As before, the channel was demultiplexed before being optically sampled at the rate of 10.7 GHz. Different filter configurations are investigated to obtain the most rectangular bit pattern, as for the initial ASK channel. Fig.4.14 shows the eye-diagram over more than two periods for a selection of four filter configurations.

The corresponding optical spectra are presented in Fig.4.15. In the first configuration, the delay lines used have a FSR of 21.4 GHz and 42.8 GHz respectively. The additional amplitude modulation observed on the high level can be explained by linking the time trace to the spectrum where strong secondary components were observed due to inappropriate filtering. Such additional spectral components would affect the adjacent channels when interferometrically recombined with the super-channel. The second configuration based on a Yenista tunable narrow filter is capable of sub-10 GHz bandpass with a steep roll-off. The optimum eye-diagram shows an over-filtering as the clear slow transitions are visible, when broadening the filter bandpass range was resulting in large amplitude modulation. The third configuration was based on the programming of a WSS with the matching transfer function for the reshaping i.e. the sinc function. However because of a resolution limitation of 10 GHz Gaussian filter shape of available WSS devices, complex transfer functions such as sinc can only be approximated. Degraded eye-diagrams were observed because of

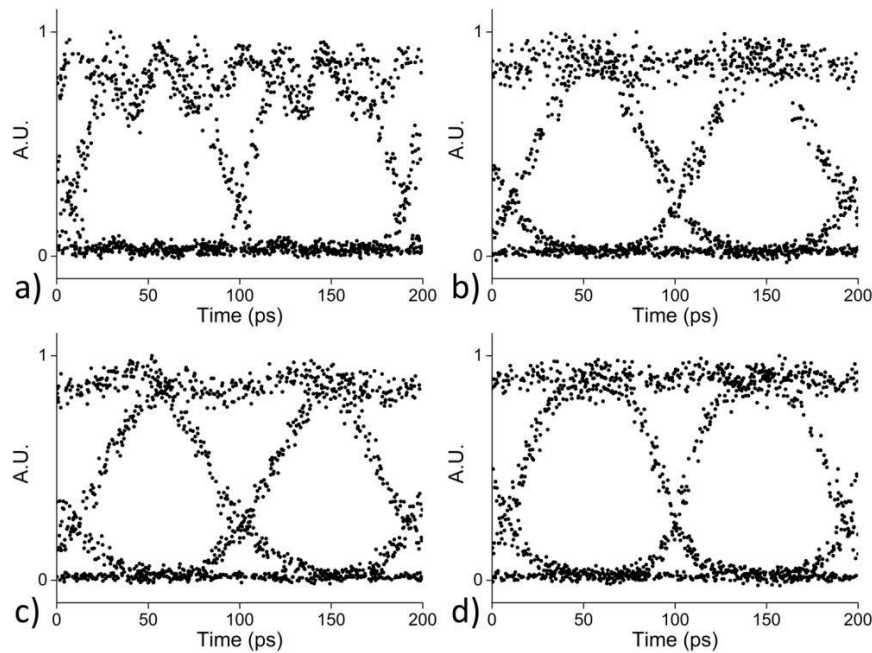


Figure 4.14: Eye-diagram of the reshaped channel for different filter configuration (from ASK AO-OFDM, 10.7 GHz symbol-rate ) a) Two cascaded delay line interferometers, b) Narrow filter (Yenista), c) Sinc function programmed WSS with dual pass configuration, and d) Two cascaded delay line interferometers follow by a 35 GHz bandpass programmed WSS.

limited extinction and filter shaping, the WSS device was used in a dual pass configuration so as to apply the transfer function twice to the optical signal. As for the Yenista filter configuration, very strong over-filtering was observed due to the limit of the device at such a narrow channel setting. The last configuration was a combination of the two cascaded DLI, to handle the narrow filtering function, and of the flexibility of the WSS programmed as a 35 GHz bandpass filter. The eye-diagram presented faster transitions as the spectrum broadened with no excessive amplitude modulation.

In the case of the full experimental implementation of the TIDE node with the 100 Gb/s BPSK AO-OFDM super-channel, the reshaping could only be setup using a first stage 20 GHz DLI followed by a WSS programmed as a 18 GHz bandpass filter. That resulted in an over-filtering of the channel in order to keep higher frequency component perturbation at a minimum. However, the eye-diagram E) from Fig.4.9 shows appropriate reshaping of the channel to be extracted, with a large sampling point free of crosstalk, proving the full reconstruction of the channel demultiplexed from the AO-OFDM super-channel.

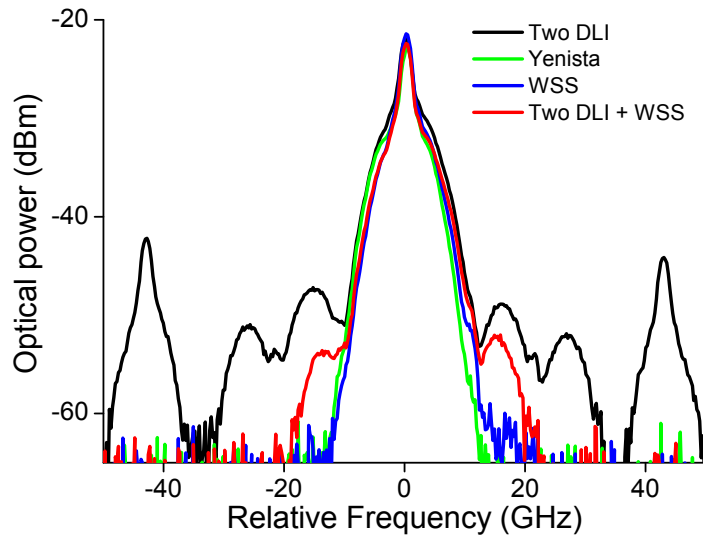


Figure 4.15: Spectra of the reshaped channel for different filter configuration (from ASK AO-OFDM, 10.7 GHz symbol-rate)

#### 4.3.4 All-Optical TIDE node experimental results

The channel dropped, gated and reshaped was combined with the copy of the original AO-OFDM signal. Consequently, the channel of interest was suppressed from the super-channel when the two arms were path matched, polarization aligned, power matched, and out of phase, as illustrated in Fig.4.16. Channel rejection higher than 20 dB may be observed at the output of the ROADM. However, the experimental node demonstration was based on optical fiber and discrete devices in a research laboratory environment, where the optimum interference condition may only be achieved for a short period of time. A second stabilization circuit was implemented in order to mitigate the thermally and mechanically (fan) induced phase difference between the two arms of the extract interferometer. A phase locked loop circuit (stabilization circuit 2 in Fig.4.1) was implemented by controlling the phase relation between the interferometer arms using a second PZT fiber stretcher. The power at the output of the drop interferometer was monitored with a low speed photodiode to control the signal of both arms to be out of phase. In order to follow the power variation at the wavelength of the dropped channel a narrow filter (bandwidth less than the signal bandwidth) was placed before the photodiode. In addition to the filter and to increase the sensitivity of the stabilization circuit, a 27 kHz dithering tone was added to the super-channel. The optical signal carrying the small variation

was down converted using the photodiode before being amplified and mixed with the original dithering signal. The lock-in amplifier circuitry followed by appropriate electrical filtering allows for high sensitivity and consequently good stabilization performance. Digital processing was used to close the loop and control the phase difference between the interferometer arms through a fiber stretcher. The feedback circuitry stabilized the drop function operation, with a reasonable channel rejection in the range of 10-15 dB. Note that since different filters were used for each function in this demonstration, with an electrical filter shaping the transmitter pulses and an optical FFT filter was the pulse shape within the node, a small mismatch in the pulse shapes was observed, which in consequence slightly degraded the quality of the interference pattern.

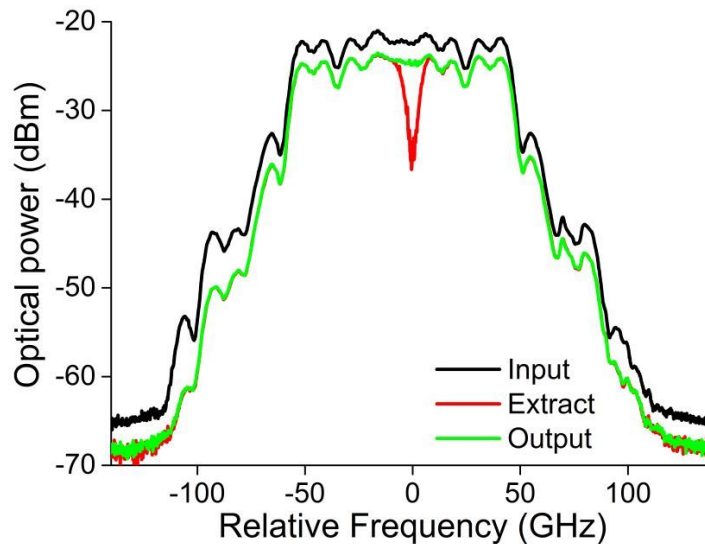


Figure 4.16: Optical spectrum of the BPSK AO-OFDM signal at the input of the node (black), after one channel was extracted (red) and after the addition of a new channel at the output of the node (green).

The add function was implemented by adding a third arm to the optical interferometer. As previously stated, this arm had to be carefully aligned to the two other arms both in power, polarization, and time. The time delay was set to be an exact integer number of bits and the polarization alignment was controlled using a polarization beam splitter at the output of the node. The new channel to be combined to the OFDM super-channel was generated using the second port of the pattern generator through a different data modulator to the OFDM transmitter. However, the optical carrier originated from the same laser so the added channel was well aligned to the freed spectrum after the drop function. Optical



carrier extraction has been previously demonstrated and could be readily implemented in order to obtain a system with solely an external optical reference [33]. The output of the TIDE node was consequently a single polarization AO-OFDM super-channel carrying a new set of information on one of its subcarriers. Since the matched filter in the coherent receiver closely approximated the ideal pulse shape the residual crosstalk was low, and no phase control was required for the add channel.

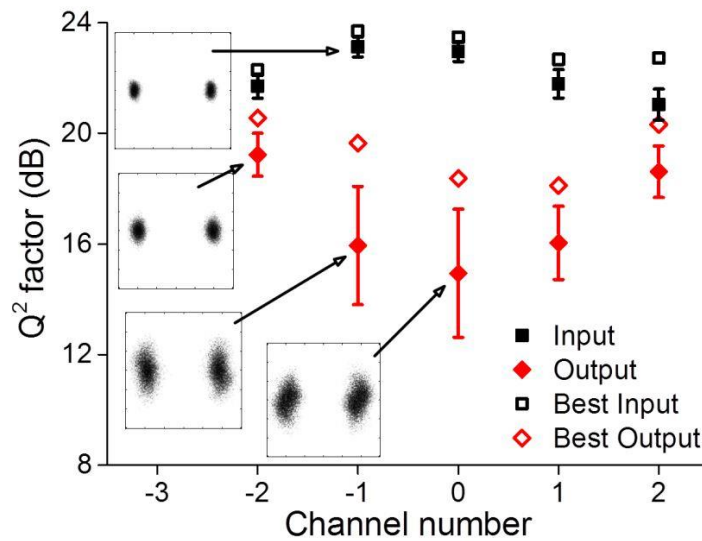


Figure 4.17:  $Q^2$ -factor measurement for the five central channels BPSK modulated: Input (square) and Output after extraction and addition (diamond). Channel zero carrying new data after extract function. 160k sample per acquisition, statistics over 40 continuous acquisitions.

Performance measurements were taken at the coherent receiver for the AO-OFDM signal before and after the optical node. Fig.4.17 presents the  $Q^2$ -factor measured for the five central channels, the channel labeled no.0 being the one where the drop and add function occurred. The error bars represent one standard deviation obtained from 40 measurements of 160k samples and illustrate the fluctuations in  $Q^2$ -factor due to residual drop interferometer variations. In addition, the mean  $Q^2$ -factor (solid symbols) and the best  $Q^2$ -factor (open symbols) from these sets of measurement are presented to show the potential of such scheme if it was integrated and/or fully stabilized. When a new channel was added in place of the vacant spectrum, penalties were observed due to the imperfect channel drop.  $Q^2$ -factor degradations are believed to be due to: (i) a residual mismatch between the pulse shape of the original and reshaped signals, (ii) mean phase errors due to phase dithering to stabilize the TIDE node and (iii)

excess amplified spontaneous emission due to noise sampling and the insertion loss of the FFT's and the optical gate. Due to a sharp trade-off experienced during WSS profile optimization between under-filtering, resulting in sharp transitions but residual sidebands from the optical gating, and over-filtering, resulting into slower bit transition and poor interferometric suppression, we believe that pulse shape matching dominated the performance. Comparing the subplot A) and E) in Fig.4.9 is a good illustration of the limitation of this first experimental implementation. The degradation of the reshaped channel can be observed from the broadening of the transition period in the bit period, along with the residual crosstalk due to the imperfect demultiplexing filter. The use of higher FFT order, appropriate transmitter pulse shaping and/or a more versatile WSS should therefore reduce the observed penalty significantly. The Fig.4.17 insets display the BPSK constellation diagrams for  $Q^2$ -factor values for individual measurements close to the average value for each channel. The figure clearly shows good performance at the output of the TIDE node. As expected, the penalty was greatest for the wavelength at which channel had been extracted and added, even if it is interesting to note it remained with considerable margin above the 7% FEC threshold (8.3 dB).

Fig.4.18 presents the BER measured after off-line processing of channels at different points of the TIDE node versus OSNR. The signal to noise ratio was degraded before the receiver by attenuating the received power at the input of the receiver amplifier while the signal optical power was kept constant at 3 dBm at the photodiode. The "add channel" was the set of new data inserted in the super-channel to occupy the frequency slot freed by the extraction function, and so represents the optimum performance of a single channel for this experimental implementation. The measurements called "OFDM" and "demux" represent the performance of the central channel contained in the AO-OFDM super-channel and demultiplexed by two cascaded DLI and a 0.4 nm filter. It is interesting to notice the identical performance as the adjacent channel crosstalk is still present after the demultiplexing and thus equally so when embedded. A small improvement in sensitivity was observed for the channel sampled and reshaped as the gating function inherently removes part of the crosstalk and the reshaping function is mainly spreading the sampled information from a fraction of the period to the full bit period. The output of the node was measured with the central channel, which sees a channel extraction and a channel addition, as well the two immediate neighbors, situated left and right. Due to the causes described earlier on, sensitivity degradation was observed for the three channels with a

greater impact on the central channel. However, measurements show performance within the requirement for a 7% FEC algorithm even for an OSNR of 10 dB.

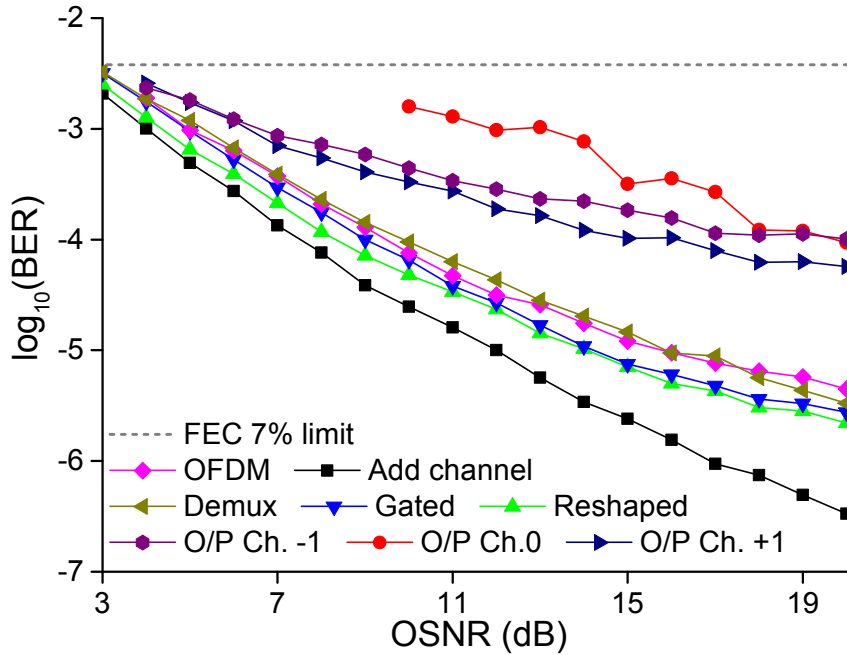


Figure 4.18: BER measurement in function of OSNR at receiver at different point of the TIDE node. OFDM: sub-channel to be extracted at the input of the node (Ch.0, at the center of the super-channel), Add channel: single channel performance, Demux.: sub-channel being demultiplexed from the superchannel, Gated: sub-channel being optically sampled, Reshaped: sub-channel copy before the recombination with the super-channel. O/P: performance measurement at the output of the node after the extraction and the add of the central sub-channel (Ch.0), Ch. $\pm$ 1 are the adjacent sub-channels.

The first experimental implementation [20] of the TIDE node concept was successful as it demonstrated the extraction of a BPSK channel from a AO-OFDM signal, by means of demultiplexing, optical gating and optical reshaping before its interferometric suppression from a super-channel. While signal degradation was observed due to FFT function approximation, laboratory environment implementation and penalties inherent to the use of standard discrete devices, it is remarkable that the performance was maintained above standard FEC correction mechanisms.

## 4.4 Experimental implementation with dual quadrature signal super-channel

Whilst the positive result presented in the previous section is encouraging, little net benefit is derived from overlapping carriers at the symbol rate if only one quadrature is used for modulation. While it is clear that the TIDE node will be compatible with broader super-channels, it is critical that the concept is compatible with more spectrally efficient modulation formats employing both quadratures. Here we verify compatibility with QPSK formatted super-channels.

### 4.4.1 Experimental setup modifications

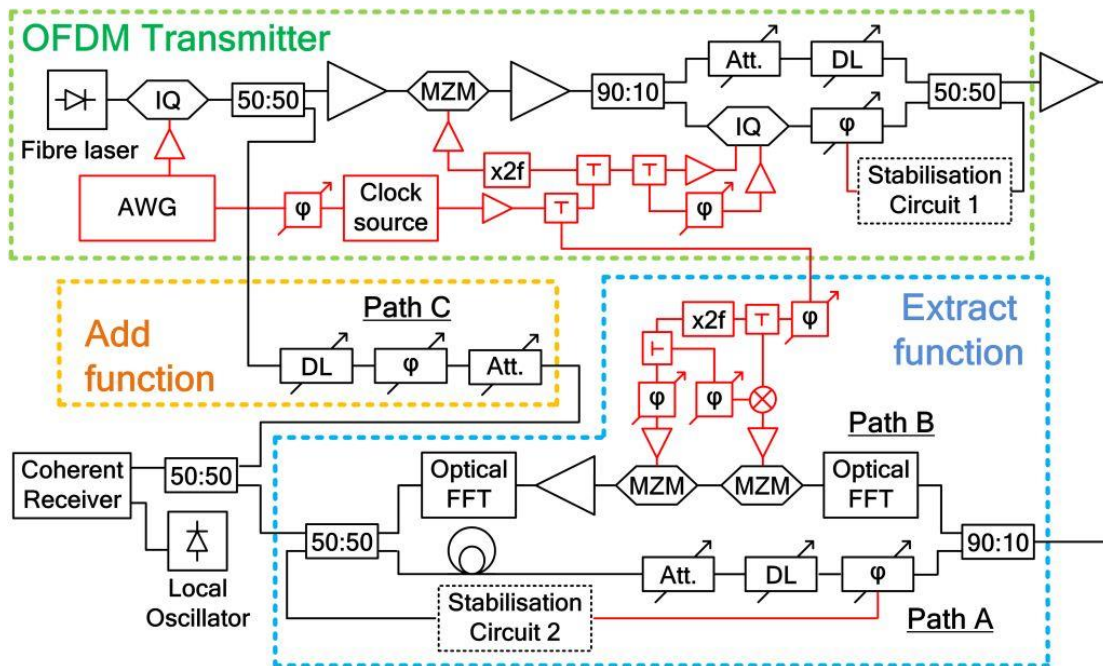


Figure 4.19: Top: Experimental setup of the QPSK AO-OFDM transmitter (top, green frame) and of the proposed all optical ROADM with drop and extract function (bottom, blue frame, path A and B) and emulation of the add function (middle, orange frame, path C). Polarization controllers and monitoring couplers not pictured for clarity. Black and red lines signify optical and electrical paths respectively. MZM: Mach-Zehnder modulator, AWG: arbitrary waveform generator, DL: tunable delay line,  $\varphi$ : tunable phase shifter, Att.: tunable attenuator, IQ: dual parallel MZM, triangles represent optical or electrical amplifiers.

A small number of minor modifications were applied to the experimental implementation of the node. In order to minimize the amount of ASE noise generated

from the amplifier situated in the reshaping arm of the interferometer, all monitor taps were removed before the gating function. In addition, an improved optical FFT was used for both channel selection and reshaping. The channel selection was obtained using a cascade of tunable DLI of FSR 20 GHz and 42.8 GHz respectively, and a WDM interleaver of FSR 50 GHz was used to select a single channel. Although a slight frequency misalignment was unavoidable in the second (athermal) DLI used, the overall transfer function of the optical filter offers a large improvement in the channel selection particularly for the suppression of the channel located at  $\pm 40$  GHz from the channel selected, as for Fig.4.20.

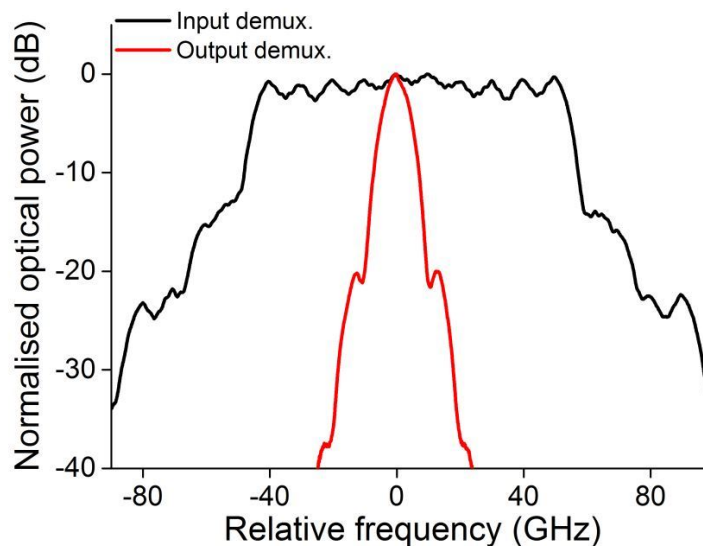


Figure 4.20: Spectrum of the QPSK AO-OFDM super-channel at the input of the node (black) and spectrum of the channel demultiplexed for the reshaping (red).

#### 4.4.2 QPSK channel reshaping

The reshaping function was obtained by cascading two DLIs, of FSR 20 GHz and 40 GHz, along with a sharp optical filter to remove the additional frequency components remaining from the incomplete optical FFT function. Similarly to the improvement observed on the demultiplexing sub-function by the experimental setup modification, the use of the two DLI devices offered a closer approximation to the FFT function filter shape and thus improved reshaping was obtained. Fig.4.21 shows the broad spectrum of the RZ-QPSK after the optical

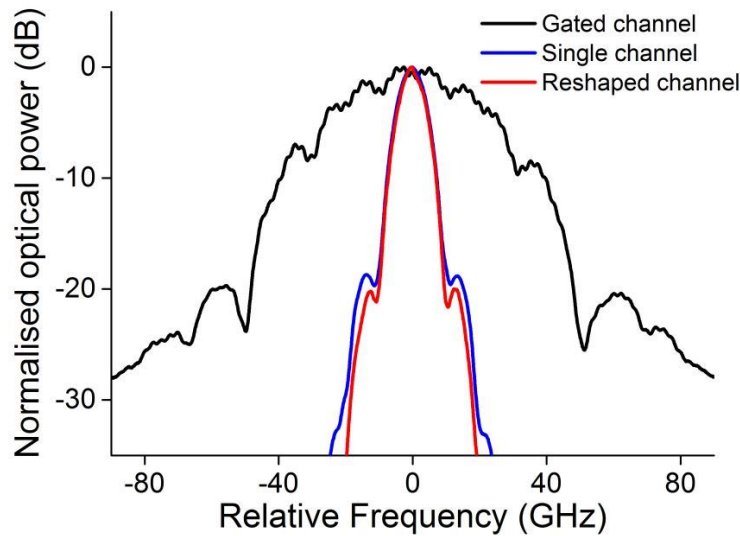


Figure 4.21: Spectrum of the QPSK channel at the output of the gating function (black), at the output of the single channel transmitter (blue), and after the reshaping functions.

gating and the spectrum of the reshaped channel to be extracted as well the original QPSK channel for comparison. Small over-filtering is observable at the first and second lobe of the spectrum.

Fig.4.22 shows the eye-diagrams and time trace of the channel to be extracted at different points of the reshaping path of the extracting interferometer. Subplot 4.22a presents the accumulation of approximately 20 eye-diagrams over a two bit period. While the crosstalk is contained within one half of the bit period, because of a denser QPSK signal transition point, the optimum sampling point is more difficult to select than for the BPSK experiment. However, subplot 4.22b shows a clear RZ-QPSK pulse pattern with low unwanted signal. Subplot 4.22c and 4.22d are the time trace, with a horizontal scale of 200 ps/div, of the "Add" channel acting as reference and the reshaped channel at the same time position. Despite a slower transition for the reshaped channel, the signal was properly extracted from the super-channel, sampled and reshaped into a clear single channel.

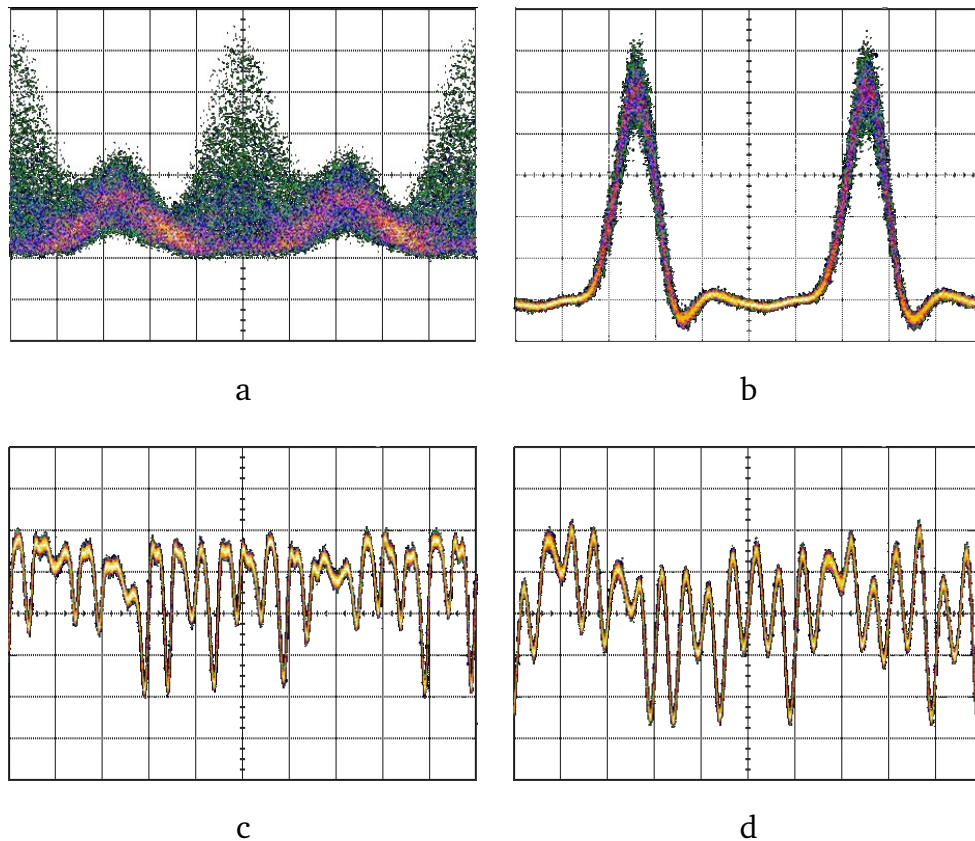


Figure 4.22: Eye-diagram and time trace of the reshaped QPSK channel. a) Eye-diagram of the demultiplexed QPSK channel (two symbols long time window). b) Eye-diagram of the sampled QPSK channel (two symbols long time window). c) Time trace of the QPSK single channel (20 symbols long time window). d) Time trace of the QPSK reshaped channel (20 symbols long time window)

### 4.4.3 All-Optical TIDE node experimental results

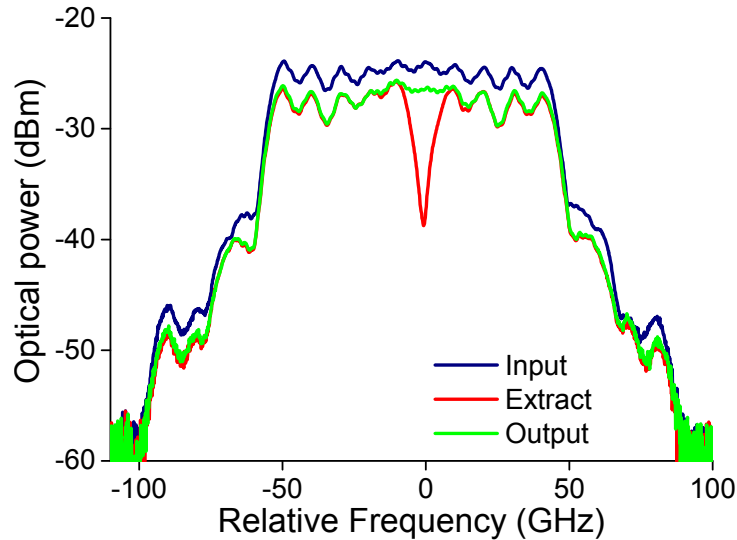


Figure 4.23: Optical spectrum of the QPSK AO-OFDM signal at the input of the node (black), after one channel was extracted (red) and after the addition of a new channel at the output of the node (green)..

The TIDE node was completed by adding new data to the channel cleared by the extract function. For QPSK data, the same optical modulator was used for the original super-channel and for the channel added, with the add channel data decorrelated from the super-channel by the path length delay. Fig.4.23 displays the optical spectrum for the input super-channel, the channel drop and the resulting super-channel with the new channel added. With the assistance of the second stabilization circuit, the channel suppression was maintained higher than 10 dB. This is identical to the previous section, since the dither based feedback loop, based on the suppression of the channel power, is not affected by the modulation format.

For each data point, the coherent receiver recorded 40 sets of 160k samples that were processed offline. When receiving a single QPSK channel, the average  $Q^2$ -factor measured from the EVM was 21.5 dB. The laser, used both at the transmitter and at the receiver had a narrow tunable range only allowing the measurement of the central channel where the drop and add occurred and the adjacent channels. Fig.4.24 presents the measurement of the super-channel at the input of the optical node and at its output when the central channel had been suppressed and new data had been added. Identically to the data in Fig.4.17,



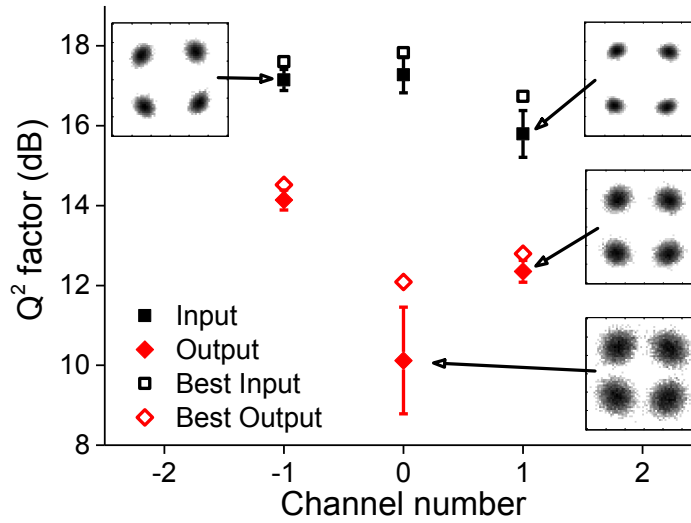


Figure 4.24:  $Q^2$ -factor measurement for the five central channels QPSK modulated: Input (square) and Output after extraction and addition (diamond). Channel zero carrying new data after extract function. 160k sample per acquisition, statistics over 40 continuous acquisitions.

the main degradation is observed on the central channel. Nevertheless the performance is maintained above FEC limits. Adjacent channels were somewhat affected but to a lesser extent due to the improved channel reshaping implemented for the quadrature modulation format. The standard deviation of the  $Q^2$ -factor results for those channels was also reduced, demonstrating a regime closer to the optimum orthogonality and hence the independence of one channel to the other. In this section, improvements were made on the experimental setup and thus the compatibility of the TIDE node with a dual quadrature modulated super-channel was experimentally demonstrated.

## 4.5 Chapter summary

In this chapter, the first implementation of an optical node capable of the drop, add, and extract function compatible with a super-channel of spectrally overlapping signals is presented. Extensive simulations have been carried out to study the feasibility of the scheme as well as the parameters required such as the pulse width and extinction ratio [17]. The first real-time implementation of an all-optical node was demonstrated using an AO-OFDM super-channel [20]. Furthermore in order to confirm the capability of the TIDE node, experimental measurements have been carried out for both single quadrature (BPSK) and dual-quadrature (QPSK) signal, resulting in performance well above the standard error-correction algorithm threshold [21]. Further enhancements are required to study the cascability of the TIDE node. The limitations due to the unmatched filtering have been extensively described, as well as the stabilization of the setup. However, all the components required are available, such as FFT-filters based on array waveguide for the matched filter or a full integration of the gate function and interferometer for the system stability, and simulations have shown that small penalty (0.8 dB) can be attained per node [18].

# Chapter 5

## Conclusion

For the investigation of all-optical systems for future optical networks supporting multi-terabit super-channels, three schemes were investigated and systems were developed: Optical comb sources based on electro-optical modulators, all-optical transmitter with overlapping spectra, and an all-optical node capable of managing individual channel from super-channel supporting optical link.

The first step was the generation of multiple optical carriers using an optical comb source based on Mach-Zehnder modulators. While previously reported techniques based on electro-optic modulators were driven by a single frequency RF signal [38,49], a multi-harmonic driven modulator was investigated in order to reduce the overall electrical power and/or the optical device count. A new concept was successfully developed and experimentally demonstrated using an electrical comb to generate a 9 line comb of excellent quality using a single optical modulator [10]. Furthermore, in conjunction with the cascaded modulator technique, a broad rectangular optical comb source was obtained with 36 lines spaced by a constant 10 GHz. The multi-harmonic comb generator has shown that large optical combs are obtainable without the need for non-linear fiber effects [113,114]. In addition, the high number of controls through driving power and biasing of the modulator allowed for the high quality of the comb demonstrated and hence mitigated the need for a shaping optical filter commonly used to exclude unwanted sidebands [36, 115]. Furthermore, the 9 line comb was obtained using a low power RF drive signal providing a cost-effective and overall low power comb source, later confirmed [41]. The multi-harmonic nature of the RF signal reduces the requirement for high gain and high output power for the electrical amplifier as well as for the maximum input power that the

optical modulator can tolerate. Instead of working at the limits of both the electrical and optical devices, the multi-harmonic comb source combines the strong performance of electronics at frequency lower than few tens of GHz and the large bandwidth of optical modulators. Finally, the comb generator presented is highly flexible as individual RF components can be suppressed following the demand for optical carriers, from 1 to 9 lines by increment of 2 lines, in the case presented in this work. Associated with a flexible transmitter [116], the multi-harmonic comb source could hence provide large combination of number of comb lines and line spacing.

The second part of the work reported focused on the implementation of a transmitter generating experimental super-channel signals. An All-Optical OFDM super-channel was obtained and tested with single and dual quadrature modulation formats. The transmitter was based on an odd/even multiplexing structure, with in its core a frequency shift function given by a DP-MZM device [16]. The transmitter implementation allowed for the first demonstration of the optical node for an OFDM super-channel and future testing of different types of super-channels.

The final part reported the development and first implementation of an optical node capable of managing individual OFDM super-channel components. Initial simulations were carried out to determine the limitation and requirements for the implementation of the Terabit Interferometric Add, Drop, and Extract multiplexer [17, 18]. The first real-time implementation of an all-optical node was reported for BPSK AO-OFDM [20], before an improved experimental setup allowed for a dual quadrature modulation format first real-time demonstration [21]. This work has shown it is possible to perform in real-time the functions required of a node (drop, extract, and add), while maintaining the signal in the optical domain. These two first demonstrations open the way for higher modulation format and future optical network capable of routing high spectrally efficiency super-channels. Penalties due to this first experimental implementation were observed, with limitations that have been determined to be linked to the matched filter coarse approximation, the interferometer fluctuation, and some excess ASE noise. However, the numerical simulations carried have shown that the penalties are not inherent of the concept and consequently the TIDE node is capable to route channels embedded into a super-channel. The next step, requiring the improvement of the matched filters and the interferometer stabilization, is to study and demonstrate the cascability of the TIDE node and show that the performance can be maintained over many nodes.

## 5. CONCLUSION

# References

- [1] Cisco Visual Networking Index. "The zettabyte era: trends and analysis." Cisco white paper, (2013).
- [2] M. Borner. "Electro-optical transmission system utilizing lasers." U.S. Patent 3,845,293, issued October 29, (1974).
- [3] A. D. Ellis, J. Zhao, and D. Cotter. "Approaching the non-linear Shannon limit." *Journal of Lightwave Technology*, vol. 28, no. 4 (2010).
- [4] S. Sygletos, I. Tomkos, and J. Leuthold. "Technological challenges on the road toward transparent networking." *Journal of Optical Networking* vol. 7, no. 4, (2008).
- [5] S. Gringeri, B. Basch, V. Shukla, R. Egorov, and T. J. Xia. "Flexible architectures for optical transport nodes and networks." *Communications Magazine*, vol. 48, no. 7, (2010).
- [6] G. Charlet, E. Corbel, J. Lazaro, A. Klekamp, R. Dischler, P. Tran, W. Idler et al. "WDM transmission at 6 Tbit/s capacity over transatlantic distance, using 42.7 Gb/s differential phase-shift keying without pulse carver." *Journal of Lightwave Technology*, vol. 23, no. 1, (2005).
- [7] R. J. Essiambre, G. Kramer, P. J. Winzer, G. J. Foschini, and B. Goebel. "Capacity limits of optical fiber networks." *Journal of Lightwave Technology*, vol. 28, no. 4, (2010).
- [8] T. Healy, F. C. Garcia Gunning, A. D. Ellis, and J. D. Bull. "Multi-wavelength source using low drive-voltage amplitude modulators for optical communications." *Optics Express*, vol. 15, no. 6, (2007).
- [9] R. Maher, P. M. Anandarajah, S. K. Ibrahim, L. P. Barry, A. D. Ellis, P. Perry, R. Phelan, B. Kelly, and J. O'Gorman. "Low cost comb source in a coher-

- ent wavelength division multiplexed system." In European Conference on Optical Communication (ECOC), (2010).
- [10] S. J. Fabbri, S. Sygletos, and A. D. Ellis. "Multi-harmonic optical comb generation." In European Conference on Optical Communication, Mo-2, (2012).
- [11] R. J. Mears, L. Reekie, I. M. Jauncey, and D. N. Payne. "Low-noise erbium-doped fibre amplifier operating at 1.54  $\mu\text{m}$ ." *Electronics Letters*, vol. 23, no. 19 (1987).
- [12] I. B. Martins, I. Aldaya, G. Perez-Sanchez, and P. Gallion. "Optimization of spectral band utilization in gridless WDM optical network." In SPIE OPTO, (2014).
- [13] F. Poletti, N. V. Wheeler, M. N. Petrovich, N. Baddela, E. Numkam Fokoua, J. R. Hayes, D. R. Gray, Z. Li, R. Slavik, and D. J. Richardson. "Towards high-capacity fibre-optic communications at the speed of light in vacuum." *Nature Photonics*, vol. 7, no. 4, (2013).
- [14] D. Kilper, K. Guan, K. Hinton, and R. Ayre. "Energy challenges in current and future optical transmission networks." *Proceedings of the IEEE* vol. 100, no. 5, (2012).
- [15] A. Morea, and J. Poirrier. "A critical analysis of the possible cost savings of translucent networks." In International Workshop on Design of Reliable Communication Networks (DRCN), IEEE, 2005.
- [16] S. J. Fabbri, C. O'Riordan, S. Sygletos, and A. D. Ellis. "Active stabilisation of single drive dual-parallel Mach-Zehnder modulator for single sideband signal generation." *Electronics letters*, vol. 49, no. 2, (2013).
- [17] S. Sygletos, S. J. Fabbri, E. Giacomidis, M. Sorokina, D. Marom, M. F. C. Stephens, D. Klonidis, I. Tomkos, and A. D. Ellis. "A novel architecture for all-optical add-drop multiplexing of OFDM signals". In European Conference on Optical Communication (ECOC), (2014).
- [18] S. Sygletos, S. J. Fabbri, E. Giacomidis, M. Sorokina, D. M. Marom, M. F. C. Stephens, D. Klonidis, I. Tomkos, and A. D. Ellis. "Numerical investigation of all-optical add-drop multiplexing for spectrally overlapping OFDM signals." *Optics Express*, vol. 23, no. 5, (2015).

- [19] S. Sygletos, S. J. Fabbri, F. Ferreira, M. Sorokina, A. Perentos, and A. D. Ellis. "All-optical add-drop multiplexer for OFDM signals." In International Conference on Transparent Optical Networks (ICTON), (2015).
- [20] S. J. Fabbri, S. Sygletos, E. Pincemin, K. Sugden, and A. D. Ellis. "First experimental demonstration of terabit interferometric drop, add and extract multiplexer." In European Conference on Optical Communication (ECOC), (2014).
- [21] S. J. Fabbri, S. Sygletos, A. Perentos, E. Pincemin, K. Sugden, and A. D. Ellis. "Experimental implementation of an all-optical interferometric drop, add, and extract multiplexer for superchannels." *Journal of Lightwave Technology*, vol. 33, no. 7, (2015).
- [22] S. J. Fabbri, S. Sygletos, A. Perentos, E. Pincemin, K. Sugden, and A. D. Ellis. "Experimental demonstration of an all-optical interferometric drop, add, and extract multiplexer for OFDM super-channel." In Summer Topicals Meeting Series (SUM), IEEE, (2015).
- [23] G. P. Agrawal. "Nonlinear fiber optics." Academic press, (2013).
- [24] G. P. Agrawal. "Fiber-optic communication systems." John Wiley, (2002).
- [25] R. Hui, and M. O'Sullivan. "Fiber optic measurement techniques." Academic Press, (2009).
- [26] A. H. Gnauck, and P. J. Winzer. "Optical phase-shift-keyed transmission." *Journal of Lightwave Technology*, vol. 23, no. 1, (2005).
- [27] Y. Chen. "Integrated Optoelectronics for coherent receivers and transmitters." In Asia Communications and Photonics Conference, ATTh4A-4, OSA, (2014).
- [28] E. Yamada, S. Kanazawa, A. Ohki, K. Watanabe, Y. Nasu, N. Kikuchi, Y. Shibata, R. Iga, and H. Ishii. "112-Gb/s InP DP-QPSK modulator integrated with a silica-PLC polarization multiplexing circuit." In Optical Fiber Communication Conference (OFC), PDP5A-9, (2012).
- [29] G. T. Reed, G. Mashanovich, F. Y. Gardes, and D. J. Thomson. "Silicon optical modulators." *Nature photonics*, vol. 4, no. 8, (2010).
- [30] J. J. O'reilly, P. M. Lane, R. Heidemann, and R. Hofstetter. "Optical generation of very narrow linewidth millimetre wave signals." *Electronics Letters*, vol. 28, no. 25, (1992).



- [31] C. Cox, E. Ackerman, H. Roussel, P. Staecker, R. Osgood, T. Izuhara, D. Djukic, and N. Jain. "Design of a broadband electro-optic modulator with very low  $V_{\pi}$ ." Technical Paper, Photonic Systems (2003).
- [32] M. McCarthy, S. J. Fabbri, and A. D. Ellis. "Signal Processing Using Opto-Electronic Devices." In *All-Optical Signal Processing*, pp. 291-323. Springer International Publishing, (2015).
- [33] M. Kourogi, K. I. Nakagawa, and M. Ohtsu. "Wide-span optical frequency comb generator for accurate optical frequency difference measurement." *Journal of Quantum Electronics, IEEE*, vol. 29, no. 10 (1993).
- [34] J. Wu, S. Tsao, H. Tsao, and J. Wu. "Tunable subcarrier comb generator using phase modulator with high modulation index." In *SPIE's International Symposium on Optics, Imaging, and Instrumentation*, (1993).
- [35] K. Ho, and J. M. Kahn. "Optical frequency comb generator using phase modulation in amplified circulating loop." *Photonics Technology Letters*, vol. 5, no. 6 (1993).
- [36] T. Sakamoto, T. Kawanishi, and M. Izutsu. "Widely wavelength-tunable ultra-flat frequency comb generation using conventional dual-drive Mach-Zehnder modulator." *Electronics Letters*, vol. 43, no. 19, (2007).
- [37] I. L. Gheorma, and G. K. Gopalakrishnan. "Flat frequency comb generation with an integrated dual-parallel modulator." *Photonics Technology Letters*, vol. 19, no. 13, (2007).
- [38] C. O'Riordan, S. J. Fabbri, and A. D. Ellis. "Variable optical frequency comb source using a dual parallel Mach-Zehnder modulator." In *International Conference on Transparent Optical Networks (ICTON)*, (2011).
- [39] M. Fujiwara, M. Teshima, J. Kani, H. Suzuki, N. Takachio, and K. Iwatsuki. "Optical carrier supply module using flattened optical multicarrier generation based on sinusoidal amplitude and phase hybrid modulation." *Journal of Lightwave Technology*, vol. 21, no. 11 (2003).
- [40] R. Wu, V. R. Supradeepa, C. M. Long, D. E. Leaird, and A. M. Weiner. "Highly flat and stable optical frequency comb generation using intensity and phase modulators employing quasi-quadratic phase modulation." In *IEEE International Topical Meeting on Microwave Photonics*, (2010).

- [41] A. K. Mishra, R. Schmogrow, I. Tomkos, D. Hillerkuss, C. Koos, W. Freude, and J. Leuthold. "Flexible RF-based comb generator." *Photonics Technology Letters*, vol. 25, no. 7, (2013).
- [42] T. Saitoh, M. Kourogi, and M. Ohtsu. "Expansion of span-width of an optical frequency comb using a higher harmonic wave modulation." *Photonics Technology Letters*, vol. 8, no. 10, (1996).
- [43] Y. Lu, Y. Xing, and Y. Dong. "Equal-amplitude optical comb generation using multi-frequency phase modulation in optical fibers." *Chinese Optics Letters*, vol. 8, no. 3, (2010).
- [44] T. Saitoh, M. Kourogi, and M. Ohtsu. "Expansion of span-width of an optical frequency comb using a higher harmonic wave modulation." *Photonics Technology Letters*, vol. 8, no. 10, (1996).
- [45] S. Ozharar, F. Quinlan, I. Ozdur, S. Gee, and P. J. Delfyett. "Ultraflat optical comb generation by phase-only modulation of continuous-wave light." *Photonics Technology Letters*, vol. 1, no. 20, (2008).
- [46] A. Boff, J. Moll, and R. Shen. "A new high-speed effect in solid-state diodes." In *Digest of Technical Papers of Solid-State Circuits Conference*, vol. 3, pp. 50-51, (1960).
- [47] HEROTEK, "Step recovery diode comb (harmonic) generators, 0.1 to 26 GHz GC series."
- [48] I. Tomkos, S. Azodolmolky, J. Sole-Pareta, D. Careglio, and E. Palkopoulou. "A tutorial on the flexible optical networking paradigm: State of the art, trends, and research challenges." *Proceedings of the IEEE* vol. 102, no. 9, (2014).
- [49] F. C. Garcia Gunning, and A. D. Ellis. "Generation of a widely spaced optical frequency comb using an amplitude modulator pair." In *OPTO-Ireland*, pp. 469-473, International Society for Optics and Photonics, (2005).
- [50] M. Fujiwara, J. Kani, H. Suzuki, K. Araya, and M. Teshima. "Flattened optical multicarrier generation of 12.5 GHz spaced 256 channels based on sinusoidal amplitude and phase hybrid modulation." *Electronics Letters*, vol. 37, no. 15, (2001).

- [51] Q. Wang, L. Huo, Y. Xing, and B. Zhou. "Ultra-flat optical frequency comb generator using a single-driven dual-parallel Mach-Zehnder modulator." *Optics Letters*, vol. 39, no. 10, (2014).
- [52] R. R. Mosier, and R. G. Clabaugh. "Kineplex, a bandwidth-efficient binary transmission system." *Transactions of the American Institute of Electrical Engineers, Part I: Communication and Electronics*, vol. 76, no. 6, (1958).
- [53] H. F. Harmuth. "On the transmission of information by orthogonal time functions." *Transactions of the American Institute of Electrical Engineers, Part I: Communication and Electronics*, vol. 79, no. 3, (1960).
- [54] R. W. Chang. "Synthesis of Band Limited Orthogonal Signals for Multi-channel Data Transmission." *Bell System Technical Journal* 45, no. 10, (1966).
- [55] R. W. Chang. "Orthogonal frequency multiplex data transmission system." U.S. Patent 3,488,445, issued January 6, (1970).
- [56] L. J. Cimini Jr. "Analysis and simulation of a digital mobile channel using orthogonal frequency division multiplexing." *IEEE Transactions on Communications*, vol. 33, no. 7, (1985).
- [57] Armstrong, Jean. "OFDM for optical communications." *Journal of Lightwave Technology*, vol. 27, no. 3, (2009).
- [58] W. Shieh, and I. Djordjevic. "OFDM for optical communications". Academic Press, (2009).
- [59] A. Viterbi. "Nonlinear estimation of PSK-modulated carrier phase with application to burst digital transmission." *IEEE Transactions on Information Theory*, vol. 29, no. 4, (1983).
- [60] R. J. Essiambre, G. Kramer, P. J. Winzer, G. J. Foschini, and B. Goebel. "Capacity limits of optical fiber networks." *Journal of Lightwave Technology*, vol. 28, no. 4, (2010).
- [61] D. Hillerkuss, M. Winter, M. Teschke, A. Marculescu, J. Li, G. Sigurdsson, K. Worms et al. "Simple all-optical FFT scheme enabling Tbit/s real-time signal processing." *Optics Express*, vol. 18, no. 9, (2010).
- [62] J. C. Antona, E. Grellier, A. Bononi, S. Petitrenaud, and S. Bigo. "Revisiting binary sequence length requirements for the accurate emulation of

- highly dispersive transmission systems." In European Conference on Optical Communication, (2008).
- [63] S. K. Ibrahim, J. Zhao, F. C. Garcia Gunning, P. Frascella, F. H. Peters, and A. D. Ellis. "Towards a practical implementation of coherent WDM: analytical, numerical, and experimental studies." *Photonics Journal*, vol. 2, no. 5, (2010).
- [64] A. D. Ellis, I. D. Phillips, M. Tan, M. F. C. Stephens, M. E. McCarthy, M. A. Z. Al Kahteb, M. A. Iqbal et al. "Enhanced superchannel transmission using phase conjugation." In European Conference on Optical Communication (ECOC), (2015).
- [65] Y. Huang, M. F. Huang, E. Ip, E. Mateo, P. Ji, D. Qian, A. Tanaka et al. "High-capacity fiber field trial using terabit/s all-optical OFDM superchannels with DP-QPSK and DP-8QAM/DP-QPSK modulation." *Journal of Lightwave Technology*, vol. 31, no. 4, (2013).
- [66] S. Chandrasekhar, and X. Liu. "OFDM based superchannel transmission technology." *Journal of Lightwave Technology*, vol. 30, no. 24, (2012).
- [67] J. Yu, Z. Dong, H. Chien, Y. Shao, and N. Chi. "7-Tb/s Signal Transmission Over 320 km Using PDM-64QAM Modulation." *Photonics Technology Letters*, vol. 24, no. 4, (2012).
- [68] D. Qian, M. F. Huang, E. Ip, Y. K. Huang, Y. Shao, J. Hu, and T. Wang. "High capacity/spectral efficiency 101.7-Tb/s WDM transmission using PDM-128QAM-OFDM over 165-km SSMF within C-and L-bands." *Journal of Lightwave Technology*, vol. 30, no. 10, (2012).
- [69] Y. Chen, J. Li, P. Zhu, B. Guo, L. Zhu, Y. He, and Z. Chen. "Experimental demonstration of 400 Gb/s optical PDM-OFDM superchannel multicasting by multiple-pump FWM in HNLF." *Optics Express*, vol. 21, no. 8, (2013).
- [70] G. Varella, F. Pitel, and J. F. Marcero. "3 Tbit/s (300/spl times/11.6 Gbit/s) transmission over 7380 km using C+ L band with 25GHz channel spacing and NRZ format." In *Optical Fiber Communication Conference (OFC)*, PD22, (2001).
- [71] L. B. Du, J. Schroeder, J. Carpenter, B. Eggleton, and A. J. Lowery. "Flexible all-optical OFDM using WSSs." In *Optical Fiber Communication Conference (OFC)*, PDP5B-9, (2013).

- [72] L. B. Du, and A. J. Lowery. "The validity of "Odd and Even" channels for testing all-optical OFDM and Nyquist WDM long-haul fiber systems." *Optics Express* vol. 20, no. 26, (2012).
- [73] K. Higuma, S. Oikawa, Y. Hashimoto, H. Nagata, and M. Izutsu. "X-cut lithium niobate optical single-sideband modulator." *Electronics Letters*, vol. 37, no. 8 (2001).
- [74] Y. Ogiso, Y. Tsuchiya, S. Shinada, S. Nakajima, T. Kawanishi, and H. Nakajima. "High extinction-ratio integrated Mach-Zehnder modulator with active Y-branch for optical SSB signal generation." *Photonics Technology Letters*, vol. 22, no. 12 (2010).
- [75] APEXTechnologies. "<http://www.apex-t.com/pdf/optical-spectrum-analyzer.pdf>", (2013).
- [76] T. Chikama, S. Watanabe, T. Naito, H. Onaka, T. Kiyonaga, Y. Onoda, H. Miyata, M. Suyama, M. Seino, and H. Kuwahara. "Modulation and demodulation techniques in optical heterodyne PSK transmission systems." *Journal of Lightwave Technology*, vol. 8, no. 3 (1990).
- [77] S. Shimizu, G. Cincotti, and N. Wada. "High frequency-granularity and format independent optical channel defragmentation for flexible optical networks." In *European Conference on Optical Communication (ECOC)*, (2014).
- [78] S. Shimizu, G. Cincotti, and N. Wada. "Key technologies for energy and spectral efficient flexible optical networks." In *SPIE OPTO*, International Society for Optics and Photonics, (2015).
- [79] E. Pincemin, N. Brochier, M. Selmi, O. Z. Chahabi, P. Ciblat, and Y. Jaouen. "Novel blind equalizer for coherent DP-BPSK transmission systems: Theory and experiment." *Photonics Technology Letters*, vol. 25, no. 18 (2013).
- [80] S. J. Savory. "Digital coherent optical receivers: algorithms and subsystems." *Journal of Selected Topics in Quantum Electronics*, vol. 16, no. 5 (2010).
- [81] R. Schmogrow, B. Nebendahl, M. Winter, A. Josten, D. Hillerkuss, S. Koenig, J. Meyer et al. "Error vector magnitude as a performance measure for advanced modulation formats." *Photonics Technology Letters*, vol. 24, no. 1 (2012).

- [82] F. Chang, K. Onohara, and T. Mizuochi. "Forward error correction for 100 G transport networks." *Communications Magazine*, vol. 48, no. 3 (2010).
- [83] S. Chandrasekhar, and X. Liu. "Experimental investigation on the performance of closely spaced multi-carrier PDM-QPSK with digital coherent detection." *Optics Express*, vol. 17, no. 24 (2009).
- [84] M. Ali, B. Dai, and X. Wang. "Time and frequency synchronisation in all-optical orthogonal frequency division multiplexing systems." *Communications, IET* vol.9, no. 5 (2015).
- [85] D. A. Jackson, R. Priest, A. Dandridge, and A. B. Tveten. "Elimination of drift in a single-mode optical fiber interferometer using a piezoelectrically stretched coiled fiber." *Applied Optics*, vol.19, no. 17 (1980).
- [86] T. Healy, F. C. Garcia Gunning, and A. D. Ellis. "Phase Stabilisation of Coherent WDM Modulator Array." In *Optical Fiber Communication Conference (OFC), OTuI5*, (2006).
- [87] S. K. Ibrahim, A. D. Ellis, F. C. G. Gunning, and F. H. Peters. "Demonstration of CoWDM using DPSK modulator array with injection-locked lasers." *Electronics Letters*, vol. 46, no. 2 (2010).
- [88] P. Frascella, S. Sygletos, and A. D. Ellis. "A novel phase stabilization scheme for DPSK CoWDM signals using high order four wave mixing." In *European Conference on Optical Communications (ECOC), We-8*, (2011).
- [89] J. A. Armstrong, N. Bloembergen, J. Ducuing, and P. S. Pershan. "Interactions between light waves in a nonlinear dielectric." *Physical Review*, vol. 127, no. 6 (1962).
- [90] M. J. Power, W. Jia, R. P. Webb, R. J. Manning, and F. C. Garcia Gunning. "Four-wave mixing for clock recovery of phase modulated optical OFDM superchannel." *Optics Express*, vol. 22, no. 6 (2014).
- [91] I. Bennion, J. A. R. Williams, L. Zhang, K. Sugden, and N. J. Doran. "UV-written in-fibre Bragg gratings." *Optical and Quantum Electronics*, vol. 28, no. 2 (1996).
- [92] T. J. Xia, S. Gringeri, and M. Tomizawa. "High-capacity optical transport networks." *Communications Magazine*, vol. 50, no. 11 (2012).

- [93] X. Liu, S. Chandrasekhar, and P. J. Winzer. "Digital signal processing techniques enabling multi-Tb/s superchannel transmission: an overview of recent advances in DSP-enabled superchannels." *Signal Processing Magazine*, vol. 31, no. 2 (2014).
- [94] A. Sano, H. Masuda, E. Yoshida, T. Kobayashi, E. Yamada, Y. Miyamoto, F. Inuzuka et al. "30 x 100-Gb/s all-optical OFDM transmission over 1300 km SMF with 10 ROADM nodes." In *European Conference on Optical Communications (ECOC)*, (2007).
- [95] E. Pincemin, M. Song, J. Karaki, A. Poudoulec, N. Nicephore, M. Van Der Keur, Y. Jaouen, P. Gravey, M. Morvan, and G. Froc. "Multi-band OFDM transmission with sub-band optical switching." In *European Conference on Optical Communications (ECOC)*, (2013).
- [96] R. Dischler, F. Buchali, and A. Klekamp. "Demonstration of bit rate variable ROADM functionality on an optical OFDM superchannel." In *Optical Fiber Communication Conference (OFC), OTuM7*, (2010).
- [97] G. Bosco, V. Curri, A. Carena, P. Poggiolini, and F. Forghieri. "On the performance of Nyquist-WDM terabit superchannels based on PM-BPSK, PM-QPSK, PM-8QAM or PM-16QAM subcarriers." *Journal of Lightwave Technology*, vol. 29, no. 1 (2011).
- [98] E. Palkopoulou, G. Bosco, A. Carena, D. Klondis, P. Poggiolini, and I. Tomkos. "Nyquist-WDM-based flexible optical networks: Exploring physical layer design parameters." *Journal of Lightwave Technology*, vol. 31, no. 14 (2013).
- [99] A. D. Ellis, and F. C. Garcia Gunning. "Spectral density enhancement using coherent WDM." *Photonics Technology Letters*, vol. 17, no. 2 (2005).
- [100] W. Shieh, and C. Athaudage. "Coherent optical orthogonal frequency division multiplexing." *Electronics Letters*, vol. 42, no. 10 (2006).
- [101] A. Sano, E. Yamada, H. Masuda, E. Yamazaki, T. Kobayashi, E. Yoshida, Y. Miyamoto, R. Kudo, K. Ishihara, and Y. Takatori. "No-guard-interval coherent optical OFDM for 100-Gb/s long-haul WDM transmission." *Journal of Lightwave Technology*, vol. 27, no. 16 (2009).
- [102] G. Goldfarb, G. Li, and M. G. Taylor. "Orthogonal wavelength-division multiplexing using coherent detection." *Photonics Technology Letters*, vol. 19, no. 24 (2007).

- [103] Y. Chen, J. Li, C. Zhao, L. Zhu, F. Zhang, Y. He, and Z. Chen. "Experimental demonstration of ROADM functionality on an optical SCFDM super-channel." *Photonics Technology Letters*, vol. 3, no. 24 (2012).
- [104] M. G. Taylor. "Coherent optical channel substitution." U.S. Patent 8,050,564, issued November 1, (2011).
- [105] P. J. Winzer. "An opto-electronic interferometer and its use in subcarrier add/drop multiplexing." *Journal of Lightwave Technology*, vol. 31, no. 11 (2013).
- [106] T. Richter, C. Schmidt-Langhorst, R. Elschner, T. Kato, T. Tanimura, S. Watanabe, and C. Schubert. "Coherent in-line substitution of OFDM sub-carriers using fiber-frequency conversion and free-running lasers." In *Optical Fiber Communication Conference (OFC)*, Th5B-6, (2014).
- [107] S. Kodama, T. Ito, N. Watanabe, S. Kondo, H. Takeuchi, H. Ito, and T. Ishibashi. "2.3 picoseconds optical gate monolithically integrating photodiode and electroabsorption modulator." *Electronics Letters*, vol. 37, no. 19 (2001).
- [108] K. E. Stubkjaer. "Semiconductor optical amplifier-based all-optical gates for high-speed optical processing." *Journal of Selected Topics in Quantum Electronics*, vol. 6, no. 6 (2000).
- [109] A. D. Ellis, T. Widdowson, X. Shan, and D. G. Moodie. "Three-node, 40 Gbit/s OTDM network experiment using eletro-optic switches." *Electronics Letters*, vol. 30, no. 16 (1994).
- [110] K. Tajima, S. Nakamura, Y. Ueno, J. Sasaki, T. Sugimoto, T. Kato, T. Shimoda et al. "Hybrid integrated symmetric Mach-Zehnder all-optical switch with ultrafast, high extinction switching." *Electronics Letters*, vol. 35, no. 23 (1999).
- [111] A. Naka, T. Matsuda, and S. Saito. "Receiver performance analysis and basic design for optical time division multiplexed transmission systems." *Electronics and Communications in Japan (Part I: Communications)*, vol. 83, no. 4 (2000).
- [112] S. K. Ibrahim, S. Sygletos, R. Weerasuriya, and A. D. Ellis. "Novel real-time homodyne coherent receiver using a feed-forward based carrier extraction scheme for phase modulated signals." *Optics Express*, vol. 19, no. 9 (2011).



- [113] L. Boivin, M. C. Nuss, Wayne H. Knox, and J. B. Stark. "206-channel chirped-pulse wavelength-division multiplexed transmitter." *Electronics Letters*, vol. 33, no. 10 (1997).
- [114] D. Hillerkuss, T. Schellinger, M. Jordan, C. Weimann, F. Parmigiani, B. Resan, K. Weingarten et al. "High-quality optical frequency comb by spectral slicing of spectra broadened by SPM." *Photonics Journal*, vol. 5, no. 5 (2013).
- [115] A. K. Mishra, I. Nellas, I. Tomkos, C. Koos, W. Freude, and J. Leuthold. "Comb generator for 100 Gbit/s OFDM and low-loss comb-line combiner using the optical inverse fourier transform (IFFT)." In *International Conference on Transparent Optical Networks (ICTON)*, (2011).
- [116] T. Goh, H. Yamazaki, T. Kominato, and S. Mino. "Novel flexible-format optical modulator with selectable combinations of carrier numbers and modulation levels based on silica-PLC and LiNbO<sub>3</sub> hybrid integration." In *Optical Fiber Communication Conference (OFC), OWV2*, (2011).